PAUL SCHERRER INSTITUT

PSI

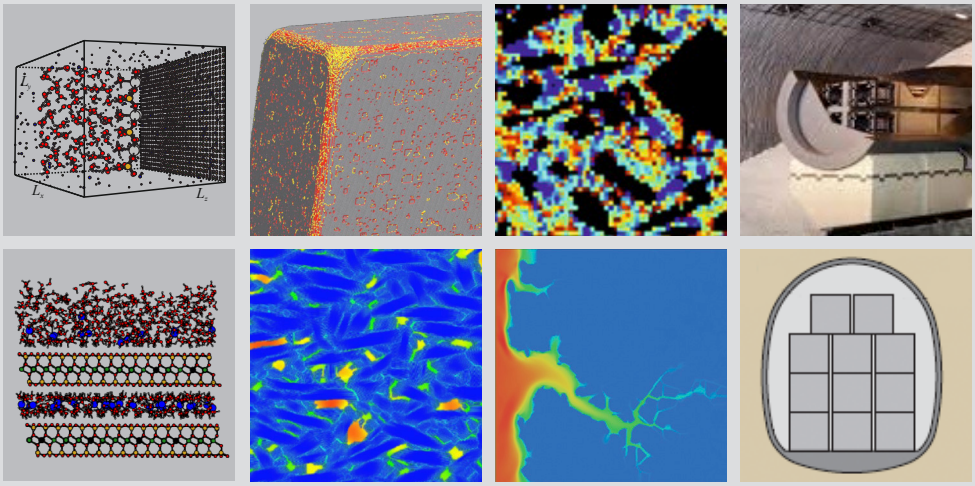

Progress Report 2018

Laboratory for Waste Management :: Nuclear Energy and Safety Department

Cover
Hierarchical coupling of reactive transport processes at different time- and length scales. Most fundamental aspects of mineral reactivity are provided by atomic scale simulations. Pore scale modelling offers an elegant way to link idealized nanometer scale atomistic description of mineral reactivity with structural and compositional heterogeneities of natural systems. The effective transport parameters obtained at different scales are the input for the continuum scales modelling of complex geochemical system over geological times.

PAUL SCHERRER INSTITUT

PSI

Progress Report 2018

Laboratory for Waste Management
Nuclear Energy and Safety Department

See also our web-page
http://www.psi.ch/les/

Preface

The mission of the Laboratory for Waste Management (LES) is to carry out a comprehensive research and development (R&D) programme in support of Swiss radioactive waste disposal options. In particular, the aim is to be one of the world-leading laboratories in the fields of geochemistry of disposal systems and transport mechanisms of radionuclides, including geochemical retardation and immobilisation.

The laboratory serves an important national role by supporting the Swiss Federal Government and Nagra in their tasks to safely dispose of radioactive wastes from medical, industrial and research applications as well as from nuclear power plants. The research activities cover fundamental aspects of repository geochemistry, chemistry and physics of radionuclides at geological interfaces, and radionuclide transport and retardation in geological and technical barriers. The work performed is a balanced combination of experimental activities conducted in dedicated laboratories for handling radioactive isotopes, field experiments and computer simulations. The work is directed towards repository implementation and the results are used by Nagra in their comprehensive performance assessments studies. The finalisation of the site selection process and the implementation of repository in the next decades will require strong expertise in model-based assessment of the repository *in situ* conditions for specific repository designs. The long-term strategy of LES is thus to develop experimental and modelling expertise necessary for fully coupled description of relevant processes in the repository in order to assist safety driven implementation of disposal options in Switzerland.

Since many years LES maintains best practices and standards in the laboratory management and data processing. In the year 2018, LES and two other laboratories from the department of Nuclear Energy and Safety have merged their quality practice in an Integrated Quality Management System. Further, LES received its first QM certification according to the ISO9001:2015 from the Swiss Safety Center (www.safetycenter.ch). The certificate covers the research and scientific services for agencies in the area of nuclear waste disposal and environmental sciences.

This report summarizes the research activities and results achieved in 2018. It gives a detailed overview of research projects, personnel management, national and international collaboration, and individual contributions achieved by scientists in the four research groups at PSI and the Chair of Mineralogy at the University of Bern.

We gratefully acknowledge the support of our work by the PSI management and Nagra.

Table of Contents

1 OVERVIEW

S.V. Churakov

1.1 Introduction

Overall progress made in the Laboratory for Waste Management (LES) over the period from January 1st, 2018 to December 31th, 2018 is summarized in the first part of the report. The report is organised thematically according to seven overarching research topics. These topics are multidisciplinary in nature and include contributions from different research groups at LES and the mineralogy group at the University of Bern.

1.2 General

The site selection process for geological disposal of radioactive waste in Switzerland, the so-called Sectoral Plan for Deep Geological Disposal (SGT), has entered its final stage. The successful finalisation of Stage 2 and initialisation of Stage 3 (SGT E3) have been approved by the Swiss Government on November 22nd, 2018. Three sites, viz. "Jura Ost, Nördlich Lägern" and "Zürich Nordost" are proposed for the further investigations. All proposed siting regions are located in the Opalinus Clay formation. The goal of Stage 3 is to select one disposal site for Spent Fuel/High Level Waste (SF/HLW) and one disposal site for Low/Intermediate Level Waste (L/ILW). Both repositories can in principle be located in one and the same siting region, as a so called "Kombi-Lager" option, given the safety criteria are fulfilled. For either option, safety has the highest priority.

In the course of 2018, LES and Nagra conducted a critical evaluation of the research needs and made a general planning of the technical documentation necessary for Stage 3 of the SGT. These planning provided a basis for the next framework agreement between PSI and Nagra which comprises research, development and demonstration activities for the period 2019-2023.

In the coming years, LES will continue research aimed at filling the gaps in understanding the sorption and transport behaviour of radionuclides and provide scientific justification for model assumptions made in safety assessment studies. Present and future research activities focus on the behaviour of modern spent fuel at repository conditions, the chemical evolution of the repository near field, sorption competition phenomena, the behaviour of redox-sensitive elements, the role of mineral surface induced redox reactions, the transfer of sorption models and data from dispersed to compacted systems. LES has further strengthened its experimental and modelling expertise in reactive transport phenomena. These capabilities are particularly important for understanding the long-term evolution of *in situ* repository conditions and the interaction between repository barriers causing an alteration of their retention and transport properties. Special attention is paid to understanding the role of heterogeneities in the waste forms, which can lead locally to very specific chemical conditions. In this context, LES develops a state-of-the-art expertise in multi-scale reactive transport modelling which enables rigorous stepwise upscaling of model parameters from atomistic to repository scale. LES' long-term goal is to maintain existing datasets for safety analysis, including sorption, diffusion and thermodynamics and to develop beyond state-of-the-art expertise in the quantitative description of the long-term repository evolution.

In the year 2018, LES has continued acquisition of competitive funding for PhD projects and postdoc fellowships. Several incoming scholarships for foreign researchers have been approved. A 3 years PhD project *"Technetium immobilization and remobilization by clays and soils"* was supported by the China Scholarship Council (CSC). The PhD student Ping Chen from the Sun Yat-sen University, Nuclear Science and Technology, China, has arrived on November 1st, 2018. The student will be hosted at University of Bern and conduct experimental work at PSI.

Another PhD student Yuankai Yang from the Tsinghua University, China, supervised by Prof. Moran Wang, has spent 6 months internship at LES to work on the development of a *"Multiscale modelling concept for ion diffusion in cement paste"* aimed at incorporation of molecular scale ion-ion correlation effects in the Nernst-Plank equation for simulations of ion transport in cement paste.

Our long-term scientific collaborator Prof. Kenichiro Nakarai from the Hiroshima University in Japan has received support for a 4 years research project *"Advanced Technology development for treatment/disposal of hazardous materials with unified evaluation of cementitious and geotechnical materials"* granted by the Japanese Society for the Promotion of Science. Within this project Prof. Nakarai and his research team will collaborate with LES on experimental and modelling studies of cement-clay interaction in waste disposal systems.

In 2018, Andra has coordinated the submission of the Joint European Research Proposal COFUND-EJP NFRP-2018-6: *"European Joint Research Programme in the management and disposal of radioactive waste"*. The preparation of the project took place in 2017 and 2018. LES participated in several working groups and actively contributed to the development of the project content. In the framework of submitted project proposals, LES participates in six individual work packages (WP):

FUTURE: Fundamental understanding of radio-nuclide retention

DONUT: Modelling of process couplings and numerical tools applied to performance assessment

ACED: Assessment of chemical evolution of ILW and HLW disposal cells

GAS: Mechanistic understanding of gas transport in clay materials

CORI: Cement-organics-radionuclide-interactions

UMAN: Uncertainty management multi-actor net-work

LES leads and co-leads several tasks in the WPs: FUTURE, DONUT and ACED. The evaluation of the project proposal is ongoing. The results are expected in the spring 2019.

The second phase of the collaborative project *"Thermodynamik und Speziation von Actiniden bei höheren Temperaturen"* (ThermAc) funded by the German Ministry of Education and Finances (BMBF) has been completed. The project activities within this phase were focused on the development of a database for high temperature properties of actinides.

LES continues participation in the follow-up phase of the THEREDA project coordinated by GRS (Gesellschaft für Anlagen- und Reaktorsicherheit GmbH, Germany). This project aims at a critical evaluation of the thermodynamic data for highly saline environments. The thermodynamic data for cement minerals in the THEREDA database is covered by the PSI-Nagra database. Further, LES contributes in the development of the THEREDA project with advanced solid solution models for cement phases.

The development and testing of an experimental set-up for compound-specific analysis of ^{14}C released by the corrosion of irradiated steel is ongoing. The focus of the work conducted in 2018 was on the development of analytical techniques for compound specific analysis of ^{14}C bearing molecules in the gaseous phase.

Over decades LES actively maintains collaborations with national and international research institutes in the field of waste management and environmental research. The main multi- and bi-lateral co-operations with external institutions and universities are summarized in Table 1.1.

Table 1.1: National and international co-operations.

Co-operations
National Nagra* Major financial contribution Various technical working groups
Multinational 7th EU FP (CAST) NEA Thermodynamic Database Project EURATOM HORIZON2020 (SITEX-II) EURATOM HORIZON2020 (CEBAMA) EURATOM HORIZON2020 (DisCo) Mont Terri Projects (diffusion retardation, clay-cement interaction)
Universities Bern*, Switzerland (mineralogy, petrography, water chemistry, C-14 AMS) EPFL, Switzerland (cement systems) Dijon, France (molecular modelling) ETH*, Zurich, Switzerland (GEMS) Hiroshima University, Japan (clay-cement interaction) University of Luxembourg (porous media) Sino-French Institute of Nuclear Engineering and Technology, Sun Yatsen University (diffusion)
Research Centres CEA*, France (chemistry of near- and far-field) EMPA*, Switzerland (cement) IFR, HZDR*, Germany (XAS, TRLFS) INE, KIT*, Germany (near- and far field; TRLFS) FZJ, Germany (sorption/diffusion of Ra) SCK/CEN, Belgium (clay and cement systems) UFZ*, Germany (reactive transport, clay systems) *formal co-operation agreements

Ongoing PhD and postdoc projects hosted at LES are listed below:

L. Hax Damiani (PhD student): *"Modelling transport across reactive interfaces with the Nernst-Planck approach"*. Start date: January 2016 (Funding: EU).

A. Keri (PhD student): *"Shedding light on metal adsorption processes on clay minerals inferred from atomistic simulations and X-ray absorption spectroscopy"*. Start date: January 2015 (Funding: SNSF).

P. Luraschi (PhD student): *"Evolution of transport properties, mineralogy and porosity of cement-clay interfaces"*. Start date: April 2017 (Funding: Nagra, PSI).

Ph. Krejci (PhD student): *"Multispecies cation transport in compacted clays"*. Start date: December 2016 (Funding: SNSF).

M. Mahrous (PhD student): *"Resolving dissolution-precipitation processes in porous media: Pore-scale lattice Boltzmann modelling combined with synchrotron-based X-ray characterization"*. Start date: March 2018 (Funding: SNSF).

A. Mancini (PhD student): *"Thermodynamic and spectroscopic investigations of the Fe and S speciation in anoxic cementitious systems"*. Start date: April 2016 (Funding: SNSF).

L. Nedyalkova (PhD student): *"A structural and thermodynamic study of the intercalation of selenium(IV), selenium(-II), sulfur(-II) and I(-I) in AFm-phases"*. Start date: February 2016 (Funding: EU).

R. Schliemann (PhD student): *"Dissolution, growth and ion uptake at phyllosilicate surfaces: Coupling atomistic interactions at the mineral water interface with Kinetic Monte Carlo model"*. Start date: July 2016 (Funding: SNSF).

S. Wick (PhD student): *"Sorption of thallium on illite and birnessite and its impact on thallium solubility in soils"*. Start date: April 2016 (Funding: SNSF).

Dr. B. Cvetković (postdoc): *"Development of C-14 AMS-based analytical methods for the identification and quantification of C-14 labelled dissolved and volatile organic compounds"*. Start date: November 2013 (Funding: Swissnuclear).

Dr. G. Geng (PSI-FELLOW-II-3i postdoc): *"Alkali-silica reaction in concrete"*. Start date: July 2017 (Funding: SNSF, EU Horizon 2020 Marie Skłodowska-Curie grant, PSI-FELLOW-II-3i).

Dr. F. Marafatto (postdoc): *"Cryo-microspectroscopy at the microXAS beamline for the investigation of redox- and radiation-sensitive samples"*. Start date: June 2017 (Funding: PSI, EAWAG).

Dr. D. Miron (postdoc): *"Effect of aluminum on C-S-H structure, stability and solubility"*. Start date: December 2017 (Funding: SNSF).

Dr. R. Patel (postdoc): *"Resolving carbonation mechanisms of cement-based materials through multi-scale microstructural simulations"*. Start date: August 2017 (Funding: EU Horizon 2020 Marie Skłodowska-Curie grant, PSI-FELLOW-II-3i).

Dr. G. Yang (postdoc): *"Pore scale control of mineral precipitation: from atomistic model to macroscopic modelling and experimental observations"*. Start date: July 2017 (Funding: EU Horizon 2020 Marie Skłodowska-Curie grant, PSI-FELLOW-II-3i).

LES comprises four research groups located at PSI (organisation chart, Fig. 1.1). A fifth research group located at the "Institute of Geological Sciences" strengthens the collaboration with the University of Bern in the field of mineral dissolution kinetics, structural studies of high porous materials and X-ray diffraction-based structure refinement. This expertise complements the LES traditional modelling and experimental capabilities. The research group in Bern is also included in the organisation chart.

The LES annual report 2018 is organised in seven thematic research projects addressing specific aspects of repository geochemistry and radionuclide transport:

Chapter 2: Geochemical evolution of repository near field

Chapter 3: Development of mechanistic sorption models and experimental validation

Chapter 4: Radionuclide transport and retention in compacted systems at full and partial saturation

Chapter 5: Cement-waste interaction and upscaling to the field scale

Chapter 6: Waste characterisation

Chapter 7: Thermodynamic models and databases

Chapter 8: Fundamental aspects of mineral reactivity and structural transformations

The following section provides an overview of activities related to the Sectoral Plan for Deep Geological Disposal, repository near- and far-field, reactivity of barrier systems and code benchmarking activities.

1.3 Sectoral plan for deep geological disposal

The potential radiological impact of a repository is one of the main safety relevant criteria employed in the site selection process. Sorption and diffusion databases are the basis for such calculations. The sorption databases are derived based on thermodynamic calculations. Therefore, a reference Thermodynamic Data Base (TDB) must be available before the development of the sorption databases and the modelling of the *in situ* repository conditions can start. A high-quality core TDB is currently in place. For other elements, a critical evaluation of data is ongoing. In 2018, the thermodynamic data for Nb and Sn were updated and several new inventory-relevant elements, namely Ti, Ag, Ac, Pa and Cf have been included in the database for the first time. The ongoing review work will continue with the aim to release a new updated TDB in 2020. This database will be the reference for all consequent thermodynamic calculations to be conducted within the SGT E3 (see section 7.2).

Calcium silicate hydrates (C-S-H) determine the most relevant properties and the durability of hydrated cement pastes and concretes. C-S-H shows a complex structure and a wide variation of chemical compositions. Accurate thermodynamic predictions of stability, density, composition and solubility of C-S-H (including water content and minor cations Na, K, Al, Sr, U, Zn, ...), in response to changes in cement recipe, water addition, humidity, temperature, carbonation, leaching, and other factors are still one of the major challenges in cement chemistry. Thermodynamic modelling further provides a scientific basis for the modelling of cement materials as a waste matrix or repository backfill. In chemical thermodynamic terms, C-S-H can be expressed as a solid solution by mixing of several structural sub-lattices. Recently, we have developed an advanced self-consistent model for the C-N-K-A-S-H system. The model was built in three steps. An initial model for the C-S-H subsystem was calibrated based on C-S-H solubility data and NMR data for mean chain length. Next, selected experimental datasets on the Na and K uptake in C-S-H were used to refine standard thermodynamic data and interaction parameters for Na and K end-members while keeping constant those previously optimized. Finally, the model was extended to incorporate Al in the system. A comparison with experimental data shows that the newly developed modular C-N-K-A-S-H solid solution model is capable of describing composition, solubility, density, non-gel water content, and the mean silicate chain length (MCL) in a wide range of Ca/Si ratios (see section 7.3).

The thermodynamic database Cemdata18 (www.empa.ch/cemdata) contains standard thermodynamic data and the temperature dependence of the most important cement phases such as portlandite, calcium aluminate, calcium sulfoaluminate present in blended cements, as well as alkali-activated materials for the temperature range from 0 to 100°C and ambient pressure. These data were critically reassessed and documented in the ThermoMatch library included in the GEMS package. To promote the use of the Cemdata18 database with other speciation codes such as PHREEQC, the data were exported from the GEMS library into a PHREEQC compatible data format and made available for the community (see section 7.4).

1.4 Repository near field

1.4.1 Repository chemistry

Dissolution of spent fuel and vitrified nuclear waste defines the radionuclide‘s release after breaching of the disposal casks containing high-level radioactive waste. Therefore, this source term has been intensively studied for decades. The manufacturing recipe of nuclear fuels is evolving to improve the reactors performance. The modern fuel types are doped with Cr or Al to increase the grain-size of the UO_2 particles. Within the EU project DisCo (Modern spent fuel Dissolution and chemistry in failed Container conditions), LES develops solid solution models for Cr-doped UO_2 fuel. The thermodynamic modelling then helps to evaluate the role of the dopant on the oxygen potential of the fuel which is a central parameter affecting the system behaviour and modifies the oxidation state of redox-sensitive fission products, both under in-reactor and repository conditions. Preliminary results suggest that Cr in the fuel should be present in the 3+ oxidation state and the oxygen fugacity in the Cr doped fuel is close to the one measured in non-doped fuel. Current calculations are based on a model of three component ideal solid solutions and need to be further extended (see section 6.3).

The L/ILW repository contains a variety of materials embedded in a cement matrix. The barrier function of the cementitious near field is expected to change over time due to the interaction of hydrated cement with CO_2 produced by chemical degradation of organic waste forms, the corrosion of activated metallic waste and the interaction of highly alkaline cement porewater with silica aggregates present in concrete or by groundwater ingress from the host rock. To investigate the extent of this processes we selected typical waste sorts conditioned (solidified) in concrete. The chemical reactions that are expected to take place inside the waste packages are i) metal corrosion,

ii) degradation of organics, iii) dissolution of silicate aggregates, and iv) carbonation of the cementitious materials. These reactions are believed to control the degradation of the waste materials (organics, metals) and to be primarily responsible for cement-waste interaction as the degradation products can react with the solidifying concrete inside the waste packages (see section 5.1).

Thermodynamic modelling reveals that the degradation of organic materials is the key process controlling the evolution of chemical conditions (solution composition, mineral composition of the solidifying concrete) in the waste packages. The latter reaction produces CO_2 which gives rise to carbonation of the solidifying concrete. This process largely controls the evolution of pH with time. Furthermore, the potential formation of zeolites has a notable effect on the availability of water in the waste packages ("closed system") and on the pH as they bind alkalis. Metal corrosion produces H_2, which was treated as a non-reactive species in the modelling, and corrosion products which may react with the solidifying concrete (see section 5.2).

Previous studies on the thermodynamic simulation of a L/ILW repository were based on the concept of a homogeneously mixed tank representing averaged compositions of waste and cement. This concept has strong limitations due to large heterogeneities of the waste. In cooperation with Y. Huang and H. Shao from the Department for Environmental Informatics of the Helmholtz Centre for Environmental Research – UFZ (Leipzig, Germany) we implemented a set of parametrised equations for source/sink terms describing gas production and consumption into the OpenGeoSys-MP (OpenGeoSys6-MultiPhase-LookupTable) code. This source/sink terms were represented as an interpolatable lookup table. The extended code allows simulations of reactive multi-component multi-phase systems considering the degradation of cementitious materials. The lookup table approach and the implementation were tested against fully coupled simulations with explicit modelling of chemical equilibria. The verified code was then applied to assess the evolution of a waste package during intermediate storage. The simulations demonstrate that the heterogeneous material distribution in the waste package and the spatio-temporal evolution of saturation with water affects the gas generation process. Gas generation, material evolution and humidity transport are coupled in a complex feedback loop involving various chemical and physical (transport) processes. The modelling clearly demonstrates the importance of coupled process simulations for a realistic assessment of gas generation rates in a repository (see section 5.3).

1.4.2 Clay systems

The most successful and widely used mechanistic sorption model for clay systems (2SPNE SC/CE model) describes the retention of cations assuming a fixed density of surface sites and cation specific surface complexation constants. Experimental observations confirm that chemically similar cations (similar valence and hydrolysis constants) occupy the same sorption sites (e.g. compete for the same sorption site). Recent dedicated experimental studies further suggest that elements in different valence state can also be competitive and that the sequence of the element's addition may influence the retention. Further open scientific questions are related to reaction kinetics and sorption reversibility.

Stable elements are ubiquitous in the repository near field, as they are supplied by the porewater from multiple sources such as tunnel backfill materials and host rock formations, corrosion of the carbon steel canister, and finally dissolution of the spent fuel and vitrified HLW. These stable elements and the released radionuclides themselves can all compete with one another for the sorption sites of clay minerals in backfill material and the host rocks. The sorption competition phenomena will therefore reduce the retention of radionuclides. Such competitive effects should therefore be considered for the selection of sorption values for sorption databases used in the safety assessment of radioactive waste repositories.

In the reporting year, the competitive adsorption behaviour of Ni^{2+}, Eu^{3+} and U^{6+} on montmorillonite was determined in a multi-element matrix (containing high concentrations of Co^{2+} and Mn^{2+}) as function of time. No major kinetic effects could be observed over the time scales investigated (3 to 213 days). The sorption of Ni and Eu tracers decrease in the presence of background ions, whereas the U^{6+} sorption is not affected. From these results, one can qualitatively conclude that the divalent and trivalent elements are competitive among each other, whereas uranyl appears to be non-competitive with di- and trivalent metals. A detailed analysis of the results and a quantitative interpretation of the data with the help of sorption models is provided in section 3.2.2.

Selectivity coefficient measurements for Pb^{2+}cation exchange on illite and montmorillonite were completed. The obtained data for the Pb^{2+}-Na^{+} exchange on montmorillonite are in the range of values commonly found for exchange of divalent transition metals. On the other hand, the corresponding value for illite was found to be a factor 4 higher compared with montmorillonite. The reason for the higher affinity of Pb towards illite is not clear. The new data and the previous sorption edge measurements were used to develop a 2SPNE SC/CE

model for Pb^{2+} uptake on illite and montmorillonite (see section 3.2.1).

The influence of temperature on the sorption behaviour of radionuclides on clay minerals is still an open question. The mechanism of Zn adsorption by montmorillonite at 25 and 90°C at neutral pH was investigated by EXAFS. The Zn-spectra obtained at high temperature were compared with Zn-spectra of samples from long-term experiments. The results indicate that at higher temperature and after long reaction time, neo-formation of Zn-bearing silicates is the dominating uptake process. A significant amount of Zn is irreversibly incorporated in the structure of phyllosilicates. Based on this observation the long-term uptake of Zn on montmorillonite can be better described as incorporation rather than as adsorption. The EXAFS study provided clear spectroscopic evidence that at elevated temperatures precipitation processes prevail, even at Zn concentrations characteristic for weak sites (2-20 mmol/kg) (see section 3.2.3).

In the past, the 2SPNE SC/CE sorption model has been successfully used to model adsorption of cations by clay minerals and poly-mineral rocks. To further assess the role of illite in Tl^{+} adsorption and fixation in soils, the solubility and exchangeability of geogenic Tl in topsoils from the Erzmatt site (Swiss Jura Mountains) was investigated. Thermodynamic calculations and EXAFS data analysis indicate that a major fraction of geogenic Tl is fixed in the interlayers of illite, and that short-term Tl solubility is controlled by the minor fraction of the geogenic Tl (see section 3.2.4). The applicability of this model to compacted soils was further tested in diffusion experiments (see section 4.4).

The use of EXAFS for a quantitative analysis of elements with a mixed structural environment requires representative reference spectra. These reference spectra may not be available experimentally and have to be obtained by theoretical calculations. To this aim, reference EXAFS spectra of Fe^{2+} and Fe^{3+} in various *cis*- and *trans*- octahedral positions of montmorillonite as well as in the tetrahedral position were obtained by quantum mechanical calculations. These spectra were used for the interpretation of measured K edge spectra of iron structurally incorporated in montmorillonite. The results suggest that Fe is present as Fe^{3+} and is equally distributed between *cis*- and *trans*- octahedral sites. The presence of tetrahedral iron often discussed in the literature can be excluded (see section 3.2.6).

1.4.3 Cement systems

Carbon-14 has been identified as a major contributor to the long-term release of radioactivity from a cement-based repository into the host rock. Corrosion of activated steel is the main source of ^{14}C in the Swiss waste disposal system. The mobility of the ^{14}C depends on its speciation. While the overall ^{14}C inventory in the radioactive waste is well known, the chemical form of ^{14}C-bearing compounds is poorly understood. The aim the ^{14}C project (see section 6.2) is to investigate i) the release of ^{14}C-bearing organic compounds from waste materials (e.g. during the corrosion of activated steel) and their speciation, ii) the chemical stability of these organic compounds in repository relevant conditions, and iii) the retardation of the organics in the near field of a repository for radioactive waste.

One of the major difficulties associated with the compound-specific analysis of ^{14}C-bearing species is their extremely low concentration, which is far below the detection limit of the conventional measurement's techniques such as gas and liquid chromatography. Accelerated mass spectrometry (AMS) is the most powerful technique, which would allow detection of ^{14}C species in the system. A combination of liquid (LC) and gas (GC) chromatography with accelerated mass spectrometry for the compound specific analysis of ^{14}C species in the gas and liquid phase is being developed and tested.

The focus of the current years was on the development of measurement protocols for gaseous species. To this aim, the GC system operated in the PSI HOTLAB has been extended to allow a separation of individual ^{14}C-bearing gaseous organic compounds. These species are oxidised to $^{14}CO_2$ in a combustion reactor and sampled as $^{14}CO_2$ in a fraction collector. The dedicated fraction collector was developed exclusively for this project by the commercial partner Brechbühler AG. Performance of the combustion reactor was evaluated and optimized in 2017. The testing and optimizing performance of the fraction collector is still ongoing. In particular, the connection between the fraction collector and the AMS is being tested and the injection of CO_2 collected in the sampling loops into the gas injection system (GIS) of the AMS is optimized (see section 6.2.2).

Corrosion experiments with non-activated steel powders conducted in the last 3 years have been completed. In these experiments, both aqueous and gaseous carbon-containing compounds produced during anoxic corrosion were measured. They show that only a limited number of organic compounds are formed during anoxic iron corrosion. These compounds have less than five carbon atoms and thus a low molecular weight. The corrosion studies with non-activated materials are complementary to parallel experiments conducted with activated steel. These experiments help to quantify the impact of gamma

irradiation on the carbon speciation during the anoxic corrosion of activated steel (see section 6.2.3).

Low molecular weight (LMW) organic molecules, such as formate and acetate, are expected to be released during the anoxic corrosion of activated steel in a cement-based L/ILW repository. These LMW organic molecules are metastable at the *in situ* conditions prevailing in the L/ILW repository and should decompose into CO_2 and/or CH_4. The decomposition process is very slow and depends on the presence of microbial activity or catalytic agents. To obtain a first conservative estimate of maximal rates for the LMW decomposition, a series of stability experiments were conducted at ambient conditions and higher temperature up to 150°C under total gas pressure of 5.5 atm for different concentrations of $Ca(OH)_2$. The preliminary results show that the decomposition of formate also takes place even at lower temperatures relevant to the near-field conditions of an L/ILW repository (see section 6.2.4).

The immobilization of selenium and iodine in AFm phases is investigated in the framework of a joined PhD study with Empa (B. Lothenbach) funded by the Horizon 2020 EC project "CEBAMA". In 2018, the characterization of SeO_4^-, $S_2O_3^-$, and I-AFm phases was completed with a study of the water sorption by Dynamic Vapour Sorption (DVS) analysis. The sorption of Se and I on various AFm phases was investigated in a series of batch sorption experiments at pH ~13. The goal of these sorption studies was to test whether the various AFm solid solution models developed in the previous years, are able to describe the observed sorption behaviour. The obtained data from the sorption experiments will be combined with the experimental data from the solid solutions studies for the construction of thermodynamic models describing the Se and I uptake by AFm phases using GEMS. The combination of both data sets would account for sorption on the two types of sorption sites available in the AFm structure: the surface ion exchange sites and the interlayer ion exchange sites (see section 3.2.5).

Iron/steel and cement are the two main components in the planned deep geological L/ILW repository in Switzerland. After closure of the repository, conditions become strongly reducing and the anoxic corrosion of Fe(0) at the interface between cement paste and steel starts to produce Fe(II,III) corrosion products. A PhD project funded by the Swiss National Science Foundation (SNSF grant No 200021_162342) was started in 2016 with the aim of developing a mechanistic view of Fe(II,III) interaction with cement phases and thus improving the current understanding of iron/steel-cement interaction over the time scale of an L/ILW repository. In 2018, batch sorption studies with Fe(III) on C-S-H phases were continued. The speciation of the Fe(II,III) in C-S-H was investigated with EXAFS. Complementary to the Fe(II,III) sorption studies on C-S-H phase micro-spectroscopic investigations were carried out with the aim of determining the oxidation state of Fe in slag cement that had been sampled from aged concrete structures, and a laboratory sample. Redox mapping was performed at the microXAS beamline of the Swiss Light Source (SLS) on different slag-containing cement thin sections in order to identify the Fe redox states around aged slag particles. The analysis of bulk XANES spectrum shows that, as expected, magnetite (Fe_3O_4) is the main corrosion product (see section 5.4).

The alkali-silica reaction (ASR) is a deterioration mechanism, which can severely shorten the durability of concrete structures. The ASR between concrete aggregate and the alkaline pore solution produces expansive solids in the concrete porosity and initiates significant cracking. Despite decades of study, the crystal structure of the ASR products remains largely unclear. In the projects carried out in the framework of a SNSF funded Sinergia consortium (Empa, EPFL and PSI) and a Horizon 2020 research and innovation programme (Marie Skłodowska-Curie) different aspects of ASR stability and structure are investigated. Pure ASR samples with systematically varied chemical compositions are synthesized and analysed with XAS and XRD. Next, microscale crystal-chemical information about ASR collected from ASR reactions in cement samples is compared with the database of reference samples. Preliminary analysis of data from cement samples shows that the structure of ASR reactions products resemble that of minerals such as mountainite and shlykovite (see section 5.5).

1.4.4 Interface processes

The multi-barrier concept for repository design foresees the use of different materials with specific safety functions to protect the environment from a radiological impact. The engineered barrier materials are not in chemical equilibrium either with each other or with host rocks. The chemical contrast between materials will result in diffusive fluxes across the barriers and cause mineralogical and structural transformations, which in turn modify the transport and retention properties of the barriers. Further changes will result from desaturation and re-saturation of the host rocks during the construction phase or from the release of decay heat in a repository for high-level waste. These processes also need to be carefully evaluated.

Several European countries also consider the use of cement as backfill material for the high-level waste. The highly alkaline environment reduces the corrosion

rate of the steel and thus improve the performance of steel-based disposal casks. However, the thermal output from the disposed SF and HLW result in a significant temperature increase in the repository near field leading to phase changes in the cement system. Reactive transport calculations were applied to evaluate the time evolution of repository *in situ* conditions for a repository with a cementitious backfill. The simulations suggest that concrete degradation due to the contact with the host rock is a relatively slow process. Moreover, the pH close to the canister surface remains above 10.5 for at least several tens of thousands of years. The temperature increase itself may lead to temporal mineral phase transformations and accompanying changes in solid volumes, which could influence mechanical properties of the backfill concrete (see section 2.2.1).

Investigations of the cement-clay interaction is ongoing in the framework of a PhD project funded by Nagra. The changes in transport properties and porosity evolution is monitored non-destructively with the help of neutron radiography and by through-diffusion experiments. The measurements show that the interaction process and the changes of porosity at the interface are still ongoing after five years of reaction time. One of the samples was analysed with SEM/EDX. In the course of reaction, the entire cement side has been enriched with Si, Na and Al, and has been depleted in Ca. On the clay side, the analysis indicated a remarkable enrichment in Ca and a decrease in Si, Al and Mg content in the first 1.0-1.5 mm close to the interface. Combining SEM and neutron imaging observations enabled us to quantify the reaction taking place at the interface (see section 2.2.3).

1.5 Repository far field

Experimental sorption studies conducted on dispersed systems are the basis for the development of sorption models. Argillaceous rocks and compacted clays are very dense and are characterised by a high solid-to-liquid ratio. It is still questionable whether the data and models derived for dispersed systems are directly applicable to highly compacted natural rocks. Because of the complexity of the pore microstructure in clay minerals and clay rocks, answers to this question have to be given on a case-by-case basis. Furthermore, during the construction phase of the repository host rock will also be partially desaturated, and this will modify transport properties.

Sorption of Co^{2+} on compacted homo-ionic Na-montmorillonite as a function of pH and ionic strength was further investigated. No systematic discrepancy between the results obtained from disperse and compacted clay media could be observed for this system. However, the effective diffusion coefficients measured by in-diffusion experiments depend strongly on the salinity of the background electrolyte, while they remained rather unaffected by pH. This behaviour is characteristic for planar surface species exhibiting a similar mobility as the respective aqueous phase species, while the surface species bound to the amphoteric surface sites can be regarded as immobile (see section 4.2).

A surface diffusion model was further developed for a consistent description of the concentration-dependent diffusion of Cs in Opalinus Clay. Ion specific surface site mobilities, which are pertinent model parameters, were estimated by fitting model outcomes to the results of in-diffusion experiments for Cs in Opalinus Clay. This surface diffusion model was tested against new experimental data obtained from a radial diffusion experiment for Cs migration in Opalinus Clay. The model was able to reproduce the experimental data in a consistent way without adjusting the parameters (see section 4.5).

Performance assessment (PA) calculations for the Swiss SF/HLW repository predict ^{14}C to be one of the major dose-determining nuclides in safety analysis. This result is mainly a consequence of assumptions related to the anionic nature of carrier species. The transport of dissolved inorganic $H^{14}CO_3^-$ species is expected to be similar to that of other anionic radionuclides, e.g. $^{36}Cl^-$, essentially without retardation. Therefore, a zero-sorption coefficient for ^{14}C in clay is assumed in PA calculations, resulting in high calculated doses. ^{14}C through-diffusion experiments were carried out on compacted Illite-du-Puy intermixed with different amounts of grinded calcite (from 0 to 10 wt.%). The experiments were modelled in COMSOL-Multiphysics by implementing a classical 1-dimensional diffusion equation, including instantaneous reversible sorption and an additional sink term, which describes the incorporation of ^{14}C in newly formed (secondary) calcite during re-crystallisation at a fixed rate. The fitted rates of re-crystallisation agree with the values determined independently in batch isotope exchange experiments, thus indicating that the ^{14}C retention measured in the experiments can be reasonably explained by ^{14}C uptake during recrystallization (see section 4.6).

The DR-B is an ongoing meter-scale diffusion experiment performed at the Mont Terri rock laboratory. It aims at surveying the long-term diffusion of iodide. The experiment was started by adding a NaI solution of high concentration in an injection interval. A dedicated X-ray fluorescence (XRF) probe is used on demand to repeatedly measure concentrations of the tracer and of other elements, such as rubidium (Rb^+), strontium (Sr^{2+}), and barium

(Ba^{2+}) in observation boreholes placed at well-defined distances from the central borehole containing the tracer. To enable 3D monitoring of concentration profiles, the XRF probe can be rotated 360° in the horizontal plane and shifted in the vertical plane (see section 2.3.2).

Diffusion of water and anions in saturated and partially saturated samples of generic clay rocks were studied based on computer-generated 2D clay structure maps with variable particle and pore size distributions. The simulations capture the trends observed in experimental data, predicting reduction of ion mobility at lower relative humidity. This demonstrates that the developed simulation procedures lead to a good representation of molecular processes at the pore scale. In the future, it might be possible to apply them directly to tomographic images, thus allowing to derive a set of various transport properties from a single tomogram (see section 2.4.2).

1.6 Model development, code benchmarking and advanced analytical tools

Benchmarking and verification of reactive transport codes is an ongoing activity which is necessary to demonstrate the credibility of numerical simulations, and to improve the description of complex geochemical interactions and radionuclide transport in a nuclear waste repository.

The development of GEM Software has been continued and the next generation of the GEMS application programming interface (xGEMS) has been released. xGEMS (bitbucket.org/gems4/xgems) is the next generation of GEMS API (Application Programming Interface), implemented in C++, and also available via the Python interface. The xGEMS replaces the GEMS3K kernel released in 2014 and becomes the state-of-the-art numerical solver for chemical equilibria in GEMS. This library is a result of a collaborative work between LES and GEG IG ETHZ (Geothermal Energy and Geofluids – Institute of Geophysics – ETH Zurich) (see section 2.6).

Macroscopic continuum models represent simulation domains using small volume elements with averaged material properties such as porosity, permeability, etc. In a reactive transport scenario, the fluids interact with the minerals and modify the pore space connectivity and topology, sometimes in an extremely non-linear way. To describe the evolution of the pore-space and its effect on transport, macroscopic codes use simple Kozeny-Carman type of correlations to predict the change of permeability due to porosity changes. In order to improve the predictive capability of the macroscopic simulations, especially when strong chemical gradients are present, case-specific porosity-permeability relationships have to be extracted either from experiments or from pore-level simulations. Accordingly, we have developed and tested an approach allowing to use porosity-permeability relationships obtained from pore scale simulations at transport relevant conditions in macroscopic reactive transport simulations (see section 2.5.2).

The role of parameter uncertainty on radionuclide transport in clays was investigated in the framework of a master thesis on *"Uncertainty and sensitivity analysis of sorption chemistry in deep geological repositories"* (master student A. AYOUB 2018). In this project, extensive realizations of Cs breakthrough curves at different locations in clay are produced spanning the expected range of Cs arrival times and concentrations for sorption and transport parameter variations. The performed sensitivity analysis aims at quantifying the effects of uncertainties in 1) site-specific detailed equilibrium constants of the sorption reactions and 2) porewater cations' concentration, on the transport of radioactive Cs in clay. It was found that the sorption reaction equilibrium constants and the concentration of the cations are the most sensitive parameters affecting the transport of Cs in clay. Further, a classification tree was constructed to show the combination of parameters' values leading to the maximum arriving Cs concentrations at a specified location (see section 4.5).

A new SeS benchmark exercise has been proposed for modelling of Cs diffusion through clay for a single species and a multi-species reactive transport setup. So far, MCOTAC, FLOWTRAN, CORE2D, and PHREEQC-COMSOL contributed to the multispecies benchmark. General agreement could be achieved for Cs breakthrough curves obtained with the MCOTAC, FLOWTRAN and CORE2D codes. Different results were obtained with PHREEQC-COMSOL simulations. The origin of discrepancies is being investigated in more detail (see section 4.5).

Transport and retention properties of cement evolve with time due to the changes of its microstructure caused by leaching and carbonation under fully and partially saturated conditions. Such variations in saturation state are commonly encountered at cement-clay interfaces, as well as in CO_2 sequestration wells. In such systems, the ingress of a low pH solution that contains dissolved carbonate ions can lead to precipitation of calcite, and at the same time to the dissolution of calcium-bearing phases in cement. To simulate such systems, an extension in a lattice Boltzmann method based reactive transport tool was made to capture precipitation processes. The extended code was first applied to simulate the influence of the composition of an ingressing solution on an idealized porous medium consisting of portlandite ($Ca(OH)_2$) as cement phase (see section 5.6).

X-ray spectroscopy is an extremely powerful tool for the characterization of materials both structurally and chemically down to the atomic scale. Micro-resolved beamlines allow such information to be obtained with a down-to-the-micrometer resolution on spatially heterogeneous samples, at the expense of an increased photon flux density. For certain samples, the high photon intensity can lead to radiation-induced artefacts. Fortunately, these artefacts can be minimized when performing the measurements at low temperatures. To this aim, we are developing and testing a cryostatic system at the microXAS beamline of the SLS (X05LA). This new system will allow to perform micro-resolved measurements of samples at temperatures close to 4K. New collaborations may arise in disciplines that do not traditionally use synchrotron techniques, which sets the base for a considerable leap in scientific knowledge that is unmatched by other techniques (see section 3.2.7).

Clay rocks are composed by a large number of permanently charged (clay) particles. In the presence of surfaces with permanent electrical charges, the diffusive ion transport is governed by different driving forces, viz. the concentration gradients of the species in the different pore domains and the charge neutrality conditions (e.g. Nernst-Planck equation). The interaction between these driving forces and the magnitude of the resulting fluxes in compacted clay systems is not *a priori* clear from theory. The coupled multicomponent diffusion of charged solutes in charged porous media was further investigated using charged organic polymeric filter membranes as model systems and a framework of an incoming internship (see section 4.3).

The transport of ions at the surface of clay minerals is influenced by the electrostatic potential, ion-ion correlations and ion-solvent interactions. To a full extent, these phenomena can only be captured by explicit molecular simulations. So far, their effect has been ignored in most of the speciation and transport codes. Recently, we have developed a modified Nernst-Plank equation, which allows consideration of ion-ion correlation effects within the lattice Boltzmann framework for fluid transport (see section 2.5.1). Further, the effect of ion-solvent interactions was taken into account in thermodynamic calculations using a three-component classical density functional theory. The approach allows to calculate structural properties of solute and solvent molecules at the interface of charged mineral surfaces with electrolyte and to predict macroscopic thermodynamic parameters such as selectivity coefficients without the use of experimental data (see section 2.4.1).

A new open-source modelling framework for the simulation of electrochemical transport in complex geometries with multiphase chemical equilibrium has been developed based on the FEniCS finite element library and the chemical solver Reaktoro (see section 2.7). An intrinsic feature of the developed framework is the modular design which allows a vast flexibility in the coupled description of physical and chemical processes of arbitrary complexity. The code has been benchmarked against laboratory experimental data and numerical simulations of aqueous ions transport in saturated porous media. The latest version of the code has been applied to simulate reactive transport of gaseous species in the so-called "H_2-transfer" experiment at the Mont Terri underground rock laboratory (see section 2.3.1).

1.7 Fundamental aspects of mineral reactivity and structural transformations

Since 2015, PSI/LES and the Institute for Geological Science at the University of Bern (UBERN/IfG) have established research collaboration in the field of mineralogy and crystallography. Research of the Mineralogy Group at the University of Bern covers fundamental aspects of mineral dissolution and precipitation, chemical factors of crystal structure stability and temperature driven phase transitions in minerals. The dedicated laboratories operated by the group are equipped with powder and single crystal diffractometers for structural studies of minerals and atomic force microscopy laboratory for *in situ* characterization on mineral surfaces. The experimental studies are widely supported by modelling activities. Both groups at LES and the University of Bern benefit from complementary research expertise.

Currently, the main projects of the Mineralogy Group at the University of Bern aim at investigation of natural and synthetic zeolite materials and mechanisms of dissolution/precipitation reaction pathways of carbonate minerals and environmental remediation.

Natural zeolites are mainly framework silicates with large open cavities occupied by cations and H_2O molecules. Many zeolites are characterized by reversible hydration/dehydration and the ability to exchange, to different extent, their extra-framework cations in contact with aqueous solutions. Structural rearrangements in zeolite-type materials arise as a consequence of the loss of water previously bonded to extra framework cations. Such changes can involve severe structural modifications (substantial decrease of the unit-cell volume, channels contraction and in some cases structural collapse) and lead to the formation of new phases. For this reason, the study of the thermal stability of this group of minerals, from a structural point of view, is particularly interesting

considering that many applications involved a pre-heat treatment of the zeolites. These minerals are abundant all over the world and applied as ion exchangers for large-scale remediation (e.g. radionuclides extraction from contaminated soils in Chernobyl and Fukushima).

Thermal behavior of Na exchanged Na-stilbite and stellerite was investigated up to 600°C by *in situ* single crystal X-ray diffraction. Different to previous studies, stellerite B at T >300°C was found to be monoclinic (space group A2/m) (see section 8.2.1).

The dehydration behavior of natural Ca-levyne was investigated from 25 to 400°C by *in situ* single-crystal X-ray diffraction under dry conditions. The mineral group levyne belongs to the natural porous materials with **LEV** topology. Analysis of newly formed high temperature structure revealed a distinct **LEV** topology with different kind of cages, referred to as B'-levyne (see section 8.2.2).

In the SNF funded PhD project (SNF-200021 165548) *"Dissolution, growth and ion uptake at phyllosilicate surfaces: Coupling atomistic interactions at the mineral-water interface with Kinetic Monte Carlo (KMC) model"* a coarse grain simulation strategy is used to formulate a mechanistic model for clay minerals reactivity. The most important input parameters for the KMC simulations are the free energy path for attachment and detachment of the Si tetrahedra and Al octahedra to the edge surface of clay particles. To obtain these parameters, the molecular mechanism of dissolution of clay minerals at edge surfaces have been studied by DFT-based meta-dynamics simulations. The simulations provide detailed information about the reaction mechanism and the reaction kinetics (see section 8.3).

The synthesis of carbonate minerals is raising renewed interest due to the development of carbon storage techniques, which aims at the mitigation of anthropogenic release of carbon dioxide release to the atmosphere. In this context, the possibility to combine geological carbon storage (GCS) with the disposal of contaminated water could help to mitigate the high cost of conventional GCS processes. The development of industrial applications relying on geological resources requires accurate kinetic data for mineral dissolution/precipitation. These data are only partially available for the Pb-Ca-CO_2-H_2O system. The mechanism of Pb-carbonate formation has been investigated in co-precipitation experiments and *in situ* atomic force microscopy studies (see section 8.4).

Currently used dissolution models for carbonates do not consider dependence of the surface speciation on the local surface topography. We have developed a new approach, combining Grand Canonical (GCMC) and Kinetic Monte Carlo (KMC) methods to investigate the influence of water, pH and electrolyte concentration onto processes of surface charging and dissolution of carbonates. GCMC simulations of the calcite-electrolyte system were used to calculate populations of protonated sites. The modelling approach was used to systematically evaluate the behaviour of different speciation models distinguished by spatial charge distributions at the surface. The best results in comparison with the experimental AFM model were obtained by considering explicit oxygen sites on the surface. The model could reproduce both calcite dissolution rate and surface morphology as function of pH (see section 8.5).

Switzerland has a long tradition of waste incineration combustible municipal waste that cannot be recycled and has to be thermally treated in one of the 31 municipal solid waste incineration (MSWI) plants that are coupled to the distribution of district heat. The advantages of incineration are reduction of mass (75%) and volume (90%) as well as the immobilisation of metals and elimination of degradable organic compounds. However, around 6×10^5 tons of bottom ash and 6×10^4 tons of fly ash annually remain after waste incineration and have to be deposited due to their elevated concentrations of toxic substances. The mobility of hazardous metals disposed in the landfill sites depend on the mineralogical composition of the waste. A series of detailed studies has been initiated to better understand the mineralogical composition of the bottom and fly ash and their resistance to leaching in landfills (see section 8.6).

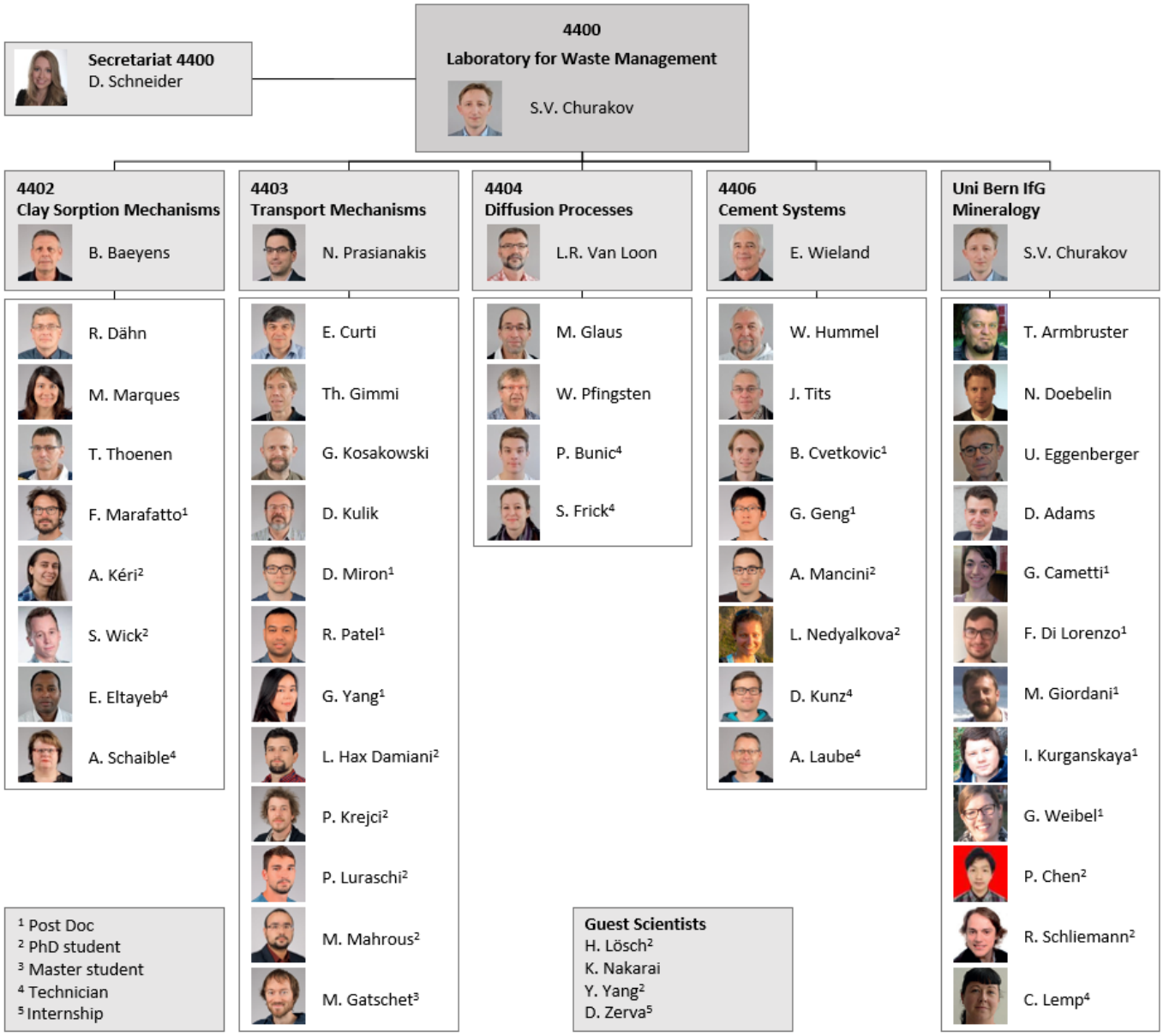

Fig. 1.1: Organisation chart of LES.

2 GEOCHEMICAL EVOLUTION OF REPOSITORY NEAR FIELD

N.I. Prasianakis, S.V. Churakov, L.R. Van Loon, E. Curti, Th. Gimmi, A. Jakob, G. Kosakowski, D.A. Kulik, W. Pfingsten, P. Bunic, S. Frick, D. Miron (postdoc), G. Yang (postdoc), R. Patel (postdoc), L. Hax Damiani (PhD student), P. Luraschi (PhD student), M. Mahrous (PhD student), Y. Yang (exchange PhD student), M. Gatschet (master student), D. Zerva (MSc Internship)

2.1 Introduction

This project aims at providing model-based descriptions for the long-term evolution of the repository near field with different conceptual design of the multi-barrier system. This expertise is essential for the site selection process in the Sectoral Plan for Deep Geological Disposal Stage 3 (SGT E3) as well as for the subsequent development and optimisation of the detailed repository design. Currently, the project is focusing on three main topics: 1) Numerical modelling of the *in situ* condition in the technical barriers and at their respective interfaces, e.g. cement evolution and cement-clay interaction; 2) Interpretation of experimental observations from finalized and running laboratory and field experiments, as well as scoping calculations for the design of the future experiments at the Mont Terri Underground Rock Laboratory (URL); 3) Development of models and concepts for the multiscale simulations and upscaling of parameters, relevant to reactive transport phenomena. The development, benchmarking and validation of coupled THMC reactive transport simulations are an integral part of these activities. Overarching thematic contributions and modelling support is provided in the area of radionuclides retention in host rock, heterogeneities, uncertainties and diffusion in disperse/compacted systems.

In the area of repository design, the temporal evolution of repository near field with an alternative, namely cementitious backfill material has been evaluated. The model takes into account the thermal pulse due to the decay heat, chemical degradation of the cement paste and chemical evolution of the near field in contact with Opalinus Clay (CLOET et al. 2018).

The effect of mineralogical and porosity changes at interfaces of technical barriers (e.g. cement-clay), are further investigated within a PhD project *"Evolution of transport properties, mineralogy, and porosity of cement-clay interfaces"*, partially supported by Nagra (P. Luraschi). By combining diffusion experiments, SEM, and neutron imaging observations, it was possible to better understand the processes and reactions that take place at the cement-clay interface.

Within the HORIZON 2020 collaborative project *"Cement-based materials, properties, evolution, barrier functions"* (CEBAMA), the on-going PhD project "*Modelling transport across reactive interfaces"* (L. Hax Damiani), resulted in the development of an advanced reactive transport solver, the FEniCS-Reaktoro, which couples Nernst-Planck electrochemical transport in porous media with state-of-the-art geochemical codes. The developed model was successfully benchmarked and has been applied to model the Hydrogen Transfer (HT) experiment at the Mont Terri underground rock laboratory. Moreover, the first sets of measurements from the DR-B experiment (*in situ* long-term iodide diffusion) at the Mont Terri were analysed in order to test the quality of the data delivered by the first prototype of the X-ray fluorescence probe (XRF probe).

The further improvement of the predictive capabilities of reactive transport codes can be achieved through multiscale modelling of the transport mechanisms, and a subsequent upscaling. The PSI-FELLOW-II-3i project *"Pore scale control of mineral precipitation: from atomistic model to macroscopic modelling and experimental observations"* (G. Yang) focused on exploring ways to bridge atomistic and pore-level simulations. To shed light on the fluid structure at the mineral-fluid interface, the Fluid-DFT technique was extended to account for the solvent structures.

The diffusion of anions in fully and partially saturated clays was investigated using random walk simulations based on computer generated clay structure maps. The same pore structure maps were used to evaluate the gas permeability in clay at low relative humidity and water saturation using the lattice Boltzmann method. The simulations approximately capture major trends observed in the experimental data.

Within the PSI-FELLOW-II-3i project *"Resolving carbonation mechanisms of cement-based materials through multi-scale microstructural simulations"* (R. Patel), and the project *"Ion transfer mechanisms in clay and cement materials"* (Y. Yang, Tsinghua University, China), a multiscale model for ion transport in cement paste was developed. To this end, the Nernst-Planck equation has been modified to account for the steric effect near the charged surfaces. The results have been validated against Monte Carlo simulations.

Reactive transport calculations are very challenging for macroscopic codes, especially in the presence of strong chemical gradients. The porosity-permeability correlations are key parameters in predicting the geochemical evolution of materials, as well as their altered transport properties because of dissolution and precipitation reactions. Pore-level modelling has been used to extract such material-specific correlations (PRASIANAKIS et al. 2018), which were used as input for continuum scale simulations (Master Thesis of M. Gatschet). The SNSF PhD project *"Resolving dissolution-precipitation processes in porous media: Pore-scale lattice Boltzmann modelling combined with synchrotron-based X-ray characterization"* (M. Mahrous) has started in 2018. This project aims at improving the predictive power of pore-level simulations including complex and accurate description of chemical equilibria in the system.

The development of the GEM Software (lead scientist D.A. Kulik) has been continued and the next generation of GEMS application programming interface (GEMS API: xGEMS) has been released. The new interface allows coupling of codes using both C++ and python programming languages.

2.2 *In situ* conditions in repository near field

2.2.1 Modelling the evolution of a HLW repository with cementitious backfill considering the heat pulse

In alternative disposal concepts, cement is considered as backfill material in the repository for high-level waste (HLW). Feasibility of implementing such a cementitious backfill in the Swiss repository for HLW has been investigated by reactive transport simulations. The model evaluates the long-term evolution of the repository near and far field, taking into account the thermal pulse due to the decay heat, the chemical degradation of the cement paste and the chemical evolution of the near field in contact with Opalinus Clay (CLOET et al. 2018).

The estimation of the temperature distribution in the near and far field was based on the model developed by JAKOB (2013). The 3D COMSOL model considers the heat transport by conduction, and spatially and temporally constant parameters are applied. It was assumed that for the investigated design, the concrete backfill will be protected from drying out via pre-saturation prior to the installation. In accordance with the calculations done by JAKOB (2013) the initial heat output of the waste canister was set to 1500 W. The radii of the emplacement tunnels and the EDZ were adjusted to 1.5 m and 2 m, respectively. Given a repository in Opalinus Clay at 900 m depth, the expected temperature for the centre of the emplacement tunnels is 41.1°C. The thermal conductivity and specific heat capacity for Opalinus Clay and surrounding formations were taken from JAKOB (2013). The reference value for thermal conductivity of wet concrete was set to λ=2.3 $Wm^{-1}K^{-1}$ ($\pm$0.5 $W \cdot m^{-1}K^{-1}$) and the specific heat to 1300 $J \cdot kg^{-1}K^{-1}$ which is a typical value for water saturated concrete. The calculated temperature evolution at selected positions in the near field is shown in Fig. 2.1. The highest observed temperatures are for wet concrete and are only slightly above 100°C.

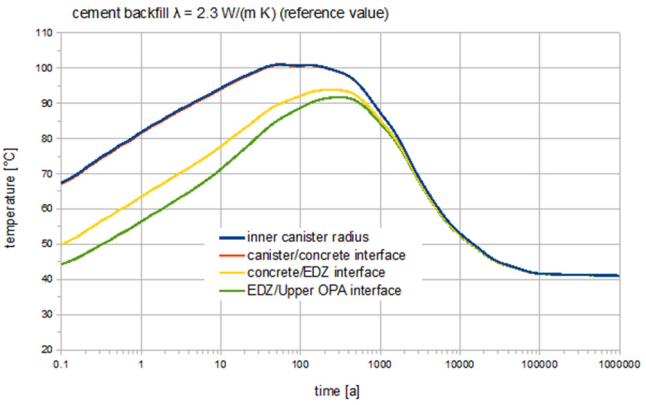

Fig. 2.1: Temperature evolution of the near field for selected monitoring points extracted from the 3D heat transport model in the HLW repository.

The calculated temperature evolution was further used as input, for calculations of the chemical evolution of the near field, thus considering the influence of the temperature pulse. The OpenGeoSys-GEM code was used for this task (KOSAKOWSKI & WATANABE 2014). Calculations are based on a modelling approach developed for analysing the long-term clay-cement interaction in the framework of the Mont Terri CI (Cement Interaction) project (KOSAKOWSKI 2018). The thermodynamic setup combines the cement model by B. Lothenbach (CLOET et al. 2018) and the model for Opalinus Clay from KOSAKOWSKI (2018). Investigated scenarios include instantaneous local thermodynamic equilibrium, kinetic control of clay and zeolite reactivity and consideration of feedback between porosity changes and solute transport. Influence of spatio-temporal temperature variation was considered during chemical equilibration, in temperature-dependent diffusion coefficients, and a temperature-dependent parametrization of mineral dissolution/precipitation kinetics following PALLANDRI & KHARAKA (2004).

Based on various former studies, and on the specific reactive transport calculations in this study, it is expected that concrete degradation due to contact with the host rock is a relatively slow process. The pH will be above 10.5 for at least several tens of thousands of years near the canister surface. The thermal pulse has limited influence on the long-term chemical evolution of concrete backfill. The temperature increase itself may lead to temporal mineral phase transformations and accompanying changes in solid volumes, which could influence mechanical properties of backfill concrete.

As shown in Fig. 2.2, the initially stable jennite phase transforms into afwillite before 0.01 years (Fig. 2.2, upper) due to the fast temperature increase at the canister/concrete interface, while jennite existing near the concrete/Opalinus Clay interface remains stable up to 0.2 years (Fig. 2.2, middle). The model predicts that afwillite is back-transformed into jennite near the canister once the temperature drops below ~50° C. This reaction is suppressed close to the Opalinus Clay due to the influx of silica from Opalinus Clay, which favours stability of the phases with lower Ca/Si ratio. At the Opalinus Clay side, the formation of calcite and zeolites causes porosity clogging in the model after few hundreds of years (Fig. 2.2, bottom). Mineral alterations in Opalinus Clay are mainly limited to a cm to dm wide zone, near the concrete backfill. Porosity clogging is very likely to occur at the concrete/ Opalinus Clay interface. Clogging times are highly uncertain. After clogging, mass fluxes between concrete and Opalinus Clay will be largely reduced and concrete degradation will be slowed down.

2.2.2 Long-term evolution of porosity and chemistry at cement-clay interfaces

Since 2013, several sets of interfaces of high porosity ordinary Portland cement (OPC)/Na-montmorillonite have been reacting in dedicated experimental cells at *in situ* relevant conditions. In 2018, the samples with reaction times of 4 to 5 years were analysed and investigated using destructive and non-destructive techniques to correlate the porosity evolution with the chemical changes at the interface. After a new series of neutron radiographs, which was recorded at the ICON beamline (PSI) to detect porosity changes, the element mapping in several samples has been obtained by Scanning Electron Microscopy/Energy dispersive spectroscopy (SEM/EDX). These data allow the evaluation of elemental profiles across the interface, which gives insight into the mineralogical changes in the reacted interfaces.

Neutron imaging (Fig. 2.3) was performed three years after the last measurements (totally 4.6 years of interaction time). The data indicate a) a further

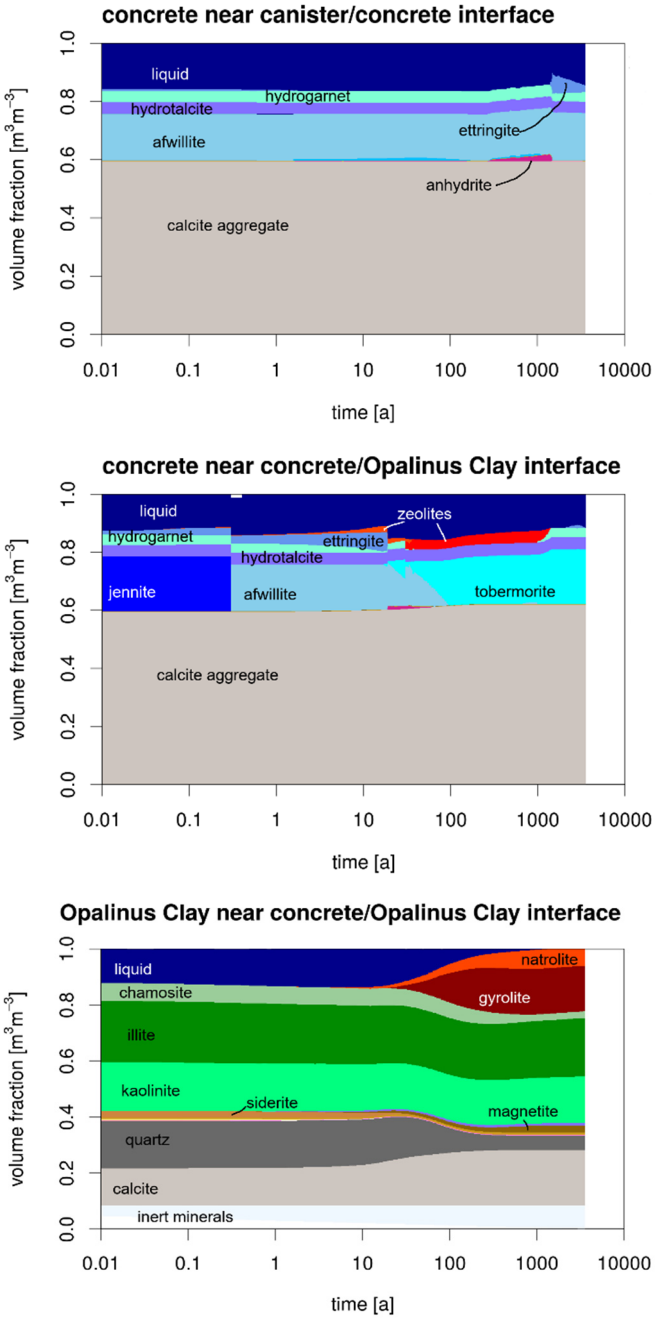

Fig. 2.2: Temporal mineralogical evolution considering kinetic control of clay minerals and porosity feedback on transport. Shown is the evolution near the canister/concrete interface (upper figure), in the concrete adjacent to the concrete/Opalinus Clay (EDZ) interface (middle figure) and in the Opalinus Clay adjacent to the concrete/Opalinus Clay (EDZ) interface (lower figure). Temperature evolution at the canister/concrete and concrete/Opalinus Clay (EDZ) interfaces follow the corresponding curves of Fig. 2.1.

extension of the high porosity region in the cement, and b) only moderate reduction of porosity in the low porosity region in the clay domain, which extends for 1-1.5 mm from the interface. Despite the reduction of porosity, the interface remains partially permeable for the diffusive water transport.

The SEM/EDX profiles across the interfaces show diffusion-controlled distribution of the element's concentrations (Fig. 2.4). In the course of reaction, the entire cement side has been enriched in Si, Na and Al, and has been depleted in Ca. On the clay side, the analysis indicates a remarkable enrichment in Ca and decrease of the Si, Al and Mg contents in the first 1-1.5 mm close to the interface (Fig. 2.4) compared to the unaltered region far away from the interface.

Combining SEM and neutron imaging observations allowed elucidating the reaction that take place at the interface. On the cement side, the measurements suggest the dissolution of portlandite ($Ca(OH)_2$), which leads to a continuous porosity increase and subsequent release and diffusion of Ca^+ and OH^- into the clay domain (Figs. 2.3 & 2.4). The alkaline plume originating from the cement side, most likely causes a partial dissolution of Na-montmorillonite and successive mobilisation of Al, Na, Mg and Si on the clay side (Fig. 2.4). Preliminary results show that Ca originating from the cement compartment is transported and precipitates as calcite inside the clay compartment. The remaining Ca is likely to participate in a cation exchange reaction with Na-montmorillonite. Possible formation of other Ca-bearing phases cannot be excluded and is currently under investigation. Comparison of Figs. 2.3 and 2.4 indicates a correlation between the spatial extension of the low porosity zone and the chemically altered region. This fact suggests that new mineral phases with different molar volume have formed resulting in porosity reduction. Further chemical investigation to better constrain the mineralogical change at the interface are planned. The follow-up analysis will include micro-XRD and Raman spectroscopy.

2.3 Field studies at the Mont Terri underground rock laboratory

2.3.1 Hydrogen Transfer (HT) experiment: Modelling of transport across reactive interfaces

The hydrogen transfer (HT) experiment started in 2009 at the Mont Terri underground rock laboratory with the purpose to investigate the diffusion of dissolved hydrogen in Opalinus Clay (VINSOT et al. 2017). The experimental setup is schematically shown in Fig. 2.5. The newly developed FEniCS-Reaktoro coupled code has been applied to re-evaluate the previously published experimental results (APPELO 2015). Compared to previous simulations our model uses a mass and volume conservative Gibbs-Energy-Minimization approach for calculating geochemical equilibria. This approach also allows calculating the multi-phase equilibrium in the borehole. The modelling results shown in Fig. 2.6 illustrate the excellent agreement between the FeniCS-Reaktoro model and the experimental data collected during the injection period, where gases (H_2, He, Ne) are injected into the borehole and diffuse into Opalinus Clay.

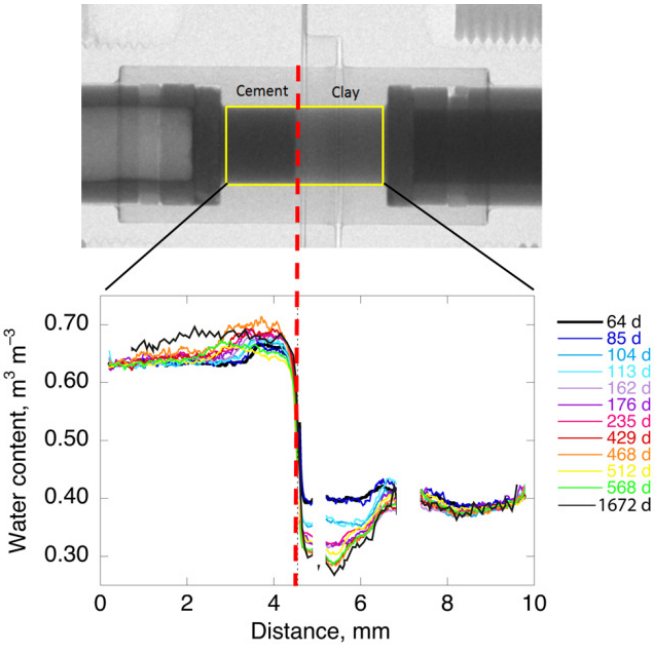

Fig. 2.3: Neutron radiograph of an interface with the corresponding water content profiles at different time.

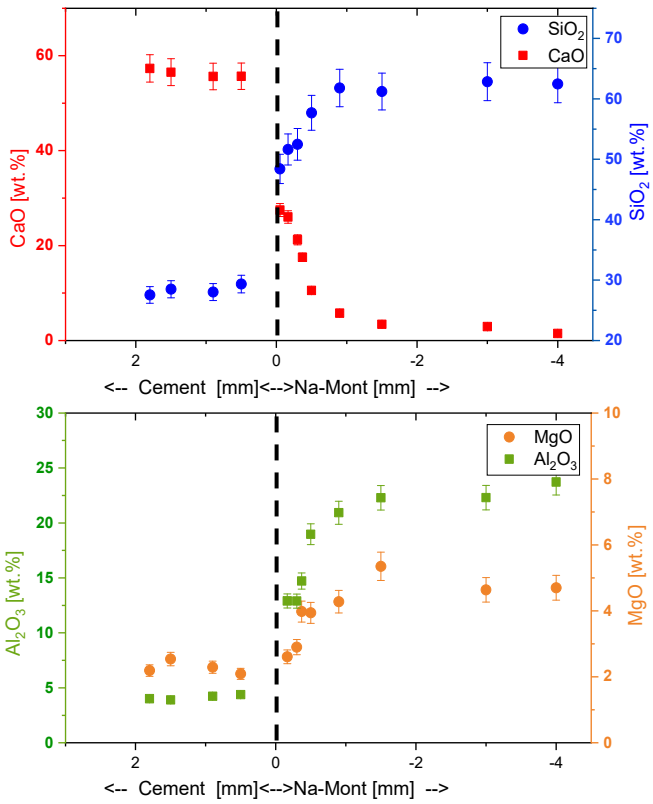

Fig. 2.4: Concentration profiles of Ca, Si, Al and Mg across the cement-clay interface after four years of interaction obtained by SEM/EDX.

It can be seen that the microbial community present in Opalinus Clay affects the existing H_2, which is modelled via a biochemical reaction in which SO_4^{2-} is reduced by H_2 followed by precipitation of FeS. The approach allows the investigation of the microbiological impact on the diffusive transport in Opalinus Clay in a flexible, goal-oriented way and shows a good agreement with the new long-term experimental data (HAX DAMIANI et al. 2018).

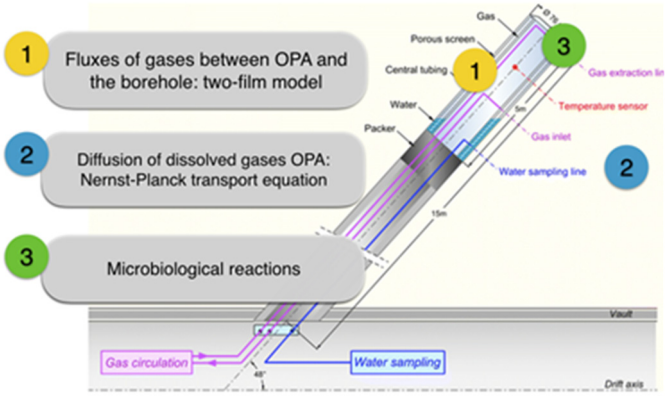

Fig. 2.5: Schematic representation of the Hydrogen Transfer (HT) experiment modified after (VINSOT et al. 2017). Three main processes are indicated: (1) the fluxes of gases and liquid between the borehole and the Opalinus Clay, modelled using the two-film model (LISS & SLATER 1974); (2) the diffusive transport of solutes in saturated Opalinus Clay, modelled using the Poisson-Nernst-Planck equation; and (3) the microbial reduction of SO_4^{2-} by H_2 controlled via a Michaelis-Menten kinetic rate law.

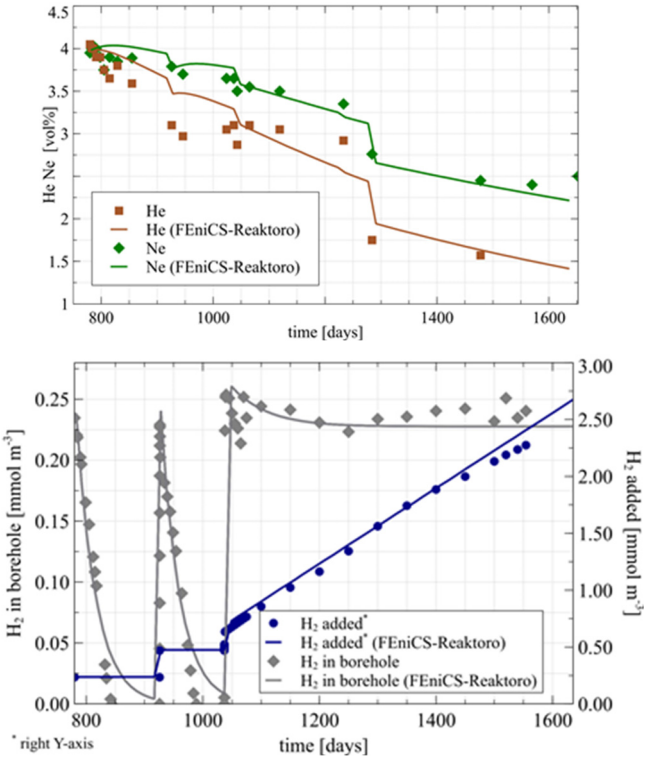

Fig. 2.6: Comparison of FeniCS-Reaktoro modelling results with the experimental data. Top: He and Ne are still present in the borehole after 800 days of their injection. Bottom: 25 mmol/m³ of H_2 is injected into the borehole and practically disappears in approximately 90 days, when a second injection of 25 mmol/m³ is performed, and the same concentration profile is noticed due to its consumption by the microbial community present in Opalinus Clay. Around the day 1000, continuous H_2 injection starts.

2.3.2 DR-B experiment: Diffusion of iodide in Opalinus Clay, analysis of first results

The DR-B is an ongoing meter-scale diffusion experiment performed at the Mont Terri rock laboratory. It aims at surveying the long-term diffusion of iodide. The experiment was started by adding a NaI solution of high concentration in an injection interval. A dedicated X-ray fluorescence (XRF) probe is used on demand to repeatedly measure concentrations of the tracer and of other elements, such as rubidium (Rb^+), strontium (Sr^{2+}), and barium (Ba^{2+}) in the observation boreholes (Fig. 2.8). To enable 3D monitoring of concentration profiles, the XRF probe can be rotated 360° in the horizontal plane and shifted in the vertical plane.

Four boreholes were drilled, BDR-B4, BDR-B5, BDR-B6 and BDR-B8. The NaI was injected in the BDR-B4 borehole. The BDR-B4, BDR-B5, and BDR-B6 are aligned perpendicular to the strike, with BDR-B5 down-dip and BDR-B6 up-dip from BDR-B4. The BDR-B8 is located along the strike from BDR-B4.

The bedding of the Opalinus Clay formation dips with ~35° at the location of the experiment. The total length of each borehole is 10.5 m for BDR-B4, 11.73 m for BDR-B5, 10.66 m for BDR-B6 and 11 m for BDR-B8 (Fig. 2.8). Each observation borehole consists of 2 parts, the upper part serving as guide, and the lower part (2.5 m) which is the measurements area.

A carbon fiber liner (CFK) was installed in the lower part of each borehole for stabilization, while keeping the transparency for the XRF probe. At the bottom of the upper part of each observation borehole, an aluminium plate (baseplate) was placed with 48 mm thickness. The BDR-B8 borehole has moreover a 50 mm thick resin layer below this bottom plate.

Two sets of measurements had been carried out to investigate the evolution of the tracer and possibly of other elements. One set of measurements took place before the injection of NaI solution, the second one approximately 7 months after the NaI injection. The measured data were further analysed within the MSc student internship of D. Zerva. A quality screening,

which included the statistical analysis of the correlations of measurement parameters (e.g. detector livetime) and of the results (Fig. 2.7), the elimination of boundary regions affected by the baseplate or the tip of the probe, and an evaluation for abnormally high concentration values were performed in Matlab (outliers, Fig. 2.9).

The "livetime" for measurement acquisition indicates the time in seconds, that the detector is effectively collecting data (e.g. livetime of 95 seconds in a measurement of 100 seconds). A typical borehole measurement consisted of more than seven thousand local measurements, which upon reconstruction can provide a 3D visualisation of the concentrations along the borehole. The actual duration of data collection (livetime) is affected by the mineral composition at the location of the measurement (Figs. 2.7 & 2.10). For boreholes BDR-B5 and BDR-B6 the top 60 mm are influenced by the baseplate (48 mm from the baseplate and 12 mm from the baseplate "noise"). For the borehole BDR-B8 the influenced interval is increased to 110 mm (48 mm from baseplate, 50 from resin layer and 12 mm from "noise"). The CFK successfully does not affect the measurements (Fig. 2.10). The reliability of the measurements conditions was checked with a comparison between the duration of each measurement (livetime) and the resulting concentration. It was found that the livetime does not affect the quality of the data, as long as it is over 90 sec.

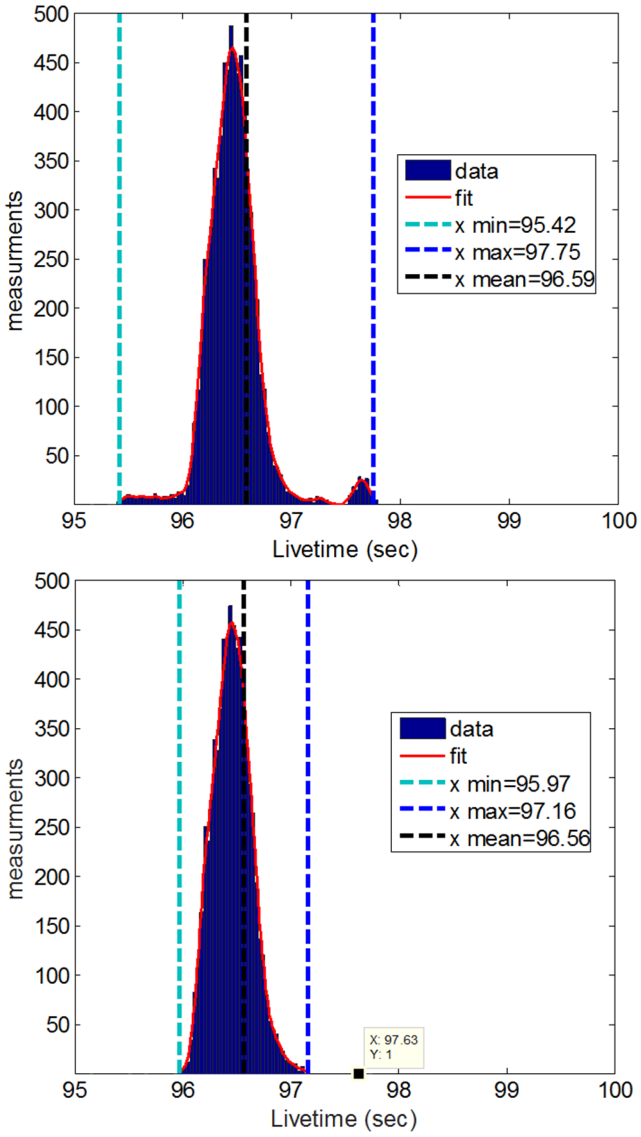

Fig. 2.7: Histogram of livetimes including measurements near the baseplate (top) or excluding these measurements (bottom).

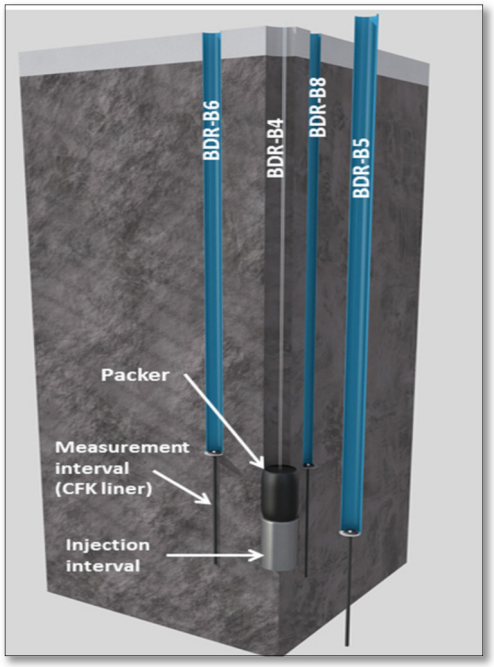

Fig. 2.8: 3D representation of the injection borehole BDR-B4 and the observation boreholes BDR-B5, BDR-B6 and BDR-B8 (Nagra AN 16-669).

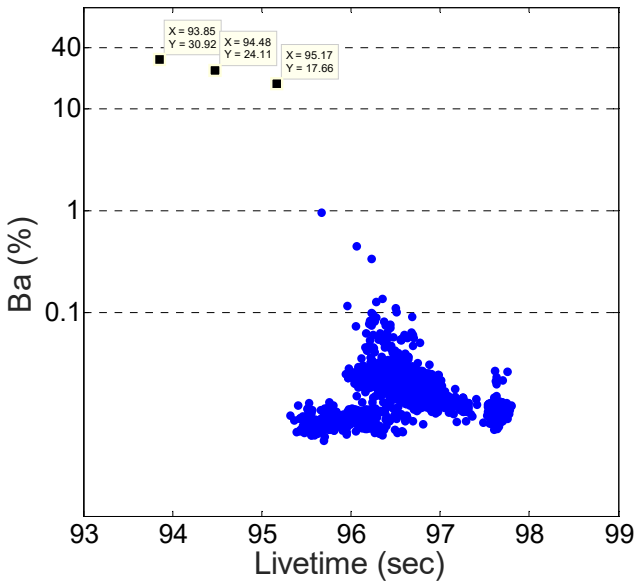

Fig. 2.9: Localization of outliers in one data set for Ba.

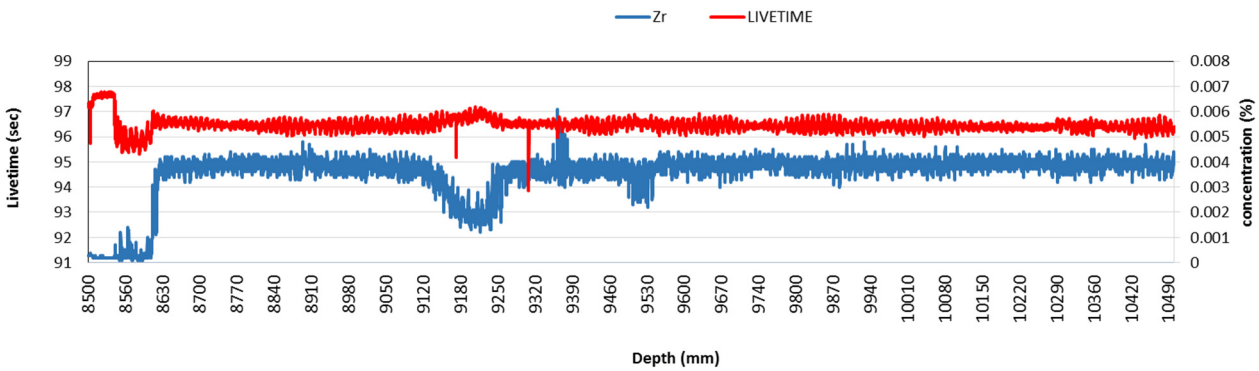

Fig. 2.10: BDR-B8 borehole: The baseplate and resin layer (depth ca. 8500 - 8630 mm) influence the livetime of the measurement, and the derived Zr concentration (note that calibration may be inappropriate in this region). An interrelation between livetime and Zr concentration in Opalinus Clay is visible in the region around the depth of 9200 mm.

2.4 Fundamental understanding of transport and sorption mechanisms

2.4.1 Fluid density functional theory (f-DFT) bridge between atomistic and pore-level simulations

The PSI-FELLOW-II-3i project *"Pore scale control of mineral precipitation: from atomistic model to macroscopic modelling and experimental observations"* (G. Yang) was initiated in 2017. The project receives partial funding from the European Union's Horizon 2020 research and innovation programme under the Marie Skłodowska-Curie grant agreement No. 701647.

Mineral surfaces often carry structural charges, which exert electrostatic potential and results in the formation of the diffuse double layer at the mineral-fluid interface. Montmorillonite is one of the most common swelling clay minerals present in argillaceous rocks. Single montmorillonite particles are made up of an (Mg, Al) octahedral (O) sheet sandwiched between two (Si, Al) tetrahedra (T) sheets, forming a so-called TOT layer. The negative charge of the TOT layer is compensated by cations in the interlayer pore space, as well as in the external pore space, forming the so-called diffuse double layer. The detailed structure of the fluid at the interface can be obtained by molecular dynamics or Monte Carlo simulations. These simulations are computationally expensive and cannot easily be applied for the thermodynamic calculations. Instead, classical density functional theory (f-DFT) was applied to model water and ion distribution at the charged mineral water interface. In our f-DFT model for montmorillonite – electrolyte interface, the solvent molecules were included in the system of equation as neutral hard-sphere particles. The developed f-DFT model was able to predict solvent and solute structure in the fluid, at the mineral interface, in good agreement with results of Molecular Dynamics (MD) simulations with the SPC-water model (Fig. 2.11) (YANG et al. 2018). The model was further applied to model cation ion exchange and was able to reproduce experimental results as seen in Fig. 2.12 (YANG et al. 2018). At the same time, this methodology can be applied to fluid systems of increased complexity, i.e. 3D systems but not restricted to system size. The computational advantage of f-DFT allows conducting very fast parametric studies (parameters: pore-size/solution concentration) and will be used in bridging the gap between atomistic and pore-level simulations.

2.4.2 Simulation of water retention and of diffusion of anions and cations in clay samples

Diffusion of water and anions in water saturated and partially saturated samples was studied in a systematic way using random walk simulations. The samples were represented by computer generated 2D clay structure maps (16'000 times 16'000 pixels, representing a 2 µm by 2 µm sample). The maps were composed of non-swelling clay particles, and smectite particles with two water layer thick interlayers. Several maps with different pore size distributions described by gamma distribution with selected Coefficients of Variation (*CV*) were investigated (Fig. 2.13). The mean of the gamma distribution for the inter-particle pore sizes was set to 3 nm. Results for diffusion of water and of anions, along the bedding, in saturated samples are shown in Fig. 2.14. Anions were assumed to be excluded from the interlayers and from a small fringe around the clay particles. The simulated diffusion coefficients of anions were lower than those of water, as a result of the partial anion exclusion. Diffusion coefficients of water and anions are largest at small *CV*, i.e. when the inter-particle pore sizes are relatively homogeneous. A more heterogeneous inter-particle pore size distribution (larger *CV*), with a few large pores and many smaller pores leads to lower pore diffusion (D_p) values.

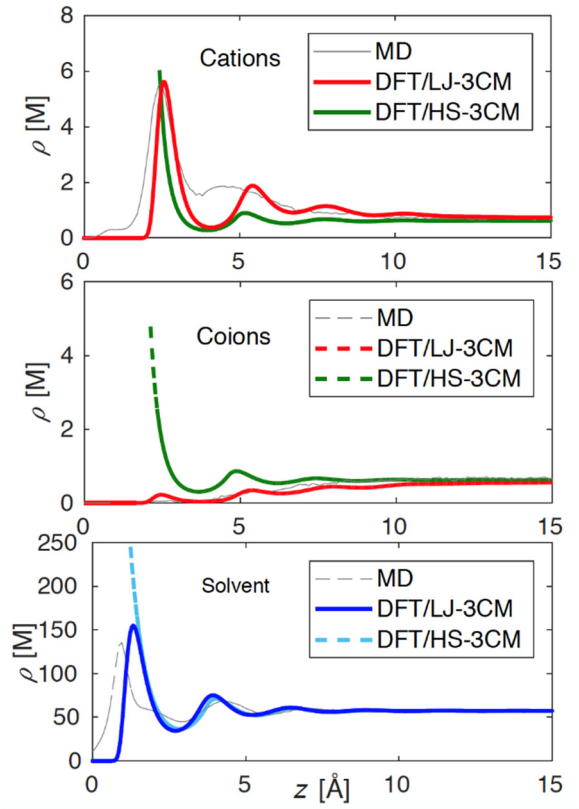

Fig 2.11. Density distributions of Na^+ (dark blue curves) Cl^- (green curves) ions and H_2O (light blue circles) from DFT calculations (YANG et al. 2018) compared with atomic simulations (YANG et al. 2017) (grey curves), in which 12 Na-Cl ions and 1800 water molecules are equilibrated in a 30 Å wide nano-channel of Na-montmorillonite.

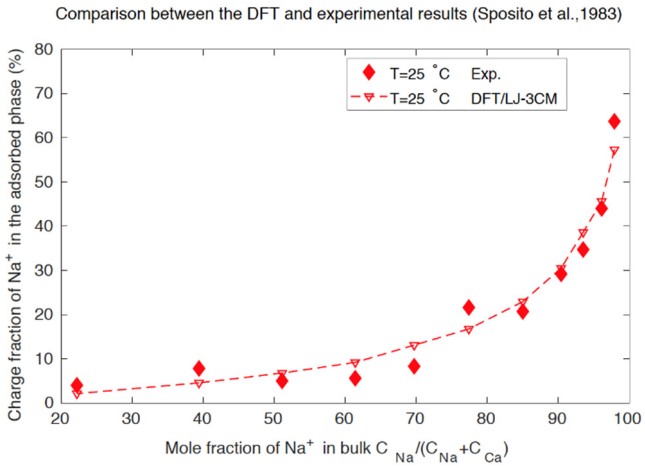

Fig 2.12: Charge fraction of sodium in the adsorbed phased $\Gamma_{Na}/(\Gamma_{Na}+\Gamma_{Ca})$ as function of the mole fraction of sodium in bulk solutions $C_{Na}/(C_{Na}+C_{Ca})$. Ca-Na exchange experiments were conducted for Wyoming Ca-MMT in chloride medium (SPOSITO et al. 1983). The DFT results are from the result of recent developments of our project (YANG et al. 2018).

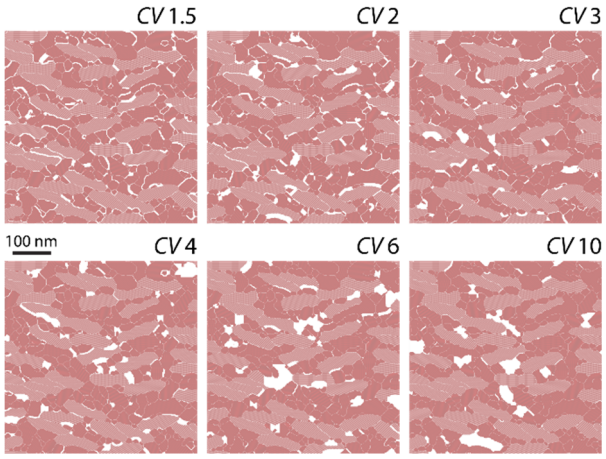

Fig. 2.13: Parts of clay structure maps used for water retention and diffusion simulations. The maps differ in the Coefficient of Variation (CV) of the width distribution used for creating interparticle pores. Pores are white, smectite particles are light red, and other particles are dark red.

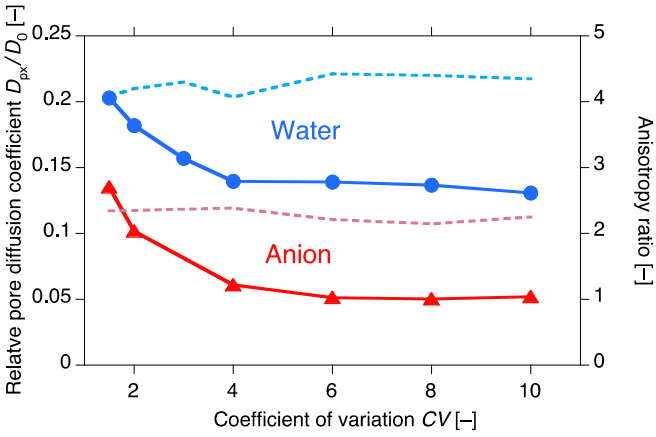

Fig. 2.14: Simulated diffusion coefficients D_{px}/D_0 along bedding at full water saturation (solid lines, left ordinate) for water (blue) and anions (red) as a function of the CV of the interparticle pore width distribution. D_{px} is the pore diffusion coefficient along the bedding, D_0 is the diffusion coefficient in bulk liquid. Also shown are the anisotropy ratios D_{px}/D_{py} (dashed lines, right ordinate).

The anisotropy ratio D_{px}/D_{py}, also shown in Fig. 2.14, appears about independent of the *CV*. This ratio is about 4 for water tracers, and about 2 for anions, which is similar to experimental findings for Opalinus Clay. The difference in the anisotropy ratio between water and anions results mainly from the differences of D_{px} along bedding, where the interlayers contribute to water tracer transport, but block anion transport. The D_{py} perpendicular to bedding is nearly identical for water and anions, meaning that the interlayers hardly contribute to transport in this direction.

Next, water retention in the clay structure maps was simulated based on the capillary law and surface adsorption effects (Fig. 2.15). Simulated water retention curves, which show the relation between equilibrium relative humidity and water content of a sample, were then used to simulate diffusion through partially saturated clay samples. Diffusion of anions is exemplarily shown in Fig. 2.16. The simulated effective diffusion coefficients, D_e, normalized by the value $D_{e,sat}$ at saturation, decrease more rapidly with desaturation for lower *CV* as compared to higher *CV*. Considering liquid surface films as well, leads to a less rapid decrease compared to simulations considering capillary forces only. For comparison, literature data (SAVOYE et al. 2010 & 2014) for various clay materials are also plotted in Fig. 2.16. The simulations capture approximately the trends of the experimental data. This demonstrates that the developed simulation procedures lead to reasonable results. In the future, it might be possible to apply them directly to tomographic images, thus allowing a set of various transport properties from a single tomogram to be derived.

At the same time, the clay structure maps derived for the simulation of diffusion coefficients under partially saturated conditions were also used to measure the gas using the lattice Boltzmann simulation framework. For this purpose, a part of a map was remeshed at a higher spatial resolution. Due to the existence of many pores with very small sizes, fully interconnected gas pathways occurred only at full or near complete gas saturation. Within this limited range, the gas permeability decreased with increasing water saturation, as expected, and effective gas diffusivities as a function of relative humidity and saturation have been calculated.

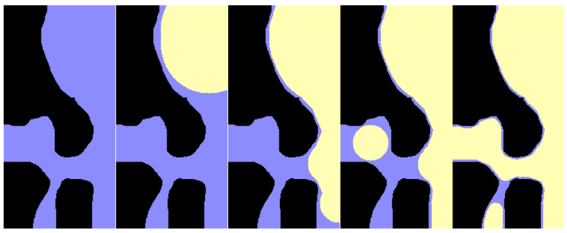

Fig. 2.15: Drainage of an example model structure map for decreasing relative humidity (frames from left to right), considering capillary effects (drainage of core of pores with decreasing radius) and surface adsorption effects (thinning of surface water films). Black: solid, blue: water, yellow: drained pore.

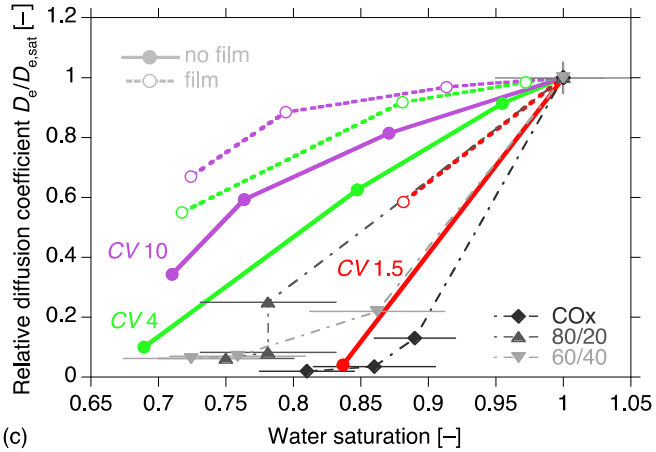

Fig. 2.16: Simulated effective diffusion coefficients $D_e/D_{e,sat}$ ($D_{e,sat}$ is the value at saturation) for clay structure maps with given CV as a function of water saturation. Solid lines: capillary condensation only; dashed lines: capillary condensation and surface films. Literature data (SAVOYE et al. 2014 & 2010) for various clay materials are shown as black to gray symbols with dash-dotted lines.

2.5 Multiscale modelling of reactive transport mechanisms and upscaling

2.5.1 Upscaling of reactive transport parameters from molecular to field scale

Reactivity of minerals is controlled by chemical processes at mineral-fluid interfaces acting at different time- and length scales. Various modelling approaches are available to characterize scale-specific aspects of mineral-fluid interface chemistry. Most fundamental aspects of mineral reactivity are provided by atomic scale simulations. Several attempts have been made to interpret macroscopic observation based on atomic scale simulations alone. Many of them have failed however, because of neglecting the pore-scale transport phenomena. One of the aims of developing multiscale modelling approaches is to upscale transport and thermodynamic parameters obtained by experimental and modelling approached to macroscopic field scale simulations. A concept for the multiscale modelling approach is summarized in Fig. 2.17 (CHURAKOV & PRASIANAKIS 2018).

2.5.2 Multiscale modelling of ion transport in cement paste

The PhD student Y. Yang from Tsinghua University, Beijing, China (supervisor Prof. M. Wang) joined LES for a 6-month internship to work on the development of a multiscale modelling framework for ion transport in cement paste. The internship was supported by the China Scholarship Council. A schematic representation of the developed multiscale modelling approach is shown in Fig. 2.18. In this work, the conventional expression of the Nernst-Planck equation has been modified to account for steric effects due to the final ion size and the ion-ion

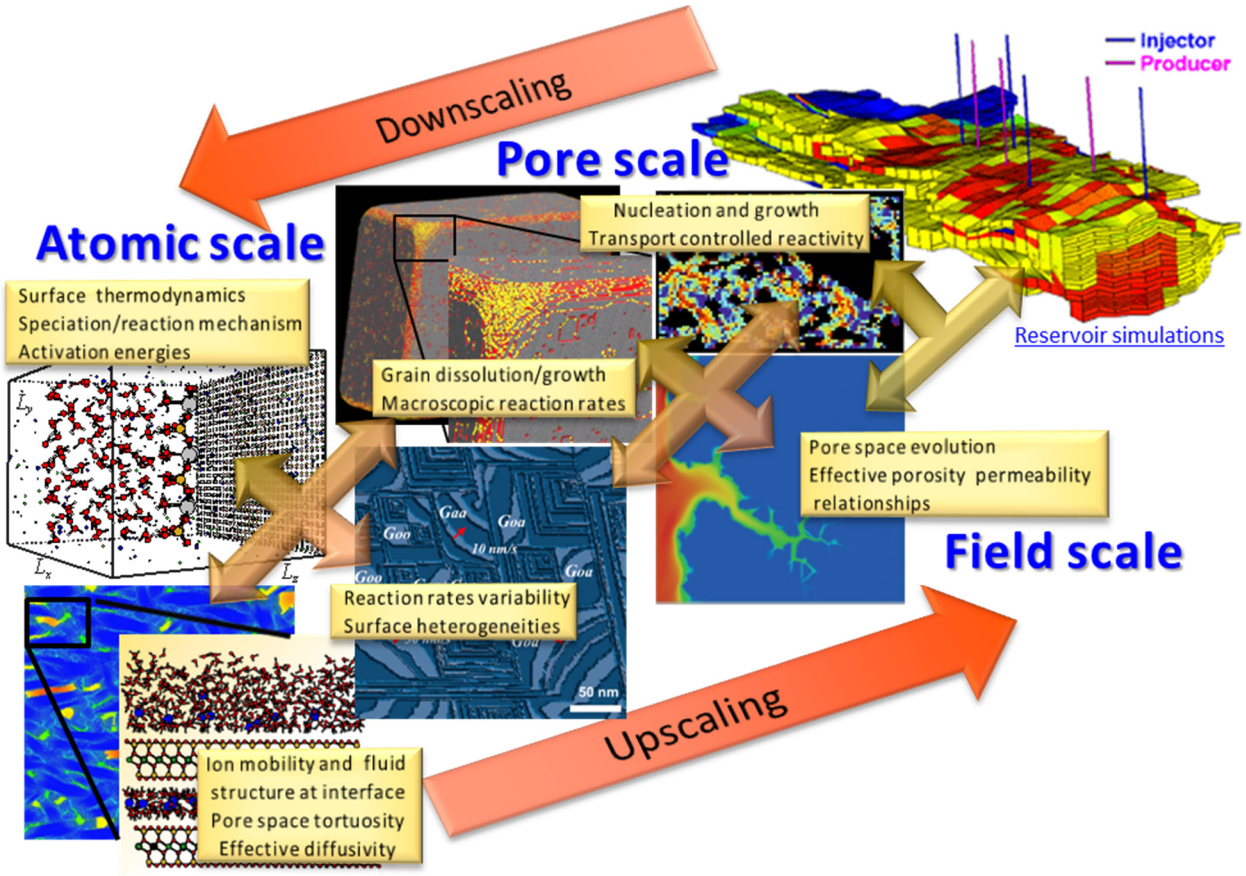

Fig. 2.17: Hierarchical coupling of processes and scales. Atomic scale modelling provides effective parameters for pore-scale simulations such as activation barriers for surface reaction and the reaction mechanism. These data are used by pore-scale simulation to obtain effective transport parameters and their evolution for continuum scale simulations (CHURAKOV & PRASIANAKIS 2018).

correlation in the electric double layer at the mineral-fluid interface. The calibration parameters for the modified Nernst-Planck equation were obtained from Monte Carlo simulations of the equilibrium between pore solution and calcium silicate hydrates (C-S-H) (CHURAKOV et al. 2014). Fig. 2.19 shows a comparison between modified Nernst-Planck equation, Monte Carlo simulations and classical Nernst-Planck equation. The simulation setup represents equilibrium between C-S-H surface and bulk electrolyte solution with 20 mM $Ca(OH)_2$. Fig. 2.19 clearly shows that the modified Nernst-Planck equation correctly captures the concentrations near the surface, while the classical Nernst-Planck equation fails to predict the charge distribution in the diffuse double layer. The developed multiscale modelling approach was further applied to explain differences in diffusivity of different ions in cement paste that has been reported in the literature.

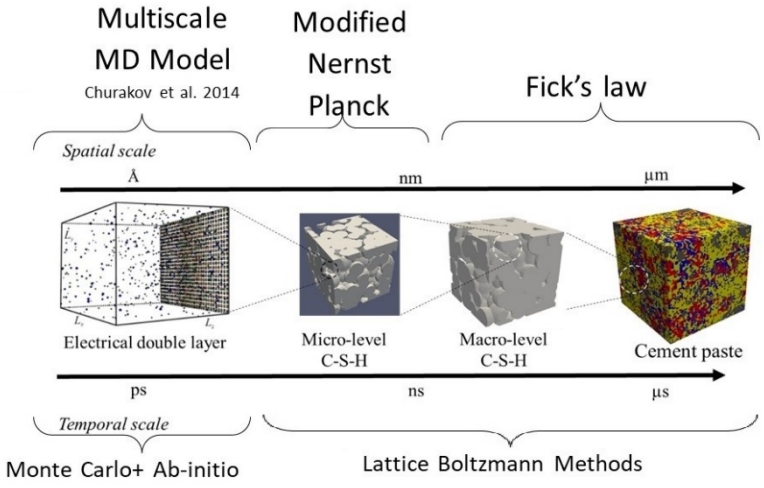

Fig. 2.18: Multiscale modelling scheme for ion transport in cement paste.

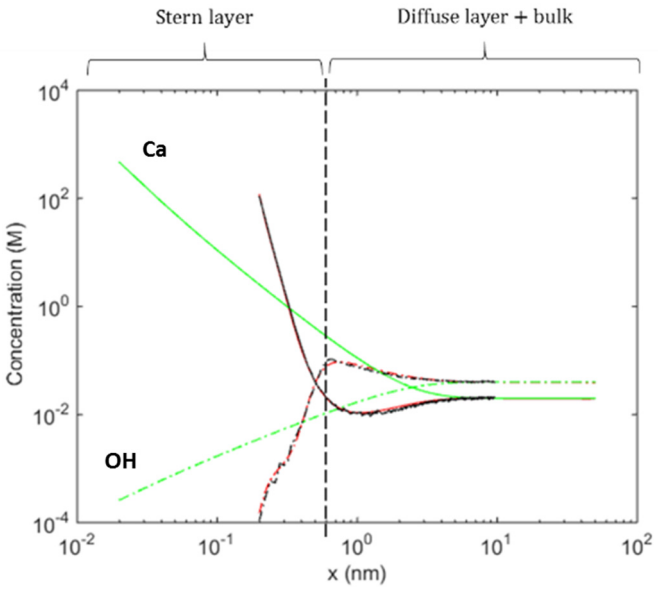

Fig. 2.19: Comparison between Monte Carlo simulations of C-S-H electrolyte interface (black), modified passion Nernst-Planck equation (red) and classical passion Nernst-Planck equation (green). Solid lines refer to calcium ion and dashed lines to hydroxide ion.

2.5.3 Bridging pore- and continuum scale simulations

Macroscopic continuum scale simulations usually represent the domain of interest as small volume elements with averaged material properties such as porosity, permeability, etc. In a reactive transport scenario, the fluids interact with the minerals and modify the pore space connectivity and topology, sometimes in an extremely non-linear way. To describe the evolution of the pore space and its effect on transport, macroscopic codes use simple Kozeny-Carman type of correlations to predict the change of permeability due to porosity changes. In order to improve the predictive capability of the macroscopic simulations, especially when strong chemical gradients are present, case-specific porosity-permeability relationships have to be extracted either from experiments or from pore-level simulations.

Pore-level modelling and simulations were conducted within the lattice Boltzmann method framework, and porosity-permeability relationships corresponding to different flow and reactive conditions were obtained (PRASIANAKIS et al. 2018). Dissolution of calcite rock, in the presence of HCl acid has been considered. The non-dimensional parameters that characterize the reactive transport problem are the Peclet, Damkohler and Reynolds numbers. As expected, the change of permeability, due to porosity changes, strongly depends on the flow and reaction characteristics, which is in contrast of using a single Kozeny-Carman type of correlation for all flow regimes. In Fig. 2.20, some of the extracted correlations are depicted. For this example, blue circles correspond to the creation of wormholes in calcite rock, while red crosses correspond to the face dissolution of the same rock (due to different flow conditions). Filled circles would be a typical Kozeny-Carman prediction.

The evolution of permeability has been fitted in terms of template power laws in order to upscale these results and use them in a macroscopic scale simulator (Master Thesis of M. Gatschet). For the macroscopic simulations, the reactive transport code MCOTAC was used. The simulation result in Fig. 2.21 highlights the sensitivity of macroscopic simulation to the underlying porosity-permeability model. For the same inlet flow rate (inlet velocity is set to 4.0×10^{-4} m s^{-1}) and pH flow conditions (pH=2), the three different correlations extracted from Fig. 2.20 are applied to simulate the dissolution of a porous carbonate rock.

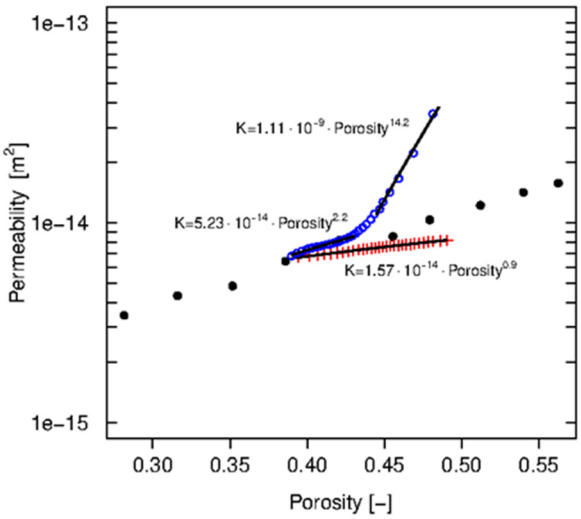

Fig. 2.20: Changes in porosity-permeability relationships strongly depend on the flow regime and reaction conditions. Blue circles correspond to the creation of wormholes in calcite rock, while red crosses correspond to the face dissolution of the same rock related to different flow conditions. Filled circles show typical Kozeny-Carman relationships. Blue circles can be fitted with a single correlation or can be split in two distinct regimes.

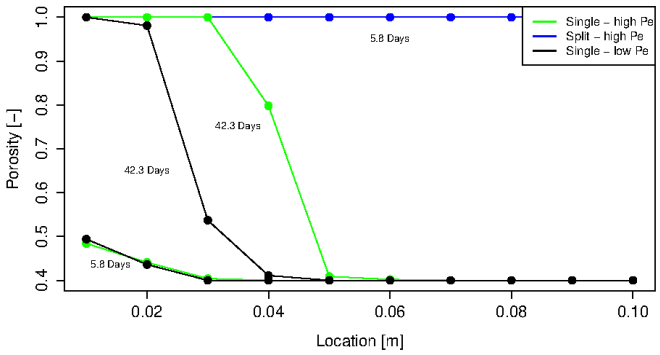

Fig. 2.21: Sensitivity analysis of the macroscopic reactive transport model to the underlying porosity-permeability correlations obtained from microscopic calculations performed for different fluid transport regimes. Given the appropriate porosity-permeability relationships, as obtained by pore-scale simulation, the continuum model is able to capture the changes in the evolution of the system.

2.5.4 Minerals precipitation/dissolution at the pore scale

The process of mineral precipitation and dissolution is of great significance in predicting and assessing the geochemical evolution of the repository near field. A cross-scale model has been recently developed and has been applied in the prediction of simultaneous dissolution and precipitation processes (PRASIANAKIS et al. 2017, POONOOSAMY et al. 2015). Reactive transport calculations on realistic 3D domains that are described by more than one billion grid cells (> 1000^3 domains) are computationally intensive, especially when full speciation is considered. The SNSF PhD project *"Resolving dissolution-precipitation processes in porous media: Pore-scale lattice Boltzmann modelling combined with synchrotron-based X-ray characterization"* has started in 2018. This project will extend the modelling capabilities to more complex reactive systems by incorporating more accurate geochemical description, and by exploiting the acceleration that GPU-based lattice Boltzmann algorithms and high-performance computing facilities. The mineral precipitation is modelled based on the Classical Nucleation Theory (CNT), allowing predicting the onset of precipitation as well as the evolution of mineral reactive surface areas. Further validation of the reactive transport models will be conducted against 3D experimental results that will be analysed at the Swiss Light Source (SLS) large-scale facilities of PSI. The project methodology is depicted in Fig. 2.22.

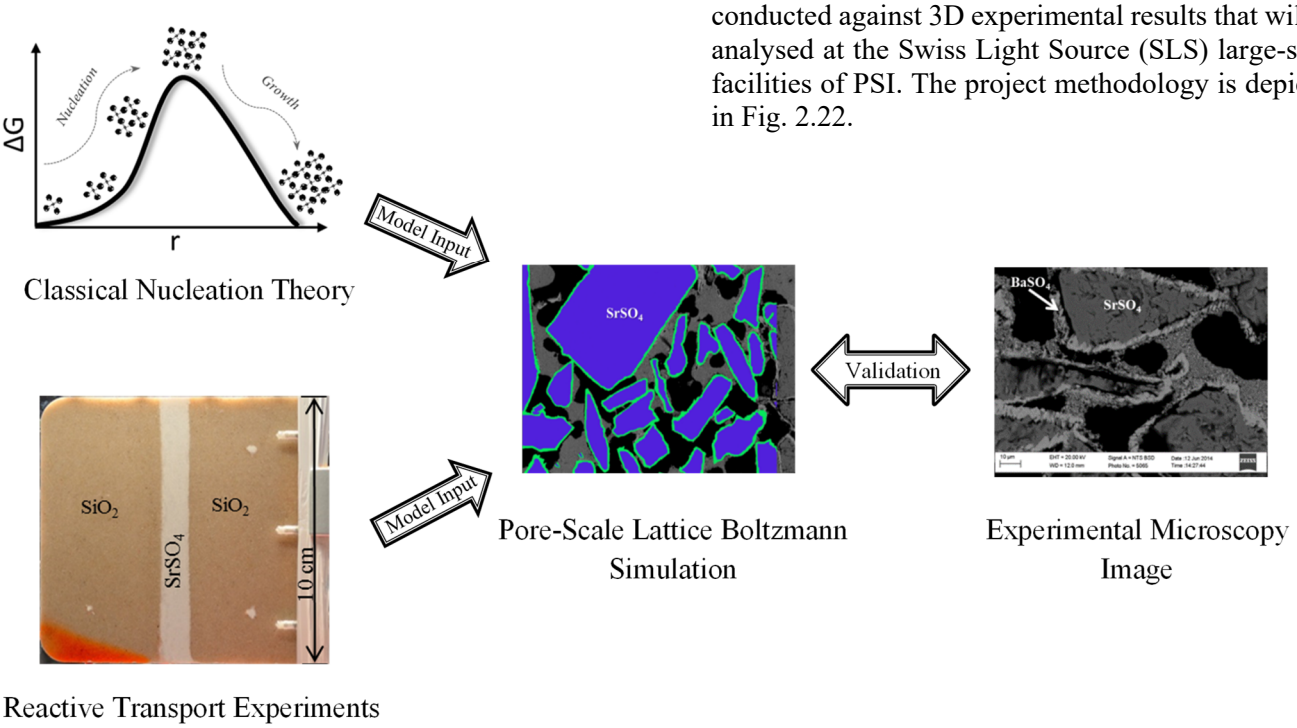

Fig. 2.22: A schematic representation of the modelling and experimental methodology adopted in the PhD project "Resolving dissolution-precipitation processes in porous media: Pore-scale lattice Boltzmann modelling combined with synchrotron-based X-ray characterization".

2.6 Thermodynamic modelling framework and thermodynamic databases: further development in GEMS project

The xGEMS code library (https://bitbucket.org/gems4/xgems) is the next generation of GEMS API (Application Programming Interface), implemented in C++, and also available via Python interface for convenience. The xGEMS replaces GEMS3K as the state-of-the-art numerical solver of chemical equilibria in GEMS (Fig. 2.23). The library is a result of the collaborative work between LES and GEG IG ETHZ (Project leader A. Leal). The xGEMS API is under continuous development with new extensions and access methods added per requests from the overarching laboratory projects, the collaborators and the modelling community. The code comes with new "ChemicalEngine" for C++ and Python APIs that share the same access methods for either C++ or Python implementations. A third-party lightweight header-only tool pybind11 is used for exposing the C++ API in Python (https://github.com/pybind/). The API provides access methods for loading the chemical system definition, setting the composition, temperature and pressure, running the chemical equilibrium, and extracting the computed speciation results as well as other system properties. For calculating chemical equilibrium, xGEMS currently uses the GEMS3K code (KULIK et al. 2013) with its TNode class API for the improved GEM IPM-3 algorithm for Gibbs energy minimization, and the TSolMod library (WAGNER et al. 2012) for activity and mixing models of phases-solutions. The xGEMS is initialized with the same set of files as GEMS3K that define the parent chemical system, which is setup in GEM-Selektor. The xGEMS code can be coupled with a mass transport simulator or any other code (e.g. a graphical user interface, a parameter optimizer, or a web application). An example for coupling xGEMS with a reactive transport code in Python is available in the code repository; it reproduces the 1-D reactive transport calcite dissolution dolomite precipitation benchmark from SHAO et al. (2009) (Fig. 2.24). A joint publication about xGEMS and latest improvements in GEMS3K is in preparation.

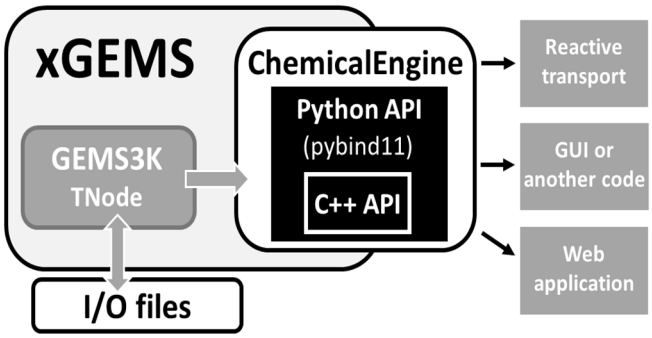

Fig. 2.23: xGEMS library with new C++ and Python APIs.

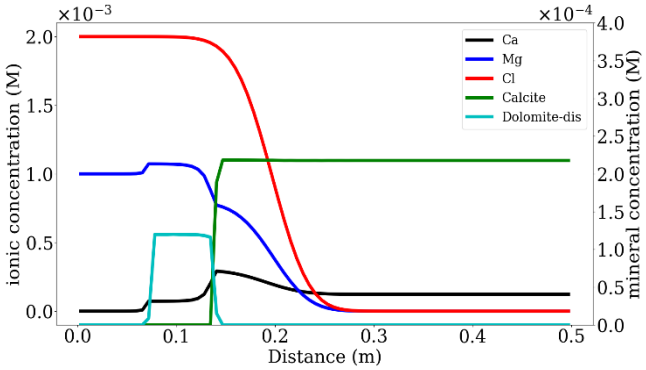

Fig. 2.24: Results of 1-D reactive transport benchmark (SHAO et al. 2009) obtained using xGEMS. A column of calcite is flushed from the left side with a 0.001 mol/L $MgCl_2$ aqueous solution.

2.7 Role of electrochemical transport in reactive transport simulations

The PhD project entitled *"Modelling transport across reactive interfaces"* (L. Hax Damiani) focuses on the development of a reactive transport code, which takes into account electrochemical interaction relevant for transport in porous media with surface-charged minerals, such as Opalinus Clay. This project is part of the HORIZON 2020 collaborative work package *"Cement-based materials, properties, evolution, barrier functions"* (CEBAMA). The developed open-source simulation framework, couples the finite element library FEniCS (ALNÆS et al. 2015) with the chemical solver Reaktoro (LEAL et al. 2016). Intrinsic feature of the developed code is the modular design which allows a vast flexibility in the coupled description of physical and chemical processes of increasing complexity. The code has been benchmarked against laboratory experimental data and numerical simulations of aqueous ions transport in saturated porous media. The latest version of the code has been applied to simulate reactive transport of gaseous species in the so-called "H2-transfer" experiment at the Mont Terri underground rock laboratory (see section 2.3.1).

2.8 References

ALNÆS M., BLECHTA J., HAKE J., JOHANSSON A., KEHLET B., LOGG A., RICHARDSON C., RING J., ROGNES M.E., WELLS G.N. (2015)
The FEniCS project version 1.5. Arch. Numer. Softw. 3. doi:10.11588/ANS.2015.100.20553.

APPELO C.A.J. (2015)
HT Hydrogen Transfer experiment TN-201258 http://www.mont-terri.ch/internet/mont-terri/de/home/experiments/documentation/gratisberichte.parsys.0788.downloadList.57712.DownloadFile.tmp/tr9804.pdf

CHURAKOV S.V., LABBEZ C., PEGADO L., MARIALORE S. (2014)
Intrinsic acidity of surface sites in calcium silicate hydrates and its implication to their electrokinetic properties. J. Phys. Chem. C 118(22), 11752-11762.

CLOET V., CURTI E., KOSAKOWSKI G., LURA P., LOTHENBACH B., WIELAND E. (2018)
Cementitious backfill for a high-level waste repository: impact of repository induced effects. Nagra Tech. Rep. (in preparation).

HAX DAMIANI L., CHURAKOV S.V., KOSAKOWSKI G. (2018)
Hydrogen Transfer modelling with NPS. PSI Technical Report TM-44-18-01, Paul Scherrer Institut, Villigen, Switzerland.

JAKOB A. (2013)
Temperature evolution in the near and far field of a Swiss repository for radioactive waste accounting for an increased heat production of the waste. PSI Technical Report TM-44-13-01, Paul Scherrer Institut, Villigen, Switzerland.

KOSAKOWSKI G., WATANABE N. (2014)
OpenGeoSys-Gem: A numerical tool for calculating geochemical and porosity changes in saturated and partially saturated media. Phys. Chem. Earth, Parts A/B/C, 70/71, 138-149.

KOSAKOWSKI G. (2018)
CI experiment: Reactive transport modeling of interface evolution with OpenGeoSys-GEM. PSI Technical Report TM-44-18-05, Paul Scherrer Institut, Villigen, Switzerland.

KULIK D.A., WAGNER T., DMYTRIEVA S.V., KOSAKOWSKI G., HINGERL F.F., CHUDNENKO K.V., BERNER U.R. (2013)
GEM-Selektor geochemical modeling package: Revised algorithm and GEMS3K numerical kernel for coupled simulation codes. Comput. Geosci. 17, 1-24.

LEAL A.M.M., KULIK D.A., KOSAKOWSKI G. (2016)
Computational methods for reactive transport modeling: A Gibbs energy minimization approach for multiphase equilibrium calculations. Adv. Water Res. 88, 231-240.

LISS P.S., SLATER P.G. (1974)
Flux of gases across the air–sea interface, Nature 5438, 181-184.

PALANDRI J.L., KHARAKA Y.K. (2004)
A compilation of rate parameters of water-mineral interaction kinetics for application to geochemical modeling (Open File Report 2004-1068). Menlo Park, California: U.S. Geological Survey. Retrieved from http://pubs.usgs.gov/of/2004/1068/pdf/OFR_2004_1068.pdf

POONOOSAMY J., KOSAKOWSKI G., VAN LOON L.R., MÄDER U. (2015)
Dissolution-precipitation processes in tank experiments for testing numerical models for reactive transport calculations: experiments and modeling. J. Contam. Hydrol. 177-178, 1-17.

PRASIANAKIS N.I., CURTI E., KOSAKOWSKI G., POONOOSAMY J., CHURAKOV S.V. (2017)
Deciphering pore-level precipitation mechanisms. Scientific Reports, 13675.

PRASIANAKIS N.I., GATSCHET M., ABBASI A., CHURAKOV S.V. (2018)
Upscaling strategies of porosity-permeability correlations in reacting environments from pore-scale simulations. Geofluids 9260603.

SAVOYE S., PAGE J., PUENTE C., IMBERT C., COELHO D. (2010)
New experimental approach for studying diffusion through an intact and unsaturated medium: A case study with Callovo-Oxfordian argillite. Environ. Sci. Technol. 44, 3698-3704.

SAVOYE S., IMBERT C., FAYETTE A., COELHO D. (2014)
Experimental study on diffusion of tritiated water and anions under variable water-saturation and clay mineral content: comparison with the Callovo-Oxfordian claystones. Geological Society, London, Special Publications, 400(1), 579-588.

SPOSITO G., HOLTZCLAW K.M., CHARLET L., JOUANY C., PAGE A. L. (1983)
Sodium-calcium and sodium-magnesium exchange on Wyoming bentonite in perchlorate and chloride background ionic media. Soil Sci. Soc. Am. J. 47(1), 51-56.

YANG G., NERETNIEKS I., HOLMBOE M. (2017)
Atomistic simulations of cation hydration in sodium and calcium montmorillonite nanopores. J. Chem. Phys. 147(8), 084705.

YANG G., PRASIANAKIS N.I., CHURAKOV S.V. (2018)
Comparison of atomistic simulations and fluid density functional theory of modeling water molecules in montmorillonite interlayer (submitted).

3 Development of mechanistic sorption models and experimental validation

B. Baeyens, R. Dähn, M. Marques Fernandes, J. Tits, S.V. Churakov, A. Schaible, E. Eltayeb, F. Marafatto (postdoc), A. Kéri (PhD student), S. Wick (PhD student), L. Nedyalkova (PhD student)

3.1 Introduction

The aim of this project is to improve the mechanistic understanding of the uptake processes of (radio)-contaminants on 2:1 clay minerals, important components of argillaceous rocks and soils, and on C-S-H/AFm phases, the main products formed during the cement hydration.

The focus in 2018 was put on the following research activities:

- Cation exchange measurements of Pb^{2+} on illite (Na^+-IdP) and montmorillonite (Na^+-SWy) were carried out to complement the surface complexation data and to finalise the Pb 2SPNE SC/CE sorption model.
- The competitive adsorption behaviour of Ni^{II}, Eu^{III} and U^{VI} were determined in a multi-element matrix (containing high concentrations of Co^{II} and Mn^{II}) as function of time on montmorillonite.
- The adsorption kinetics (3 days/2 years) and the influence of temperature (25 °C/90 °C) on the adsorption mechanism of Zn on montmorillonite were elucidated by X-ray absorption spectroscopy.
- The mechanistic model for Tl sorption on illite was developed in the framework of the SNSF funded PhD project on thallium speciation and solubility in soils.
- The immobilisation of Se and I by AFm phases was studied in the framework of a PhD project funded by the Horizon 2020 EC CEBAMA project.
- The mechanism of Fe incorporation in montmorillonite was investigated in the framework of a SNSF funded PhD project. The measured EXAFS and XANES spectra were interpreted based on ab initio atomistic simulations.
- The cryo-micro spectroscopic technique for redox- and radiation-sensitive samples was further developed at the microXAS beamline of the SLS (CROSS project).

3.2 Mechanistic sorption studies

3.2.1 Sorption of Pb on montmorillonite and illite

Pb adsorption edges and isotherms were measured on 2:1 clay mineral previously. In the current year, cation exchange and additional isotherms at pH ~ 3 and ~ 6 were measured. The entire sorption data set could be satisfactorily modelled with the 2SPNE SC/CE sorption model. The compilation of this work is currently published (MARQUES FERNANDES & BAEYENS 2019).

Pb^{2+}-Na^+ cation exchange (CE) experiments were carried out on Na-IdP and Na-SWy suspensions prior converted to 0.01 M NaCl background electrolyte by using the dialysis technique. Aliquots of the respective Na saturated clay mineral suspension were mixed with solutions containing stable Pb and Na in different proportions. The total normality of the clay-Na-Pb suspension was kept constant at 0.01 N and the Pb fractional occupancies (N_{Pb}) ranged from 0.1 to 0.9. The admixed Pb-Na solutions were labelled with ^{210}Pb to quantify the final Pb loadings. The samples were shaken end-over-end for 1 day.

The equilibrium data for the displacement of Pb^{2+} by Na^+ can be represented by the following reaction, 2 Na-clay + Pb^{2+} ⇔ Pb-clay + 2 Na^+, and is defined following the GAINES & THOMAS (1953) convention by the selectivity coefficient, ${}^{Pb}_{Na}K_c$ according to the following equation:

$$ {}^{Pb}_{Na}K_c = \frac{N_{Pb}}{N_{Na}^2} \cdot \frac{[Na]^2}{[Pb]} \cdot \frac{(\gamma_{Na})^2}{(\gamma_{Pb})} $$

where N_{Pb} and N_{Na} are the equivalent fractional occupancies, defined as the equivalent of Na (or Pb) adsorbed per kg of clay mineral divided by the cation exchange capacity (CEC) [eq·kg^{-1}]; [Na] and [Pb] are the aqueous molar concentrations and γ_{Na} and γ_{Pb} are aqueous phase activity coefficients.

The ln K_c values for the Na-Pb exchange Na-IdP and Na-SWy plotted as a function of the Pb occupancies (N_{Pb}) are plotted in Figs. 3.1a and 3.1b, respectively. The average ln K_c values obtained from the graphical integration of the ln K_c composition plots are ~ 2.7 and ~ 1.2 for illite and montmorillonite, respectively. The selectivity coefficient for the Pb^{2+}-Na^+ exchange on montmorillonite is in the range what is commonly found for simple exchange of divalent transition metals (MAES et al. 1975). On the other hand, the value of Pb on IdP is a factor of ~ 4 higher compared with SWy. The reason for the more pronounced exchange behaviour for Pb towards illite is not clear.

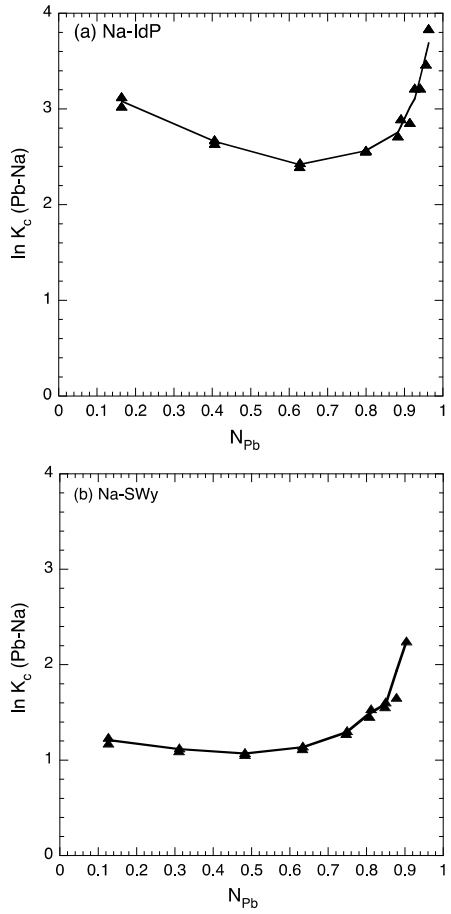

Fig. 3.1: Natural logarithm of the stoichiometric selectivity coefficient for the Pb^{2+}-Na^{+} exchange against the equivalent fraction of Pb^{2+} on (a) Na-IdP and (b) Na-SWy.

3.2.2 Reversibility and kinetics of competitive sorption of Ni, Eu and U on Na-SWy in a multi-cation matrix

Stable elements are ubiquitous in a deep geological repository for high-level waste (HLW). They are supplied by the porewater from multiple sources such as tunnel back fill materials and host rock formations, corrosion of the carbon steel canister, and finally dissolution of the spent fuel and vitrified HLW. These stable elements and the released radionuclides themselves, can all compete with one another for the sorption sites on the backfill material and the host rock, and thus reduce their uptake on them. Such competitive effects should be considered for the selection of sorption values for sorption databases used in the safety assessment of radioactive waste repositories (BRADBURY et al. 2017).

Competitive sorption experiments have been carried out in which a trace radionuclide ($^{63}Ni^{II}$, $^{152}Eu^{III}$ or $^{233}U^{VI}$) was allowed to react with Na-SWy at pH ~7 in 0.1 M NaCl background electrolyte for different periods of time in the absence (reference) and presence of competing elements. The competing element matrix contained divalent ($5 \cdot 10^{-4}$ M Ni, $5 \cdot 10^{-4}$ M Co and $5 \cdot 10^{-4}$ M Mn), trivalent ($5 \cdot 10^{-4}$ M Eu) and hexavalent ($5 \cdot 10^{-6}$ M U^{VI}) metals. The concentration of the target element ($^{63}Ni^{II}$, $^{152}Eu^{III}$ or $^{233}U^{VI}$) was reduced to trace concentration ($< 10^{-8}$ M) in each particular experimental set-up.

The sorption measurements are expressed as log R_d as function of reaction time and are shown (as symbols) in Figs. 3.2a, 3.2b and 3.2c for Ni, Eu and U, respectively. The results clearly show that over the time scales investigated (3 to 213 days) no major kinetic effects could be observed. In the case of Ni and Eu, the sorption at trace concentration in the absence of competing elements (red symbols) decreases if the competing metals were present (blue symbols) whereas for U this was not the case. From these results one can qualitatively conclude that the divalent and trivalent elements are competitive whereas uranyl appears to be non-competitive with di- and trivalent metals.

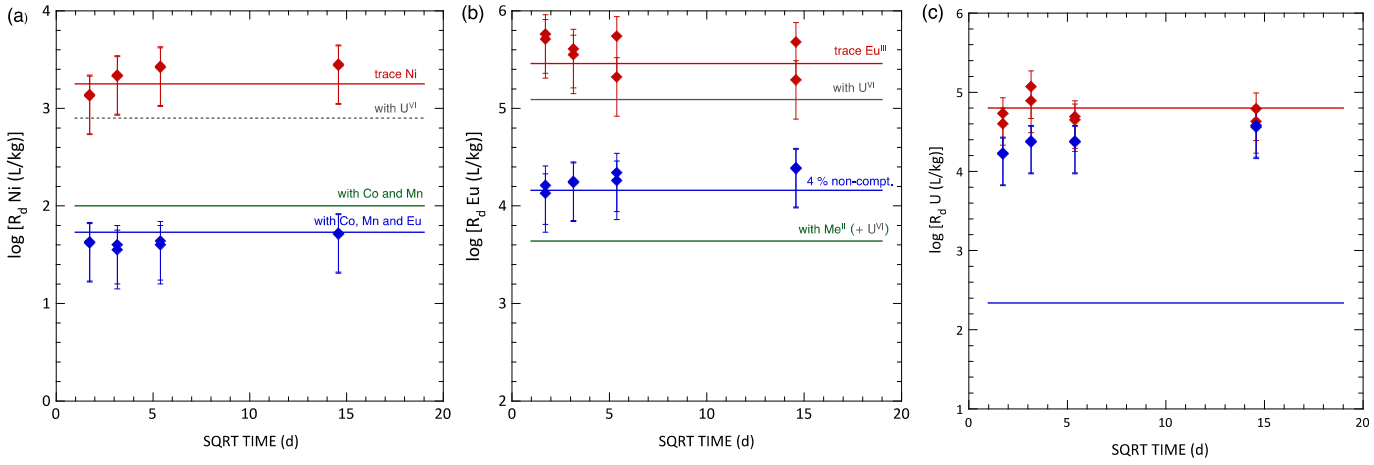

Fig. 3.2: Competitive sorption of (a) $^{63}Ni^{II}$ (b) $^{152}Eu^{III}$ and (c) $^{233}U^{VI}$ on Na-SWy at pH 7 in 0.1 M NaCl in the absence (red symbols) and presence (blue symbols) of di-, tri- and hexavalent metals. Green and gray lines are explained in the text.

By applying the 2SPNE SC/CE sorption model and the associated parameters for montmorillonite (BAEYENS & BRADBURY 2017), the data in Fig. 3.2 can be quantitatively described. Initially, the data in the absence of competing elements (reference measurements) were modelled and are represented by the red lines in Fig. 3.2 and are in good agreement with the experimental data. It should be noted that in the case of uranyl the sorption values measured in these experiments are ~0.4 log units lower than given for instance in BAEYENS & BRADBURY (2017). However, such discrepancies are in line with batch sorption measurements with high R_d values and carried out on different clay batches. For this exercise, the uranyl surface complexation constants were fitted to the experimental data in Fig. 3.2c.

In Fig. 3.2a the modelling of the competitive sorption of Ni is illustrated. In a first step, the presence of U^{VI} was modelled simultaneously with trace Ni sorption and the log R_d value for Ni is reduced by ~0.3 log units (grey line). The reason for the small decrease is that the total U^{VI} concentration is rather low because of solubility limits. In a second step, the sorption of Ni was calculated in the presence of the two other divalent metals and this calculation resulted in a clear decrease of Ni sorption (green line). The predicted decrease in Ni sorption is almost corresponding to the experimental data indicating competitive sorption behaviour between these divalent elements. Finally, in addition to Co and Mn, the Eu concentration was added in the model calculation and the predicted line (blue line) corresponds to the experimental data. The conclusion from this experiment is that trace Ni is competitive with di- and trivalent elements.

The same modelling approach was applied to the Eu sorption experiment. As in the case of Ni the presence of U^{VI} has almost no influence on the Eu sorption values for the same reason as given above. The addition of the three different divalent metals with a total concentration of $1.5 \cdot 10^{-3}$ M, however, caused a decrease of the Eu log R_d by ~ 1.8 log units indicating that di- and trivalent elements are competitive. However, the experimental Eu log R_d values were ~ 0.6 log units higher than the predicted by the model assuming full competition (green line in Fig. 3.2b). The experimental data could be fitted by the 2SPNE SC/CE model if one assumes that 4 % of the strong sites are non-competitive. This is illustrated by the blue line in Fig. 3.2b.

Finally, in the case of U^{VI} no competitive behaviour with the di- and trivalent elements was observed. If competitive sorption were present, the U^{VI} sorption should decrease by 2.4 log units (blue line) which clearly was not the case as shown in Fig. 3.2c.

3.2.3 Adsorption of Zn on montmorillonite: effect of temperature and reaction time

The influence of temperature on the sorption behaviour of radionuclides on clay minerals is still an open question. Extended X-ray absorption fine structure (EXAFS) spectroscopy investigations of Zn loaded clay samples (Na-STx-1) obtained from adsorption experiments performed at 25 and 90 °C at neutral pH were carried out. Additionally, to reduce the gap in the current knowledge between short-time sorption and long-time incorporation processes, these experiments were monitored for the period of two years. At Zn loadings corresponding to the full occupation of strong (2 mmol/kg) and weak (6 mmol/kg) site in the 2SPNE SC/CE sorption model, the investigations provided spectroscopic evidence that the reaction time and temperature have a distinct influence on the uptake behaviour. A sample loaded with 2 mmol/kg Zn reacted at 90 °C for 3 days resembles the spectra of a sample reacted for two years at room temperature. Further, for the samples with loadings of 6 mmol/kg and 3 days reaction time, the effect of temperature is even stronger. Based on the splitting of the EXAFS oscillation at 8 $Å^{-1}$ (Fig. 3.3), it can be concluded that the formation of newly formed Zn phases occurred. Based on this observation the uptake process of Zn on montmorillonite should not anymore be described as adsorption, as assumed in the 2SPNE SC/CE sorption model. The EXAFS study provided clear spectroscopic evidence that precipitation processes prevail even at Zn concentrations characteristic for weak sites (2 - 20 mmol/kg) and elevated temperatures.

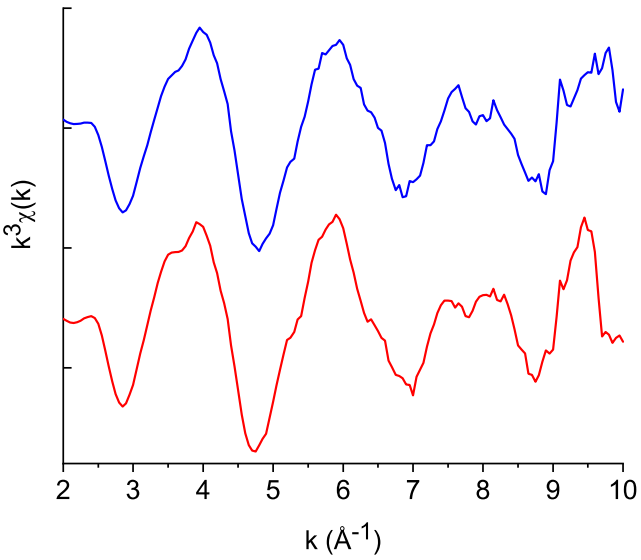

Fig. 3.3: EXAFS spectra of Zn loaded STx (6 mmol/kg) samples reacted for 3 days at room temperature (blue line) and at 90 °C (red line).

3.2.4 Thallium uptake in soils

Thallium (Tl) commonly occurs in the environment as monovalent Tl^+. It is assumed that the clay mineral illite is a key sorbent for Tl^+ in soils and sediments. This hypothesis is based on the similarity between the cations Tl^+ and Cs^+ (similar ionic radius and hydration energy, same charge), whereas the latter is known to show highly specific affinity sorption at the frayed edges of illite (BROUWER et al. 1983) and fixation in the illite interlayer (FULLER et al. 2015). The selectivity coefficients for Tl-Na, Tl-K, Tl-NH_4 and Tl-Ca exchange equilibria were derived within the framework of the 3-site cation exchange model (frayed edge sites, type II sites and planar sites) for Cs^+ (BRADBURY & BAEYENS 2000), which confirmed the high affinity of Tl^+ for illite (WICK et al. 2018). To further assess the role of Tl^+ adsorption and fixation by illite in soils, the solubility and exchangeability of geogenic Tl in topsoils from the Erzmatt site (Swiss Jura Mountains) was investigated.

The aqueous extractions of 36 topsoil samples, with geogenic Tl contents from 3 to 1000 mg/kg, with 1 M NH_4-acetate (exchangeable Tl) showed that overall 3.5 ± 1.8% of the total geogenic Tl was NH_4-exchangeable. Fig. 3.4 shows the relation between the total geogenic Tl content and the extractable Tl and reveals a nearly linear relationship indicating that the more Tl is present in the soils the more Tl is exchangeable. Tl L_{III}-edge X-ray absorption spectra of 12 soils suggested that most of the geogenic Tl was associated with illite. In combination, these findings indicate that a major fraction of geogenic Tl was fixed in the interlayers of illite over time, and that short-term Tl solubility was controlled by the minor fraction of the geogenic Tl.

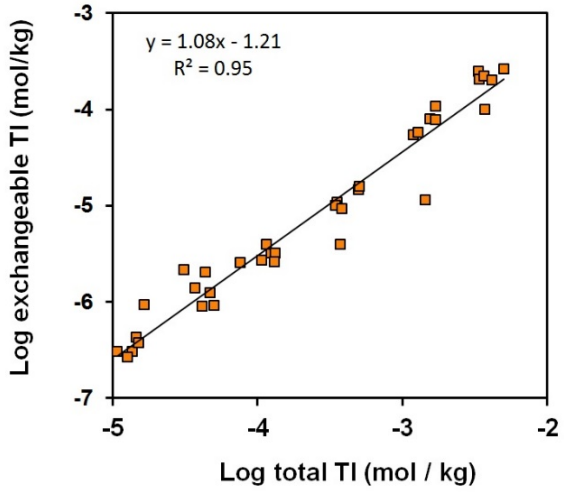

Fig. 3.4: Correlation between the total geogenic Tl and the 1 M NH_4-exchangeable Tl in 36 topsoils from the Erzmatt site (Swiss Jura Mountains).

In further work it is planned to examine how the NH_4-exchangeable pool affects Tl solubility in soils and to test the 3-site cation exchange model for Tl^+ adsorption onto illite (WICK et al. 2018) in these Tl contaminated topsoil systems.

3.2.5 Immobilisation of Se and I in cementitious systems

The potential of AFm phases to immobilize selenium and iodine is the focus of a PhD study performed in the framework of the Horizon 2020 EC project "CEBAMA". In the first two years of the PhD project, pure AFm phases containing one of the various sulfur and selenium anions (SO_4^{2-}, SO_3^{2-}, $S_2O_3^{2-}$, HS^-, SeO_4^{2-}, SeO_3^{2-}, HSe^-) as well as I^- as the intercalating anion were synthesized and characterized by XRD, TG, FTIR, and aqueous phase analysis. In addition, the formation of binary solid solutions between these end-members and also between them and the common AFm phases hemi-, monocarbonate and hydroxyl-AFm was examined.

In 2018, the characterization of SeO_4-, S_2O_3-, and I-AFm phases was completed with a study of the water sorption by Dynamic Vapour Sorption (DVS) analysis. These DVS data will be used for more accurate determination of the solubility products of these phases using GEMS. The change in the water amount of the samples as a function of the relative humidity (RH) was recorded for RH between 5 % and 95 % at room temperature (Fig. 3.5). The minimal total water content achieved for the SeO_4-AFm is 12 H_2O at 5 % RH. At 10 % RH the water content increases to 13 H_2O and remains stable. The S_2O_3-AFm shows a single absorption/desorption step at low RH with slight hysteresis.

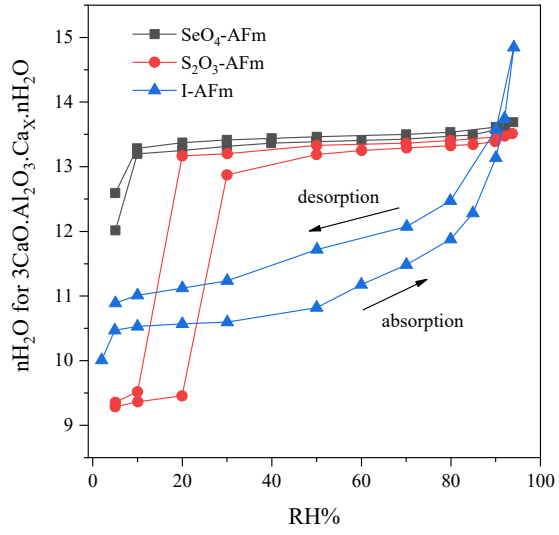

Fig. 3.5: Sorption isotherms for the SeO_4-, S_2O_3- and I-AFm phases.

The water content of the phase changes from 9 H_2O at 20 % RH to 13 H_2O at 30 % RH; the desorption step occurs at 20% RH. In the I-AFm phase, different water evolution behaviour can be observed. The sample undergoes steady water absorption starting with 10 H_2O at 5 % RH and reaching the maximum water content with 15 H_2O at 95 % RH. The SeO_3- and the SO_3-AFm are still to be measured.

The sorption of Se and I on various AFm phases was investigated in a series of batch sorption experiments at pH ~ 13. The goal of these sorption studies is to test whether the various AFm solid solution models developed in the previous years are able to describe the observed sorption behaviour. The partitioning of the radionuclides ^{75}Se and ^{125}I, respectively, between the solid and the liquid phase was measured and expressed in terms of the distribution coefficient R_d [$L \cdot kg^{-1}$]. R_d values for the sorption of Se(IV) on SO_4-AFm were determined using starting Se(IV) concentrations ($[Se]_{tot}$) between 0.1 M and 10^{-13} M. The measured R_d values range between ~ 31 $L \cdot kg^{-1}$ at high $[Se]_{tot}$ and ~ 821 $L \cdot kg^{-1}$ obtained at the lowest $[Se]_{tot}$ (Fig. 3.6a). Thermodynamic calculations using the NES thermodynamic database (OLIN et al. 2004) show that the solubility limit for $CaSeO_4 \cdot 2H_2O$ is never exceeded. The same starting concentrations ($[I_{tot}]$: 0.1 M - 10^{-13} M) were used for I sorption tests onto SO_4-AFm, HS-AFm and OH_CO_3-AFm. The measured R_d values for I are significantly lower than those observed for Se(IV) for all examined AFm phases. OH_CO_3-AFm shows the highest affinity for I with R_d values up to ~ 56 $L \cdot kg^{-1}$. The R_d values obtained for the HS-AFm show only a weak dependency on the $[I_{tot}]$ and vary between ~ 15 and ~ 41 $L \cdot kg^{-1}$. The weakest sorption is observed for the SO_4-AFm with a maximum R_d value of ~ 31 $L \cdot kg^{-1}$ (Fig. 3.6b). The experimental data suggests that the sorption of I is dependent on the type of the interlayer anion with a stronger sorption displayed by AFm phases with a singly charged anion in the interlayer.

The obtained data from the sorption experiments will be combined with the experimental data from the solid solution studies for the construction of thermodynamic models describing the Se and I uptake by AFm phases using GEMS. The combination of both data sets would account for sorption on the two types of sorption sites available in the AFm structure: the surface ion exchange sites and the interlayer ion exchange sites.

3.2.6 Mechanism of Fe incorporation in montmorillonite

In the SNF funded PhD project "*Detailed understanding of metal adsorption on clay minerals obtained by combining atomistic simulations and X-ray absorption spectroscopy*", the characteristics of structural iron in natural bulk montmorillonites were determined. The interpretation based on EXAFS and X-ray absorption near edge structure (XANES) spectroscopy modelled by atomistic calculations. Molecular dynamics (MD) simulations based on density functional theory (DFT+U) were performed on six atomistic models of iron incorporated montmorillonites. The atomic coordinates obtained from the trajectories served as a basis to calculate the EXAFS and XANES spectra. The comparison of the experimental data for Milos-montmorillonite and the simulation results suggest that structural iron is preferentially incorporated as Fe^{3+} into the octahedral sheet of bulk montmorillonite and it is equally distributed between the *cis*- and *trans*-octahedral sites (Fig. 3.7) (KÉRI et al. 2017).

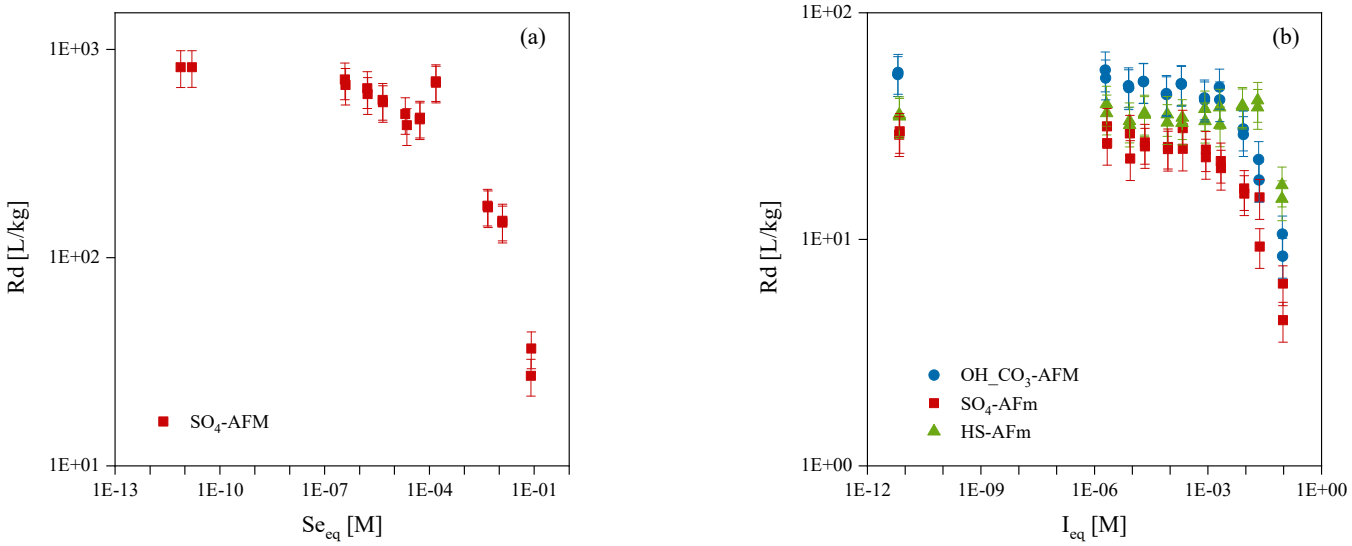

Fig. 3.6: R_d values for the sorption of Se(IV) onto SO_4-AFm (a) and I onto SO_4-, OH_CO_3- and HS-AFm (b).

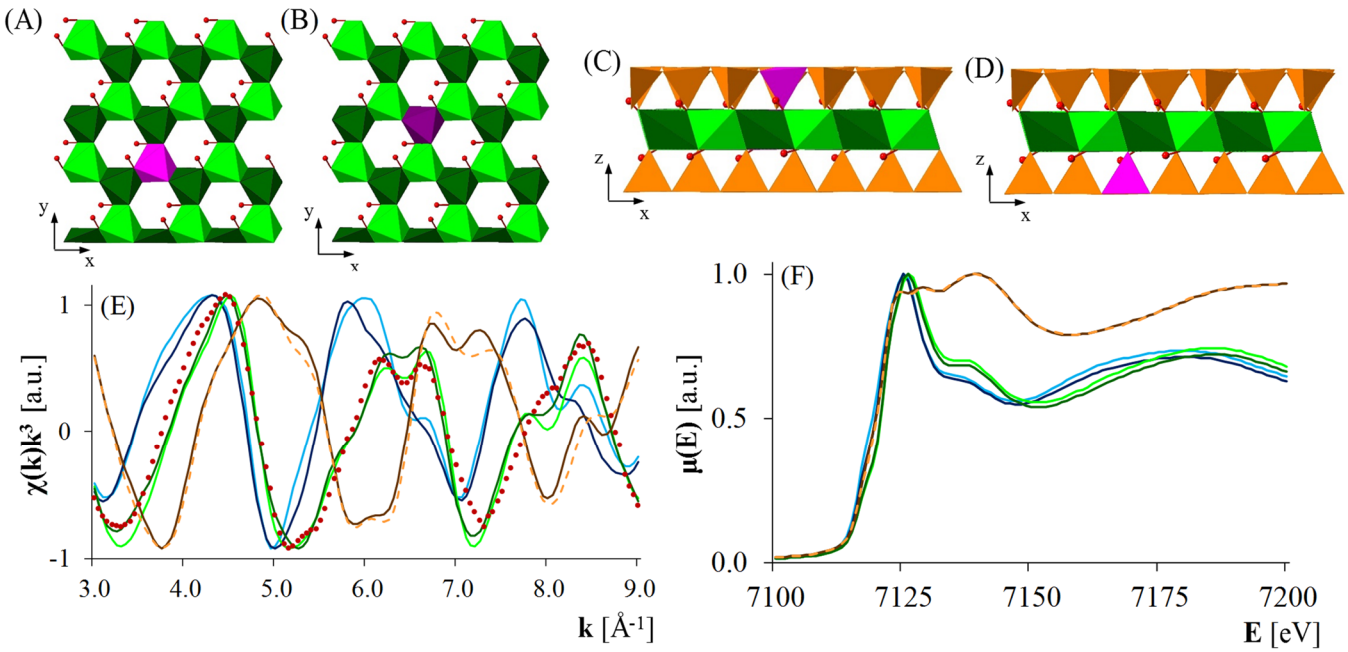

Fig. 3.7: Atomistic models of structural iron incorporation in the octahedral and in the tetrahedral sheet of montmorillonite (A, B and C, D), respectively. Orange color represents Si tetrahedra, Al octahedra are shown with green color, while Fe incorporation is marked with pink and purple colors. Darker colors of the octahedral sheet show trans- while lighter colors represent cis-sites with respect to the relative positions of the hydroxyl (OH^-) groups marked with red spheres. Panel A and B indicate only the octahedral sheet for the sake of clarity. The calculated EXAFS and XANES spectra of Fe substitution in the bulk montmorillonite for ferrous and ferric ions are shown with blue and green lines, while brown color represent tetrahedral Fe^{3+} in panel E and F, respectively. Octahedral cis-site is marked with lighter, while trans-occupational site with darker colors. Lighter brown color correspond to tetrahedral occupation shown in panel C, while darker color represent tetrahedral Fe^{3+} incorporation as it is in panel D. The measured spectra of Milos-montmorillonite are denoted with red dots.

3.2.7 Development of cryo-microspectroscopic techniques for redox- and radiation-sensitive samples

Synchrotrons are extremely powerful tools to characterize materials both structurally and chemically down to the atomic scale. Micro-resolved beamlines allow such information to be obtained with down to micrometer resolution on spatially heterogeneous samples, at the expense of an increased photon flux density. For certain samples the increased photon flux density can lead to radiation-induced artefacts which may hinder the measurements. Fortunately, these artefacts can be minimized by changing the measurement strategy and lowering the temperature of the sample through cryostat solutions. The main goal of this project was to purchase and implement a cryostat solution at the microXAS beamline of the SLS (X05LA) that would allow micro-resolved measurements of samples to temperatures down to 4K to reduce the effect of beam damage (Fig. 3.8), with a particular focus to environmentally relevant samples. The cryostat is now in commissioning phase. As a scientific goal, we investigated the speciation of Tl in Tl-rich soils from the Swiss Jura Mountains. Our results show that the speciation of Tl^{III} is linked to that of Mn, partly confirming laboratory studies (Fig. 3.9). Finally, this project has led to first-time collaborations between the Swiss Light Source and research groups at EAWAG, as well as strengthening existing collaborations with research groups at PSI-LES. New collaborations may arise in disciplines that do not traditionally use synchrotron techniques, which sets the base for a considerable leap in scientific knowledge that is unmatched by other techniques.

Fig. 3.8: A photograph of the cryostat system assembled and awaiting mounting for commissioning phase at the microXAS beamline.

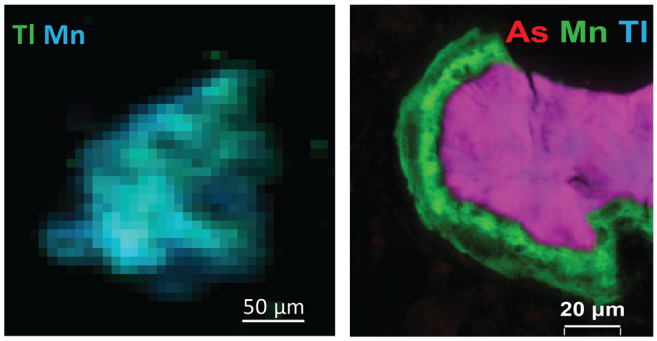

Fig. 3.9: X-ray fluorescence maps; Mn concretion with adsorbed Tl (left); Tl-rich hotspot with As surrounded by Mn rim (right). The Tl concentration is low on the rim but Tl is present.

3.3 References

BAEYENS B., BRADBURY M.H. (2017)
The development of a thermodynamic sorption data base for montmorillonite and the application to bentonite: PSI Bericht 17-05 and Nagra Tech. Rep. NTB 17-13.

BRADBURY M.H., BAEYENS B. (2000)
A generalised sorption model for the concentration dependent uptake of caesium by argillaceous rocks, J. Contam. Hydrol. 42, 141-163.

BRADBURY M.H., MARQUES FERNANDES M., BAEYENS B. (2017)
Estimates of the influence of radionuclide solubility limits and sorption competition on the sorption values in the SDBs of MX-80 bentonite and Opalinus Clay: PSI Bericht 17-04 and Nagra Tech. Rep. NTB 17-11.

BROUWER E., BAEYENS B., MAES A., CREMERS A. (1983)
Cesium and rubidium ion equilibria in illite clay. J. Phys. Chem. 87, 1213-1219.

FULLER A.J., SHAW S., WARD M.B., HAIGH S.J., MOSSELMANS J.F.W., PEACOCK C.L., STACKHOUSE S., DENT A.J., TRIVEDI D., BURKE I.T. (2015)
Caesium incorporation and retention in illite interlayers. Appl. Clay Sci. 108, 128-134.

GAINES G.L.J., THOMAS H.C. (1953)
Adsorption studies on clay minerals. II. A formulation of the thermodynamics of exchange adsorption. J. Chem. Phys. 21, 714-719.

KÉRI A., DÄHN R., KRACK M., CHURAKOV S.V. (2017)
Combined XAFS spectroscopy and ab initio study on the characterization of iron incorporation by montmorillonite. Environ. Sci. Technol. 51, 10585-10594.

MAES A., PEIGNEUR P., CREMERS A. (1975)
Thermodynamics of transition metal ion exchange in montmorillonite. Proc. Int. Clay Conf., Mexico City, Mexico, 16-23 July, p.319-333.

MARQUES FERNANDES M., BAEYENS B. (2019)
Cation exchange and surface complexation of lead on montmorillonite and illite including competitive adsorption effects. Appl. Geochem. 100, 190-202.

OLIN A., NOLÄNG B., OSADCHII E.G., OEHMAN L.-O., ROSÉN E. (2004)
In: Mompean F.J., Perrone J., Illemassène M. (eds). Chemical Thermodynamics of Selenium. Chemical thermodynamics 7. OECD Nuclear Energy Agency, Elsevier, Amsterdam.

WICK S., BAEYENS B., MARQUES FERNANDES M., VOEGELIN A. (2018)
Thallium adsorption onto illite. Environ. Sci. Technol. 52, 571-580.

4 RADIONUCLIDES TRANSPORT AND RETENTION IN COMPACTED SYSTEMS AT FULL AND PARTIAL SATURATION

L.R. Van Loon, M.A. Glaus, W. Pfingsten, B. Baeyens, M. Marques Fernandes, S. Frick, P. Bunic, T. Gimmi, S.V. Churakov, P. Krejci (PhD student), E. Curti, A. Jakob, A. Ahoub (master student)

4.1 Introduction

The sorption of radionuclides on clay minerals in engineered and geological barrier systems is a key safety function in the deep geological disposal of radioactive waste. Reliable sorption data (R_d values) and a mechanistic understanding of sorption processes are thus mandatory for a proper evaluation of this safety function. Sorption studies are mainly performed in batch systems using dispersed clay with a low solid-to-liquid ratio. In such systems the composition of the solution can be well controlled (e.g. pH, E_h, concentrations of anions and cations, organic and inorganic ligands) and/or varied in order to study their effect on the sorption. Real clay systems, however, are very dense and characterised by a high solid-to-liquid ratio. It is still an unanswered question whether data and models evaluated from dilute dispersed systems can be transferred to the real, compact system. The aim of this project is to give an answer to this open question of transferability.

A second focus of the project deals with the question whether sorbed ions are immobile or partially mobile. This has important consequences for the transport behaviour of ions in compacted systems. In the case of full immobilisation, a pore diffusion model can describe transport whereas in the case of partial immobilisation, surface diffusion models have to be applied.

Experimental techniques allowing for an unambiguous determination of sorption and diffusion characteristics, viz. sorption distribution values (R_d) and effective diffusion coefficients (D_e) are an important prerequisite for a successful realisation of these two project aspects.

4.2 Sorption/diffusion in compacted montmorillonite

The investigation of potential differences in the sorption behaviour of compacted and dispersed clay systems was extended to experiments involving compacted montmorillonite from Milos. In the in-diffusion technique applied, a compacted clay sample is contacted with a tracer-containing background electrolyte solution. The clay phase is separated from the solution phase via a thin (~ 0.14 mm) porous polymeric membrane. Such membranes were successfully applied for diffusion measurements using illite compacted to bulk dry densities of ~ 1700 kg m^{-3} (GLAUS et al. 2015). However, such membranes do not withstand the swelling pressures of a compacted montmorillonite sample. For the latter purpose, a thin punched titanium disk supported the membrane. The disk is punched by small holes leading to ~ 34% porosity. Owing to the stagnant water in these holes, an additional diffusive resistance has to be accepted by the use of the titanium support leading to increased uncertainties in the fit parameters (effective diffusion coefficients, sorption distribution ratios) for this particular type of diffusion setup. For most of the cases, these uncertainties were in an acceptable range. Fig. 4.1 shows a summary of the sorption distribution factors (R_d) for Co^{2+} in compacted homoionic Na-montmorillonite as a function of pH and ionic strength. The results of measurements in dispersed suspensions of montmorillonite from Wyoming (SWy-2) (BAEYENS & BRADBURY 2017) as a function of pH are also shown. No systematic discrepancy between the results obtained from disperse and compacted clay media can be deduced from the comparison shown in Fig. 4.1. It has to be noted that the uncertainties specified for the compacted samples (in-diffusion) probably overestimate the true uncertainties. The effective diffusion coefficients measured in the in-diffusion experiments depended strongly on the salinity of the background electrolyte (data not shown), while they remained rather unaffected by pH. This behaviour is characteristic for planar surface species exhibiting similar mobilities as the respective aqueous phase species, while the surface species bound to the amphoteric surface sites (inner-sphere complexes) can be regarded as immobile.

4.3 Diffusion in charged membranes

The coupled multicomponent diffusion of charged solutes in charged porous media was further investigated using charged organic polymeric filter membranes as model systems. A trainee student from Grenoble INP Phelma carried out this work to a larger extent. In the presence of surfaces with permanent electrical charges, the diffusive ion transport is governed by different driving forces, viz. the concentration gradients of the species in the different pore domains and the maintenance of charge neutrality (e.g. Nernst-Planck equation). The interaction between these driving forces and the magnitude of the resulting fluxes in compacted clay systems is not

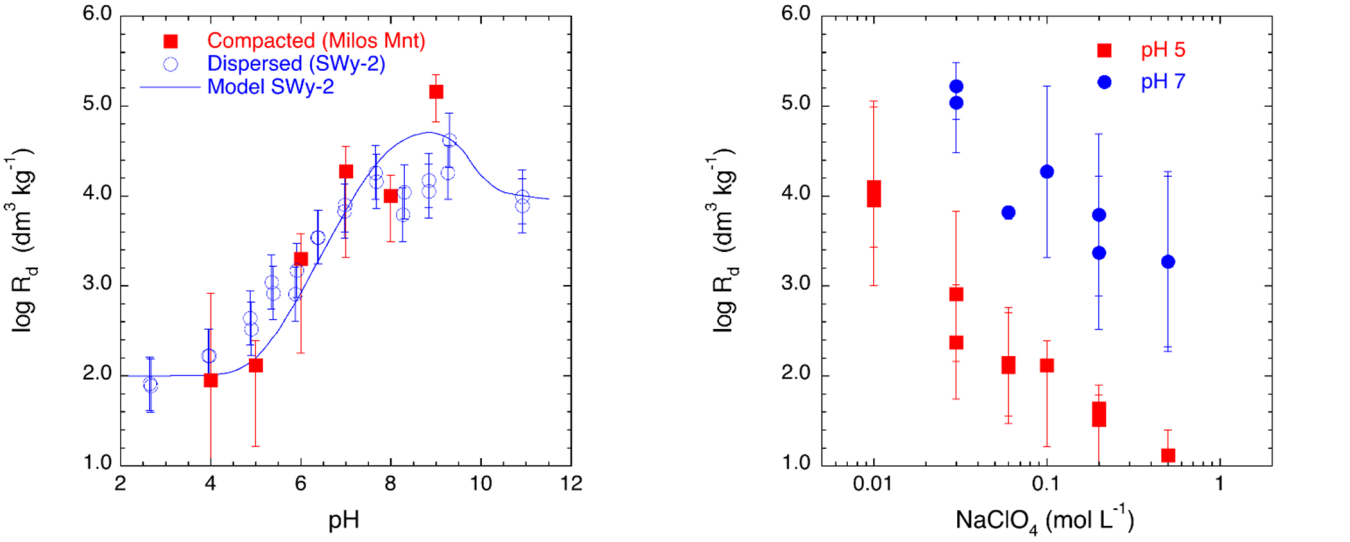

Fig. 4.1: Sorption distribution coefficients (R_d) for Co^{2+} measured in compacted homoionic Na-montmorillonite (Milos, filled symbols) as a function of pH (left-hand plot) and ionic strength (right-hand plot). The bulk density of the compacted Na-montmorillonite was of the order of 1600 kg m^{-3}. The left-hand plot shows a comparison with literature data measured for SWy-2 montmorillonite(empty symbols) in disperse suspension (BAEYENS & BRADBURY 2017).

a priori clear from theory. In the present experiments, the diffusion of $MgCl_2$ across a Nafion type membrane (cation exchanger) at concentration gradient conditions was investigated in an equilibrated KNO_3 electrolyte. Fig. 4.2 shows the evolution with time of the concentrations in the source reservoir to which the $MgCl_2$ was added.

The decrease of Mg^{2+} was accompanied by an almost stoichiometric increase of K^+ concentration, with anion concentrations being almost unchanged (data not shown). This reflects the strong perm selective behaviour of the membrane, meaning that charge is almost exclusively transported by cations or anions, respectively. The time scales involved in the equilibration of cations were compared to the behaviour of the uncharged tritiated water molecule (HTO). As can be seen from Fig. 4.2, the latter time scales are much slower despite the much larger self-diffusion coefficient of the HTO molecule compared to the cations. This observation underlines the mobility of the counter-cations and the enhancement of their diffusive fluxes induced by the concentration enrichment in the membrane pore space. Such behaviour is fully analogue to observations made for cation diffusion in clay minerals, such as smectites (GLAUS et al. 2007) and illite (GLAUS et al. 2015). However, modelling attempts for simulating the data shown in Fig. 4.2 revealed that the complexity of transport processes in charged membranes is similar to the complexity in clay media. It may thus be questionable whether such membranes can be regarded as simple model systems for transport in such porous media.

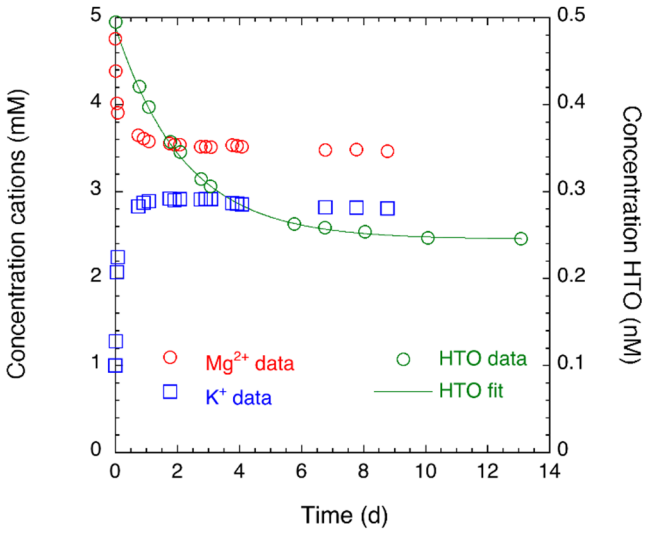

Fig. 4.2: Diffusion of electrolyte cations in an experiment in which two different solutions are separated by a Nafion membrane (cation exchanger). In an initial phase of the experiment both solutions contain 1 mm KNO_3. Subsequently, the upstream reservoir is spiked by 4.5 mm $MgCl_2$ and 0.5 nM HTO (initial concentrations after dilution). The plot shows the concentration evolution with time in the upstream reservoir.

4.4 Sorption/diffusion in Opalinus Clay

Diffusion of Co^{2+}, Mn^{2+} and Tl^+ in Opalinus Clay was investigated for both high (10^{-5} M) and low (10^{-8} M) total concentrations of the metals in solution. The behaviour of Tl^+ was studied because it has similar sorption characteristics for illite as Cs^+, which was demonstrated in a recent PhD study (WICK et al. 2018).

This means that sorption is governed by three sorption sites and that K^+ and NH_4^+ strongly compete with Tl^+. Fig. 4.3 shows the diffusion profile of $^{204}Tl^+$ measured at the lower total concentration. The data are compared with (i) a blind prediction based on a surface diffusion model for illite involving multicomponent transport in an electrical double layer (EDL) and (ii) a single-species transport model involving linear sorption after deriving the best-fit parameter values for D_e and R_d by inverse modelling.

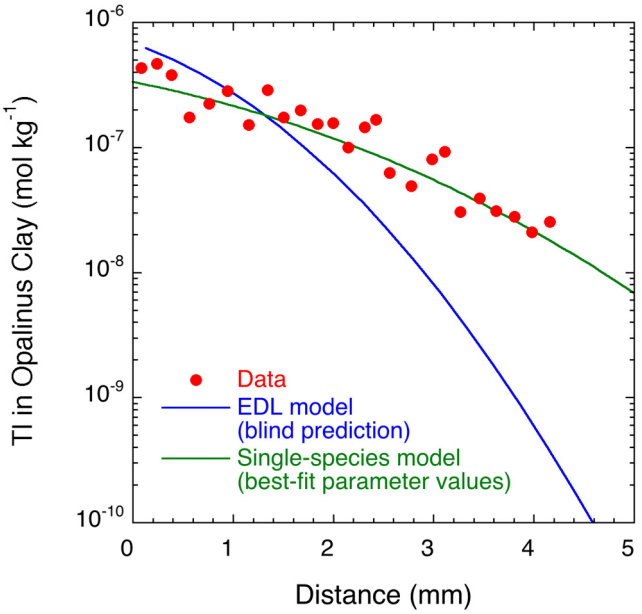

Fig. 4.3: Diffusion profiles of Tl^+ in Opalinus Clay after 14 days of in-diffusion. The total Tl concentration was 13 nM.

The EDL diffusion model is based on the approach described in GLAUS et al. (2015) and involves immobile Stern layer- and mobile diffuse layer cationic species (surface diffusion) at the planar surfaces instead of the pure cation exchange mechanism in the model of WICK et al. (2018). The site capacities were assumed to be 20% of those of the illite cation exchange capacity with selectivities left unchanged. The geometry factor for the diffusion of aqueous phase and diffuse layer cations was assumed to be identical with the geometry factor for the diffusion parallel to the bedding of tritiated water. Within the parameter ranges tested in the experiment, the calculated D_e and R_d for the EDL diffusion model can be considered to be merely constant. A comparison of the model parameters is shown in Table 4.1. In view of the unknown uncertainties for the prediction of the transport behaviour in Opalinus Clay based on an illite multicomponent transport model, the consistency between the two model parameter sets can be regarded as rather good. It has to be noted that the equilibrium distribution of $^{204}Tl^+$ between the EDL and the aqueous phase significantly determines the overall transport behaviour. Consequently, competitive effects of other cations in the porewater or complexing anions (e.g. chloride) have a direct effect on both sorption and diffusion. While a broad set of experimental data has shown that sorption data for Opalinus Clay can be reliably derived from an illite model, only sparse evidence supports so far, the validity of a similar approach for diffusion. So far, only planar surface species were assumed to be mobile. Introducing partial mobility for the other surface species (cf. section 4.5) would certainly improve the agreement between the blind prediction and the experimental data. However, no pertinent diffusion data are presently available for diffusion of $^{204}Tl^+$ in illite.

Table 4.1: Comparison of parameter values for the blind prediction (EDL multicomponent transport model) and the inverse modelling (single-species transport model) for the in-diffusion of $^{204}Tl^+$ in Opalinus Clay using an initial total Tl concentration of 13 nM.

	Blind prediction	**Inverse modelling**
D_e (m^2 s^{-1})	7.40×10^{-11}	$(1.0 \pm 0.14) \times 10^{-10}$
R_d (dm^3 kg^{-1})	53	26 ± 6

4.5 The predictive capability of a surface diffusion model for Cs in Opalinus Clay

We recently developed a surface diffusion model that is able to describe the concentration-dependent diffusion of Cs in Opalinus Clay consistently. Site-specific surface mobilities, the pertinent model parameters, were estimated by fitting model outcomes to the results of in-diffusion experiments for Cs in Opalinus Clay (Table 4.2). As a next step, the surface diffusion model with the estimated surface mobilities was now tested against other experimental data. For the test of the model we chose a radial diffusion experiment for Cs in Opalinus Clay (Fig. 4.4). The initial Cs concentration in the reservoir was 10^{-3} M and decreased during the experiment. A detailed description of the experimental setup can be found in VAN LOON et al. (2004). For the modelling we used the generalized three-site Cs sorption model of BRADBURY & BAEYENS (2000) with values for the sorption parameters from VAN LOON et al. (2009), and the previously estimated surface mobilities. Selectivity coefficients were slightly adapted within the range of their uncertainty. Fig. 4.5 shows the results of the test. The model (red line) matches the data (blue dots) well. No fitting of the Cs bulk

diffusion coefficient was necessary. The successful test shows that the surface diffusion model is able to predict diffusion behaviour of Cs in a consistent way.

Table 4.2: Surface mobilities estimated from Cs in-diffusion experiments for planar, type II and frayed-edge sites according to the generalized three-site sorption model of BRADBURY & BAEYENS (2000).

	Planar	Type II	FES
μ_s	$4.7 \cdot 10^{-2}$	0	$2 \cdot 10^{-3}$

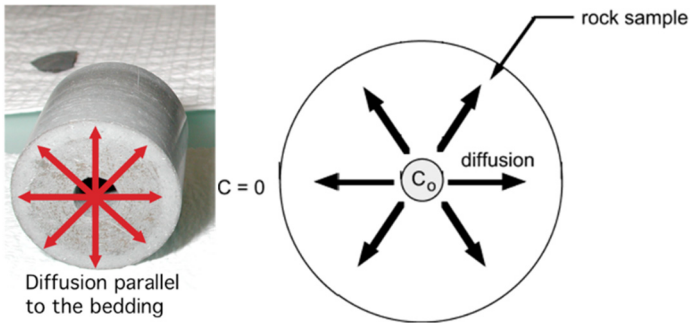

Fig. 4.4: Experimental set-up of the radial diffusion experiment from VAN LOON et al. (2004).

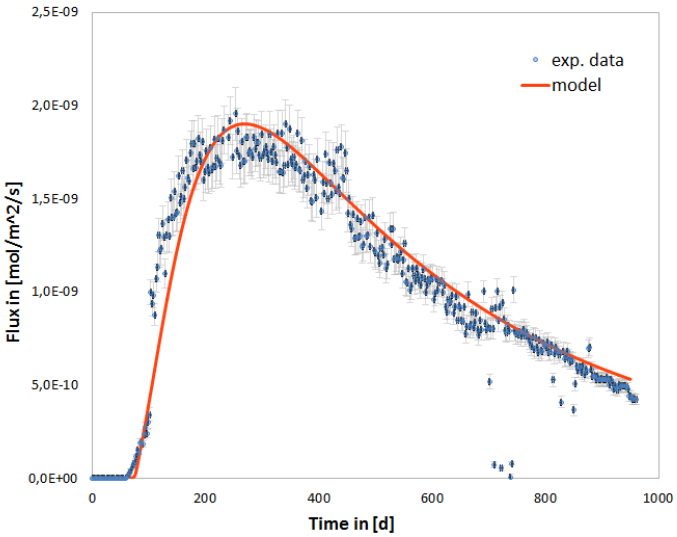

Fig. 4.5: Result of the radial diffusion experiment: Cs flux on the outer boundary of the Opalinus Clay sample. Red line: surface diffusion model; blue dots with error bars: experimental data.

An SeS benchmark example has been proposed for the modelling of Cs diffusion through clay for single species and multi-species reactive transport setup. So far, MCOTAC, FLOWTRAN, CORE2D, and PHREEQC-COMSOL contributed to the multispecies benchmark. General agreement could be achieved for calculated Cs breakthrough curves for the first 3 codes, whereas differences to all other codes' results were observed for the PHREEQC-COMSOL contribution, which has to be investigated in more detail (Fig. 4.6).

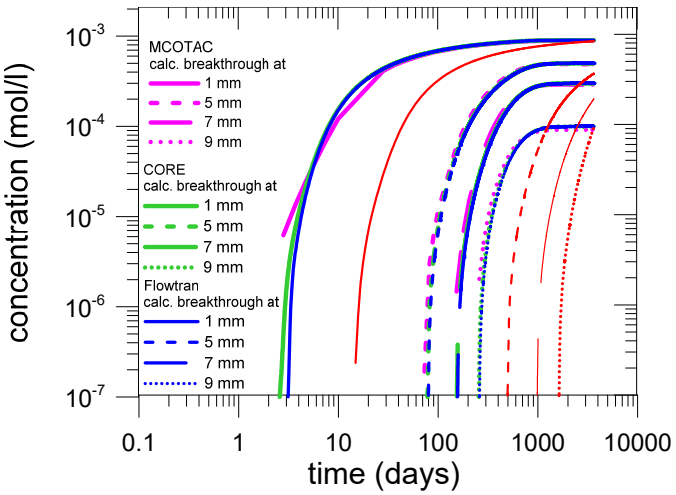

Fig. 4.6: Benchmark exercise for modelling the Cs migration through clay. Cs breakthrough at different locations (red curves are results produced so far by PHREEQC-COMSOL).

Cs diffusion in illite de Puy using the sorption model of BAEYENS & BRADBURY (2000) within MCOTAC has been modelled, allowing Cs surface/exchange-species to be (partly) mobile, and therefore contributing to the diffusive flux of Cs through illite. A systematic investigation has been started allowing different sorption model surface-species to be mobile for Cs but also the competing major cations in solution (Na^+, K^+, Ca^{2+}, Mg^{2+}) on the same surface/exchange sites. So far, some Cs surface-species could be excluded from being mobile, because calculated Cs breakthroughs and Cs concentration distribution did not fit (at all) to experimental results. However, the choice for mobile surface-/exchange-species or their individual contributing amount and the related transport parameters allows for multiple fits of the data.

In order to quantify uncertainties in the prediction of radionuclide sorption processes in clay, a methodology/tool has been developed for studying the uncertainties in detailed sorption chemistry parameters with a focus on Cs migrating through clay. This was done in the framework of a master thesis on *"Uncertainty and sensitivity analysis of sorption chemistry in deep geological repositories"* (AHOUB 2018). A comprehensive uncertainty and sensitivity analysis study was performed on detailed sorption chemistry parameters (BRADBURY & BAEYENS 2002 & 2005) used in Cs reactive transport modelling (MCOTAC, PFINGSTEN 2002). Extensive realizations of Cs breakthrough curves at different locations in clay were produced spanning the expected range of Cs

arrival times and concentrations. The performed sensitivity analysis aims at quantifying the effects of uncertainties in 1) site-specific detailed sorption reactions equilibrium constants and 2) porewater cations' concentration, on the transport of radioactive Cs in clay. The Morris method followed by an extensive Sobol sensitivity analysis was used to rank the parameters' importance and interactions. The Morris analysis quantifies the average effect of a parameter on the output of interest, i.e. the mean of the changes in the output values due to perturbations in the input parameters. Sobol, on the other hand, quantifies the relative contribution of a parameter to the variance of the output; it is more of a ranking of parameters' importance rather than a measure of the effective value. The Sobol indices are unit-less. It was found that the sorption reaction equilibrium constants on Type-II sites in addition to the concentrations of the respective cations involved in these reactions are the most important uncertainty parameters affecting the transport of Cs. Furthermore, a classification tree was constructed to show the combination of parameters' values leading to the maximum arriving Cs concentrations at a specified location. The ranges of isotherm uncertainty based on our deterministic complex chemistry calculations (MCOTAC) are visualized in Fig. 4.7. These results can be used in large-scale performance assessment to support the estimates for Cs transport parameters, with values solidly based on detailed reactive transport modelling.

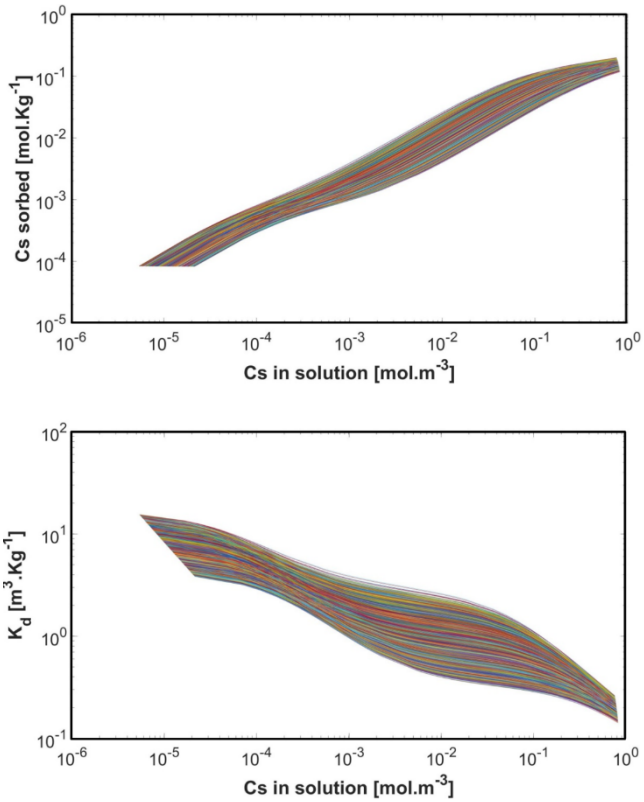

Fig. 4.7: Ranges of uncertainty of the Cs sorption isotherm calculated from the uncertainties of the individual thermodynamic sorption parameters of the complex deterministic sorption model.

4.6 Transport of inorganic ^{14}C through compacted illite-calcite mixtures

Performance assessment (PA) calculations for the Swiss SF/HLW repository predict ^{14}C to be one of the major dose-determining nuclides in safety analysis. This result is mainly a consequence of assumptions related to the anionic nature of carrier species. Dissolved inorganic ^{14}C arising from the anoxic corrosion of activated steel or Zircaloy will be transported diffusively as negatively charged $H^{14}CO_3^-$ species. Due to the negative charge and anion exclusion effects, it is expected that the transport behaviour will be similar to that of other anionic radionuclides, e.g. $^{36}Cl^-$, essentially unretarded. Therefore, a zero-sorption coefficient on clay is assumed in PA calculations, resulting in high calculated doses. Bicarbonate may, however, interact with carbonate minerals present as minor, but significant components, up to 10 wt.% in compacted bentonite and 20 wt.% in Opalinus Clay. Isotopic exchange batch experiments have shown that ^{14}C interacts with calcite and is partially immobilized during its recrystallization (AVRAHAMOV et al. 2013; BELOVA et al. 2012). This kind of interaction is a potentially effective retention mechanism which could ultimately help in reducing calculated ^{14}C doses, provided that it can be quantified via a robust model calibrated with appropriate experimental data. To this aim, ^{14}C through-diffusion experiments were carried out on compacted Illite-du-Puy intermixed with different amounts of grinded calcite (from 0 to 10 wt.%). The experiments were modelled by implementing a classical 1-dimensional diffusion equation in COMSOL-Multiphysics, including instantaneous reversible sorption and an additional sink term, which describes the incorporation of ^{14}C in newly formed (secondary) calcite during recrystallization at a fixed rate. The rate of calcite recrystallization (R, mol m^{-2} s^{-1}) was used, together with the pore diffusion coefficient (D_p, m^2 s^{-1}) and the instantaneous sorption coefficient of ^{14}C on the clay (K_d , m^3 kg^{-1}) as the only adjustable parameter to obtain the best fits of experimental data shown in Fig. 4.8. The flux data consistently show for all datasets that the peak release to the downstream reservoir occurs at about 20 - 25 days, which is indicative of a uniform retardation factor of about 0.001 m^3 kg^{-1}. The

fitted D_p also yielded uniform reasonable values between (1.0 - 1.7 × 10^{-10} m^2 s^{-1}). Finally, the fitted rates of recrystallization (0.4 – 5.3 × 10^{-11} mol m^{-2} s^{-1}) fall within the values determined independently in batch isotope exchange experiments, thus indicating that ^{14}C retention measured in our experiments can be reasonably attributed to ^{14}C uptake during recrystallization.

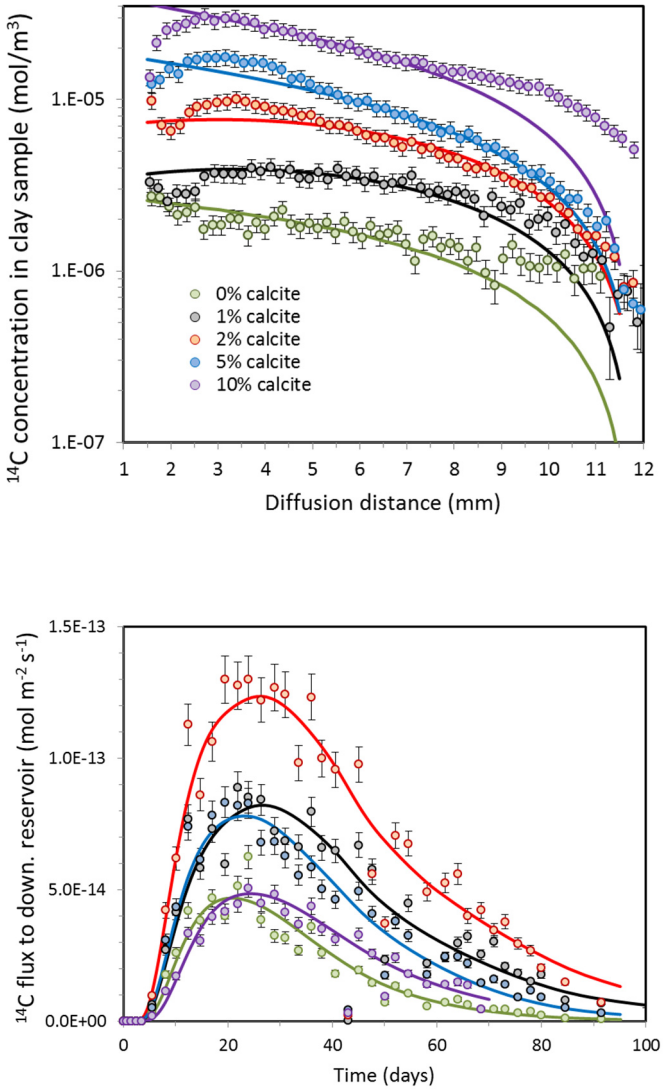

Fig. 4.8: Experimental data (circles) and corresponding best fit model curves for through-diffusion experiments on illite intermixed with different amounts of calcite: (upper) Final ^{14}C concentration profiles in the samples; (lower) ^{14}C fluxes to the downstream reservoir. Note that satisfactory fits could only be obtained assuming that the illite used already contains 1 wt.% calcite.

4.7 References

AHOUB A. (2018)
Uncertainty and sensitivity analysis of sorption chemistry in deep geological repositories. Master thesis, ETH Zurich, Switzerland.

AVRAHAMOV N., SIVAN O., YECHIELI Y., LAZAR B. (2013)
Carbon isotope exchange during calcite interaction with brine: Implications for ^{14}C dating of hypersaline groundwater. Radiocarbon 55, 81-101.

BAEYENS B., BRADBURY M. (2017)
The development of a thermodynamic sorption data base for montmorillonite and the application to bentonite. PSI Bericht 17-05 and Nagra Tech. Rep. NTB 17-13.

BELOVA D.A., JOHNSSON A., BOVET N., LAKSHTANOV L.Z., STIPP S.L.S. (2012)
The effect on chalk recrystallization after treatment with oxidizing agents. Chem. Geol. 291, 217-223.

BRADBURY M.H., BAEYENS B. (2000)
A generalised sorption model for the concentration dependent uptake of caesium by argillaceous rocks. J. Contam. Hydrol. 42, 141-163.

BRADBURY M.H., BAEYENS B. (2002)
Sorption of Eu on Na- and Ca-montmorillonites: Experimental investigations and modelling with cation exchange and surface complexation. Geochim. Cosmochim. Acta 66, 2325-2334.

BRADBURY M.H., BAEYENS B. (2005)
Modelling the sorption of Mn(II), Co(II), Ni(II), Zn(II), Cd(II), Eu(III), Am(III), Sn(IV), Th(IV), Np(V) and U(VI) on montmorillonite: Linear free energy relationships and estimates of surface binding constants for some selected heavy metals and actinides. Geochim. Cosmochim. Acta 69, 875-892.

GLAUS M.A., BAEYENS B., BRADBURY M.H., JAKOB A., VAN LOON L.R., YAROSHCHUK A. (2007)
Diffusion of ^{22}Na and ^{85}Sr in montmorillonite: Evidence of interlayer diffusion being the dominant pathway at high compaction. Environ. Sci. Technol. 41, 478-485.

GLAUS M.A., AERTSENS M., APPELO C.A.J., KUPCIK T., MAES N., VAN LAER L., VAN LOON L.R. (2015)
Cation diffusion in the electrical double layer enhances the mass transfer rates for Sr^{2+}, Co^{2+} and Zn^{2+} in compacted illite. Geochim. Cosmochim. Acta 165, 376-388.

PFINGSTEN W. (2002)
Experimental and modelling indications for self-sealing of a cementitious low- and intermediate-level waste repository by calcite precipitation. Nucl. Technol. 140, 63-82.

VAN LOON L.R., SOLER J.M., MÜLLER W., BRADBURY M.H. (2004)
Anisotropic diffusion in layered argillaceous rocks: A case study with Opalinus Clay. Environ. Sci. Technol. 38, 5721-5728.

VAN LOON L.R., BAEYENS B., BRADBURY M.H. (2009)
The sorption behaviour of caesium on Opalinus Clay: A comparison between intact and crushed material. Appl. Geochem. 24, 999-1004.

WICK S., BAEYENS B., MARQUES FERNANDES M., VOEGELIN A. (2018)
Thallium adsorption onto illite. Environ. Sci. Technol. 52, 571-580.

5 CEMENT-WASTE INTERACTION AND UPSCALING TO THE FIELD SCALE

G. Kosakowski, E. Wieland, R. Dähn, G. Geng (postdoc), A. Laube, A. Mancini (PhD student), R. Patel (postdoc), N. Prasianakis, J. Tits

5.1 Introduction

A multi-barrier concept is foreseen to ensure safe disposal of high-level waste (HLW) (spent fuel, vitrified and long-lived intermediate-level waste) and low- and intermediate-level waste (L/ILW) in Switzerland (NAGRA 2002). Barriers of the L/ILW repository include the waste matrix, the waste packages, the emplacement containers, the cavern backfill and the host rock. The L/ILW repository concept foresees the use of large amounts of cementitious materials, which will be the major physical and chemical barriers to the release of radionuclides from the cementitious near field into the host rock. For safety assessment it is of fundamental importance to understand the behaviour and performance of the barriers. In particular, cement-waste interaction processes need to be assessed, as they govern the long-term isolation of radioactive waste and the transport of radionuclides in the repository near field. The barrier function of the cementitious near field is expected to change over time due to various (geo)chemical processes that will take place, such as i) the chemical degradation of organic waste materials and the interaction of the main degradation product, CO_2 (and it bases), with hydrated cement, ii) the corrosion of metallic waste materials and potential interaction of the corrosion products with hydrated cement, and iii) the long-term degradation of hydrated cement due to interaction of highly alkaline cement porewater with silicate aggregates in concrete and backfill or by groundwater ingress from the host rock (KOSAKOWSKI et al. 2014). It has been acknowledged that cement-waste interaction may lead to the degradation of cementitious materials, which could affect the long-term performance of the barriers.

The aim of this project is to identify the physico-chemical processes controlling the temporal evolution of the L/ILW (cement-based) repository and to assess the influence of spatial heterogeneities on repository near field evolution. We evaluate the repository *in situ* conditions by modelling the interaction of waste sorts with the cement paste of the engineered barrier, by studying the relevant cement-waste interaction processes and their consequences for the long-term evolution of the chemical conditions in waste sorts such as iron corrosion at the cement-iron interface and the reaction of concrete aggregates, by assessing the impact of cement-waste interaction on gas production and humidity transport, by investigation of mineralogical alterations and porosity changes at the cement-clay interface, and by assessing the effect of porosity changes on diffusion processes. To this end, both experimental and modelling studies are carried out.

5.2 Geochemical modelling of the temporal evolution of waste packages

In 2018, the final report on the temporal evolution of waste packages containing low- and intermediate-level waste (L/ILW) was published (WIELAND et al. 2018). The aim of the study, which was partially funded by Nagra, was to evaluate chemical conditions within selected waste packages based on the currently available thermodynamic data for cementitious materials and our current understanding of the reactivity of the waste materials. For this study we selected typical waste sorts with waste materials conditioned (solidified) in concrete. The chemical reactions that are expected to take place inside the waste packages are i) metal corrosion, ii) degradation of organics, iii) dissolution of silicate aggregates, and iv) carbonation of the cementitious materials. These reactions are believed to control the degradation of the waste materials (organics, metals) and to be primarily responsible for cement-waste interaction as the degradation products can react with the solidifying concrete inside the waste packages. The simplified modelling approach is based on the assumption that the solidifying concrete and the waste materials are homogeneously distributed in the waste package ("mixing tank") implying that transport processes are fast. Two scenarios were taken into account for the modelling: limited and unlimited water availability. The first scenario is based on the assumption that the waste packages remain intact over a long time period ("closed system") while the second scenario implies that small openings (e.g. cracks, pit corrosion) exist in the walls of the waste packages already at the start of waste emplacement in the deep geological repository which allows ingress of water vapour ("semi-open system"). The two scenarios were modelled in two variants, either allowing the formation of the thermodynamically stable zeolites or inhibiting zeolite formation. The modelling study was performed for three operational and two decommissioning waste sorts.

The results from the first phase of the modelling

project revealed that the degradation of organic materials is the key process controlling the evolution of chemical conditions (solution composition, mineral composition of the solidifying concrete) in the waste packages. The latter reaction produces CO_2, which gives rise to carbonation of the solidifying concrete. This process largely controls the evolution of pH with time. Furthermore, the presence or absence of zeolites has a notable effect on the availability of water in the waste packages ("closed system") and on the pH as they bind alkalis. Metal corrosion produces H_2, which was treated as a non-reactive species in the modelling, and corrosion products, which may react with the solidifying concrete. The effect of the dissolution of the silicate aggregates (gravel) used to fabricate the solidifying concrete on the internal degradation of the concrete and the evolution of the chemical conditions was not evident from the modelling study. To this end, additional calculations were performed in 2018 for two operational waste sorts and one decommissioning waste sort based on the scenarios that either silicate aggregates, for which quartz is used as model compound, or limestone (i.e. calcite) are used as gravel to fabricate the solidifying concrete. The formation of zeolites was allowed in the modelling and water availability was not limited. The results obtained for the cement-stabilized decommissioning waste sort (denoted as SA-L-MX) are displayed in Fig. 5.2 over a time period of 2500 years. An image of the waste package is shown in Fig. 5.1 along with the inventory of this waste sort as given in MIRAM 14 (NAGRA 2014).

For this waste sort the initial composition of the solidifying concrete corresponds to a "low-pH"-type cement where portlandite is completely converted into calcium silicate hydrates (C-S-H) and the pH of the pore solution is comparatively low (LES PROGRESS REPORT 2017). Consequently, the buffer capacity of the cementitious system is very low. Carbonation caused by the degradation of the organic materials is negligible as the inventory of organic materials is very low in this waste sort. Corrosion of the metals dominates the long-term behaviour of this waste sort. Anoxic corrosion of aluminium, brass, iron, steel and zinc produces large volumes of H_2 and magnetite as corrosion product. For the current modelling study it was assumed that the aggregate material used to fabricate the solidifying concrete is either quartz, as given by the inventory in Fig. 5.1 and in accordance with MIRAM 14, or that the same amount of limestone is used for fabrication of the solidifying concrete (i.e. 1950 kg, Fig. 5.1). All other parameters and processes were retained, in particular the inventories of waste and cementitious materials (Fig. 5.1), and further the reactivity of the waste materials (WIELAND 2018). Replacing silicate aggregates (SiO_2) by

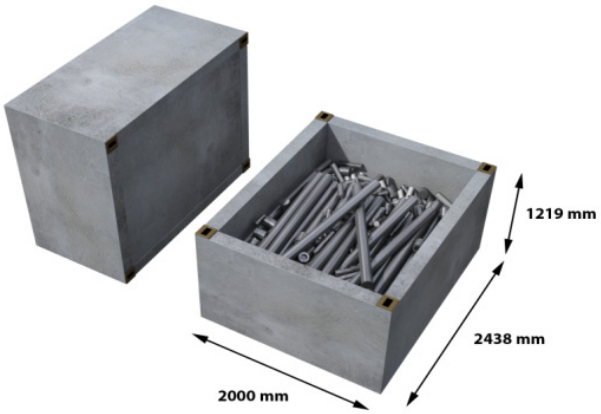

Material	Mass (kg)
LMW organics	12.92
PVC	0.75
Urea	4.49
Aluminium	3.17
Brass	124.49
Copper	139.10
Iron (cast)	210
Steel	5930
Zinc	0.58
Sand	1950
Water	757
Cementitious materials	1812

Fig. 5.1: Decommissioning waste sort SA-L-MX; top: image of the waste package; bottom: inventory.

limestone ($CaCO_3$) has a pronounced effect on the temporal evolution of the chemical conditions, which is clearly visible over the first 2500 years (Figs. 5.2 & 5.3). Silicates gradually dissolve in the highly alkaline cement porewater (Fig. 5.2a) which releases H_4SiO_4(aq). The latter species reacts with C-S-H which converts C-S-H phases with a relatively high initial Ca/Si (C/S) ratio (C/S = 1.01 in the initial mix) into C-S-H phases with C/S < 1.01. Uptake of alkalis by C-S-H phases and zeolites (Fig. 5.2c), which form below pH ~12.5, gives rise to a continuous pH drop (Fig. 5.3d). The corrosion of steel and iron is slow above the critical pH threshold of 10.5, while below pH 10.5 a 100 times higher corrosion rate is considered in safety assessment (DIOMIDIS 2014). Thus, once pH drops below 10.5 H_2 production is accelerated due to anoxic iron/steel corrosion (Fig. 5.3a) coinciding with the formation of large amounts of magnetite (Fig. 5.2c). Fig. 5.3a clearly illustrates the sensitivity of the system with respect to pH-dependent gas production by considering a 100 times difference in the corrosion rates of iron and steel above and below pH 10.5.

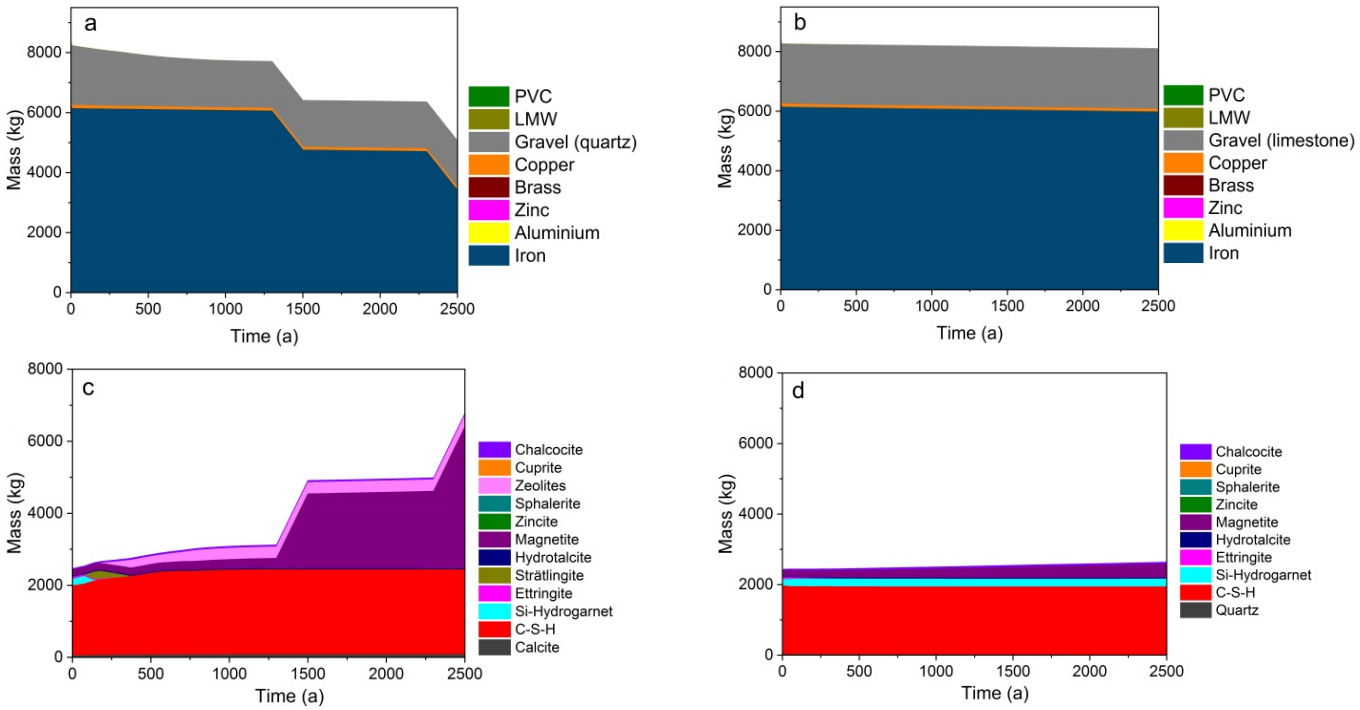

Fig. 5.2: Temporal evolution of the waste materials, gravel and mineral phases in the decommissioning waste sort SA-L-MX obtained by geochemical modelling based on the following assumptions: left: Silicate aggregate (quartz) used to fabricate the solidifying concrete: a) waste materials and gravel, c) mineral composition in the waste package; right: Limestone aggregate used to fabricate the solidifying concrete: b) waste materials and gravel, d) mineral composition in the waste package. Modelling scenario: unlimited water availability and formation of zeolites.

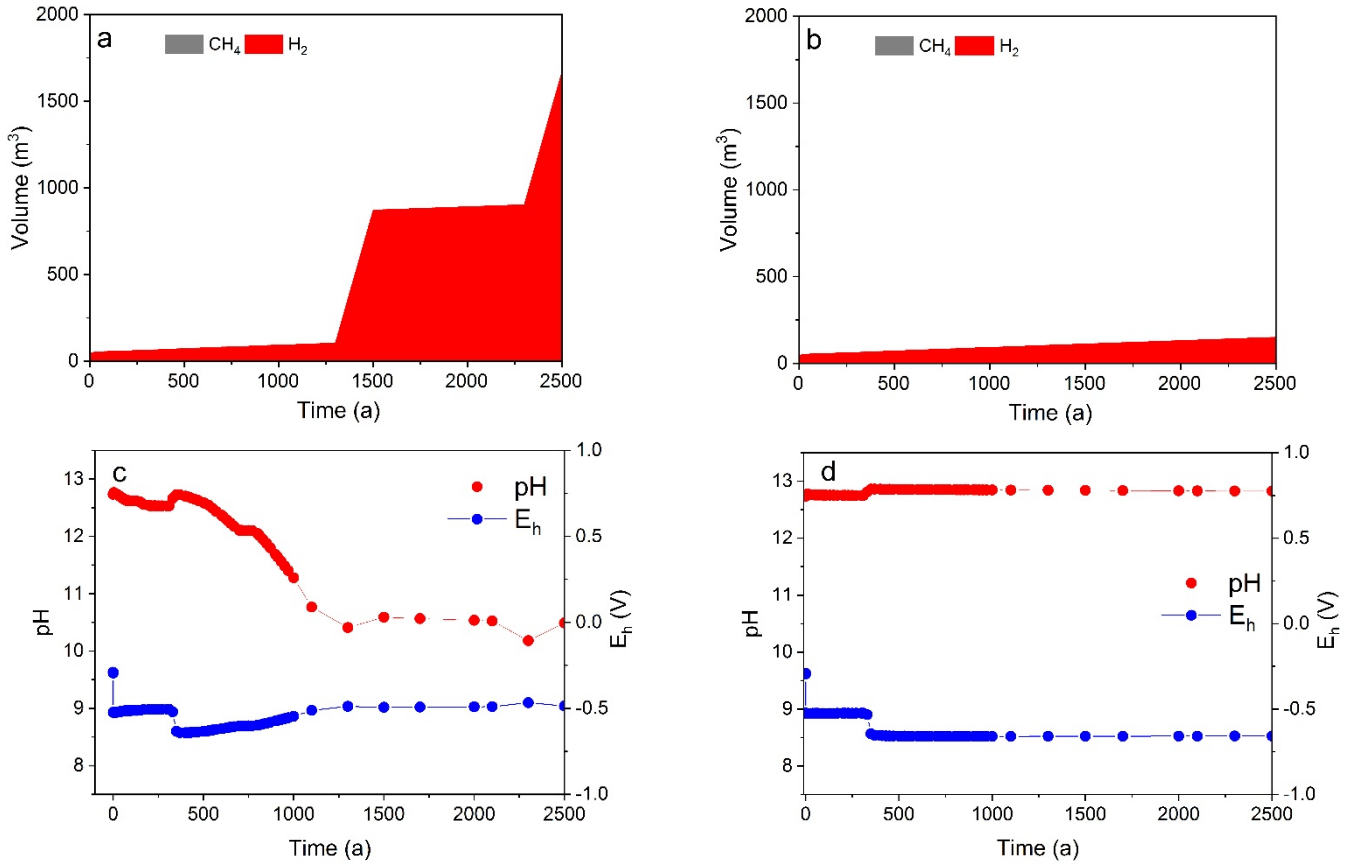

Fig. 5.3: Temporal evolution of the chemical conditions in the decommissioning waste sort SA-L-MX obtained by geochemical modelling based on the following assumptions; left: Silicate aggregate (quartz) used to fabricate the solidifying concrete: a) gas, c) pH and Eh; right: Limestone aggregate used to fabricate the solidifying concrete: b) gas, d) pH and Eh. Modelling scenario: unlimited water availability and formation of zeolites.

In contrast, a steady chemical evolution is predicted when silicate aggregates are replaced by the same amount of limestone. Calcite is stable in the highly alkaline porewater of the cementitious material. As a result, the phase composition of the solidifying concrete does not change with time and pH is buffered at ~ 12.7 due to the high concentration of alkalis in solution. In particular, no zeolites are formed which could reduce the alkali concentration in solution via structural incorporation of cations into zeolite's framework (e.g. Na- and K-phillipsite). Removal of alkalis from solution gives rise to a pH decrease as concentration of the main counter ion OH^- is reduced too.

This study reveals that the proposed geochemical modelling approach allows assessing the effect of specific parameters on the temporal evolution of the chemical conditions in different waste sorts. It further shows that the replacement of silicate aggregates by limestone for the fabrication of the solidifying concrete can significantly reduce the reactivity of some waste sorts. In the case of the decommissioning waste sort, strong alkaline conditions can be maintained over a very long time period. In particular, modelling does not predict a pH drop below 10.5, which would result in accelerated iron/steel corrosion and gas production. The latter processes are completed within a short time period compared to the entire period of concern of the repository (100'000 years). It should be noted, however, that the positive effect of limestone on the stabilization of the chemical conditions is less pronounced for those waste sorts with a high content of organic material. The degradation of the organic materials and subsequent carbonation of the solidifying concrete is the main driving force of the temporal evolution of these waste sorts. The two processes cannot be suppressed by replacing silicate aggregates by limestone (WIELAND 2018).

5.3 Multi-phase mass transport in waste packages using a process parameterization approach for description of cement degradation

This project was initiated in 2016 to investigate the influence of couplings between transport of water and (reactive) gases, chemical processes that produce gases and consume water, and the spatial heterogeneity in material parameters and chemical conditions in a near field of a deep geological repository for L/ILW. For modelling such systems on different scales, we developed a method that casts the complex chemical evolution of concrete degradation into simplified parametrization of the concrete degradation model in terms of pH, porosity and water consumption/release with respect to the degree of carbonation (mole amount of CO_2 reacted) and alkali-silica reaction (mole amount of silica aggregate dissolved and reacted).

In cooperation with Y. Huang and H. Shao from the Department for Environmental Informatics of the Helmholtz Centre for Environmental Research – UFZ (Leipzig, Germany), we implemented additional source/sink terms into the OpenGeoSys-MP (OpenGeoSys6-MultiPhase) code as a look-up table (HUANG et al. 2015, 2017). The extended code OpenGeoSys-MP-LT (LT: Look-up Table) allows simulations of reactive multi-component multi-phase systems considering the degradation of cementitious materials. The approach and the implementation were tested against a fully coupled reactive transport code with explicit modelling of chemical equilibria in a benchmarking study on accelerated carbonation of concrete due to diffusion of CO_2 in a gas phase in combination with kinetically controlled dissolution of silicate aggregates (HUANG et al. 2018).

In a second phase, we applied the approach to assess the evolution of a waste package during intermediate storage. This complements the thermodynamic modelling of the long-term evolution of waste packages described in the previous chapter (WIELAND et al. 2018). We were specifically interested in the influence of the material heterogeneity within a single waste drum on gas generation and the role of humidity transport in the waste packages as potential limiting factor for progress of chemical reactions. We have chosen a scenario (interim storage) that allows, given the existing computing resources, to evaluate the complex feedback between transport of humidity and gases, the consumption of water due to corrosion and degradation of organic matter, and the reduction of the chemical reactivity at very low water saturation. The modelling scenario does not fully represent interim storage conditions as for metal corrosion reducing conditions were assumed.

The modelled waste package is abstracted from a waste sort (BA-PH-PF see WIELAND et al. 2018) that contains mixed solid waste compacted into a steel pipe of 485 mm diameter which was embedded in a 200-l barrel of 606 mm diameter and 883 mm height (Fig. 5.4, upper left). The void space was backfilled with a cement mortar. These waste packages contain large amounts of metals (mainly steel) and fast degrading organics (cellulose). We assumed that the top of the drums are open to the atmosphere during interim storage to dry them out and to avoid overpressures. It also allows atmospheric carbonation of the cementitious backfill. For such complicated models it is not possible to present the temporal evolution of all interesting parameters and processes in a short paragraph. We thus focus on the direction of bulk gas and water fluxes after 90 years of storage and their consequences for concrete degradation and gas generation in terms of production and consumption of CO_2.

Selected results after 90 years of simulation time are shown in Figs. 5.4 and 5.5. Initially, the backfill mortar is 80% saturated with water, whereas the waste is only saturated at 35%. After 90 years, the overall water saturation is strongly reduced (Fig. 5.4, upper right), specifically near the top where the drum is in contact with the atmosphere. In the waste compartment, water saturation near the steel pipe surface is at residual values indicating locally dry conditions. This drying-out is caused by the consumption of water due to the degradation of organics and in particular due to the corrosion of the steel pipe. This observation is also reflected in the direction of the gas flow (Fig. 5.4, lower left) and the water flow (Fig. 5.4, lower right). In both cases the driving pressure field is shown as coloured surface, while the direction of flow is indicated by arrows. The general direction of advective gas transport is towards the open top. Gas transport is driven by gas production due to the degradation of organic matter and the corrosion of metal. Liquid phase flow is mainly driven by differences in saturation and liquid flow from regions of liquid saturation towards regions of low saturation.

The contact with the atmosphere at the top of the drum allows CO_2 to diffuse into the drum. This induces a carbonation front at the top, which decreases pH (Fig. 5.5, upper left) and increases porosity (Fig. 5.5, upper right). In addition, CO_2 is produced in the inner waste compartment by the degradation of organic matter. This process, as well as the corrosion of metals, consumes water. Note that the pH in the waste is relatively low. Therefore, metal corrosion and water consumption related to the corrosion process are enhanced. The combined water consumption by corrosion and organics degradation is higher near the surface of the steel pipe that causes local drying-out. The model scales the chemical reactivity with saturation like in the models of TROTIGNON et al. (2011), i.e. gas production rates and rates for concrete degradation decrease to zero at residual water saturation. This causes a spatially inhomogeneous distribution of CO_2 gas production rates in the waste compartment with very low rates near the steel pipe (Fig. 5.5, lower left). The steel pipe is a barrier for transport of water and gases. Hence, CO_2 produced in the waste compartment can only move towards the bottom or the top of the drum, where it enters the cement backfill and is immediately consumed by the carbonation of the cementitious material (Fig. 5.5, lower left and lower right). As the general transport direction of internally produced gas is towards the top boundary, carbonation (in terms of cumulative bound CO_2 by carbonation) is much more pronounced at the top interface between waste and cement backfill.

For this generic waste package, the simulations demonstrate that the heterogeneous material distribution in the waste package and the spatio-temporal evolution of liquid saturation affects gas generation. Gas generation, material evolution and humidity transport are coupled in a complex feedback loop involving various chemical and physical (transport) processes. Such insight models are necessary to gain understanding of the role of process couplings and to crosscheck the possible range of gas generation rates calculated with simpler modelling approaches.

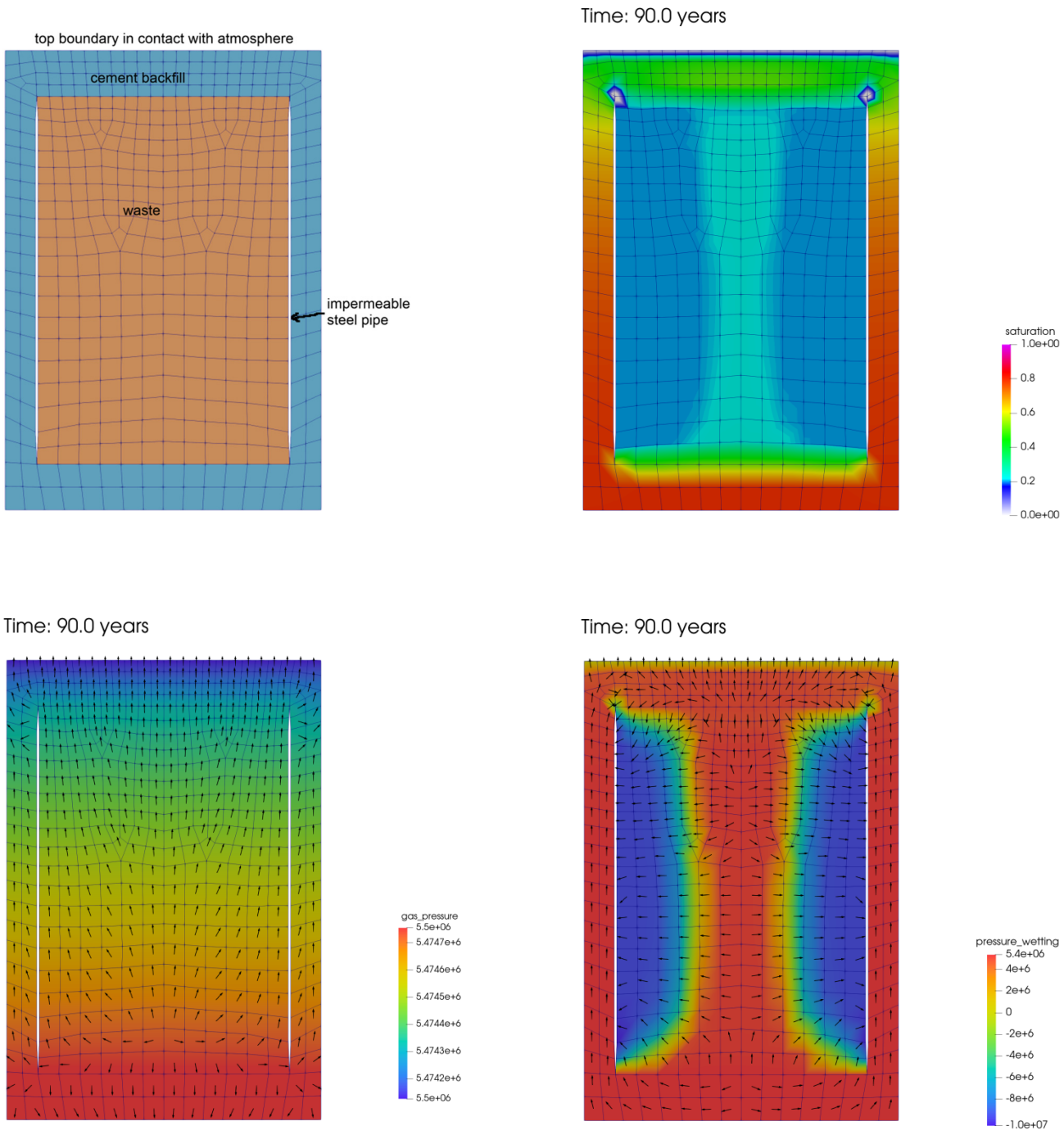

Fig. 5.4: Selected results for the evolution of the L/ILW package after 90 years. See text for detailed explanation. Upper left figure: Conceptual setup of the modelled waste package. Upper right figure: Liquid saturation state after 90 years simulation time. Lower left figure: Gas pressures (colours) and direction of advective gas transport (arrows). The arrows are not scaled to represent advective velocities. Lower right figure: Pressure distribution of the water phase (colours) and direction of advective water transport (arrows). The arrows are not scaled to represent advective velocities.

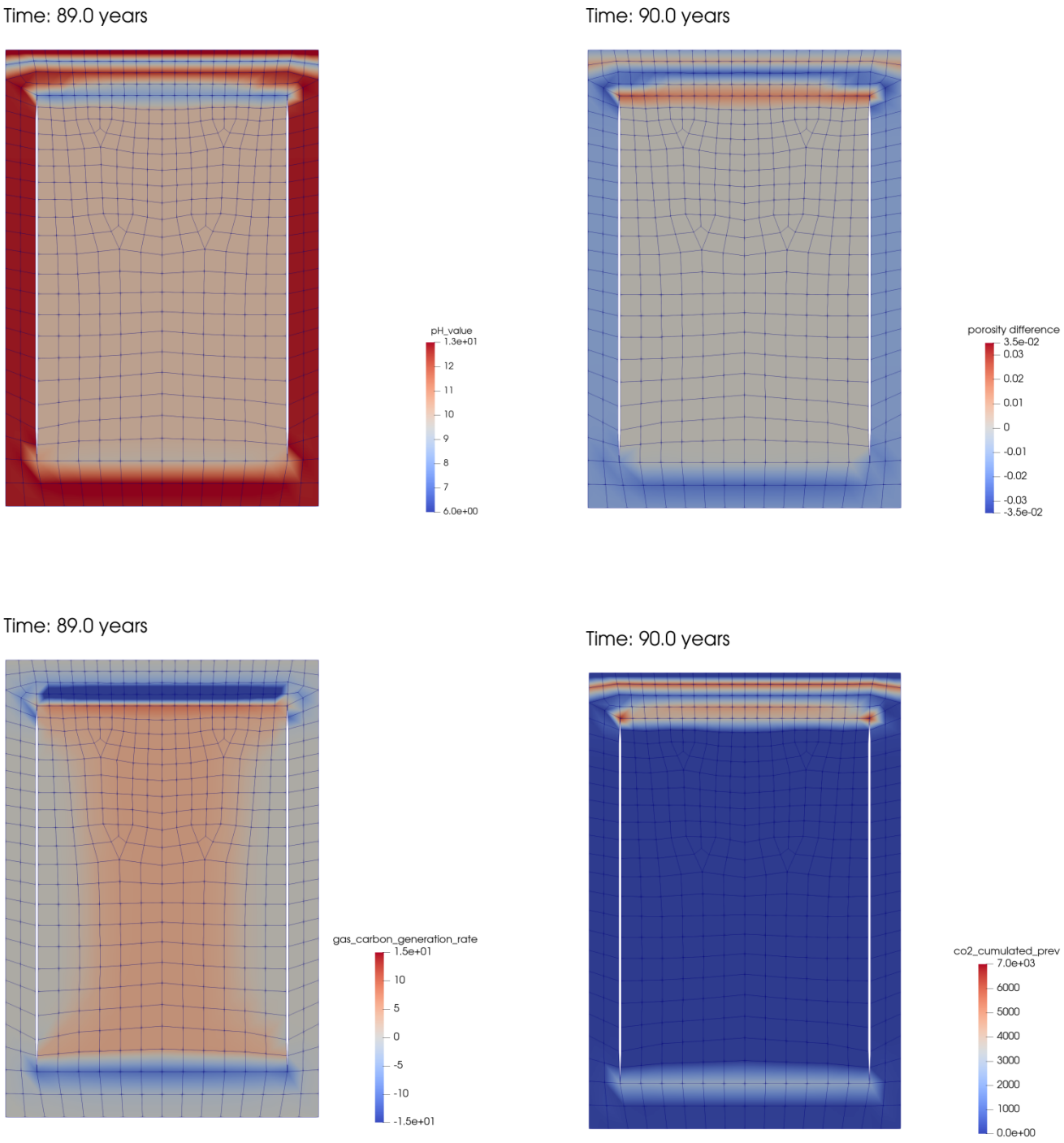

Fig. 5.5: Selected results for the evolution of the L/ILW package after 90 (89) years. See text for detailed explanation. Upper left figure: Spatial distribution of pH. Boundary nodes at the model top show very high pH values which is an artefact of the visualization. Upper right figure: Spatial distribution of porosity changes. Negative values indicate reduction in porosity; positive values indicate increase in porosity. Lower left figure: Spatial distribution of CO_2 production/consumption rates. Positive values indicate production of CO_2 by the degradation of organic matter; negative values indicate consumption due to carbonation of backfill mortar. Lower right figure: Cumulated CO_2 over time consumed by carbonation of the solidifying concrete. Note that the boundary nodes at the model top are not subject to carbonation reaction.

5.4 Interaction of iron corrosion products with cement

Iron/steel and cement are the two main components in the planned deep geological L/ILW repository in Switzerland. After closure of the repository, as soon as oxygen is completely depleted from the near field in the course of oxic Fe(0) corrosion, conditions become strongly reducing and the anoxic corrosion of Fe(0) at the interface between cement paste and steel starts to produce Fe(II,III) corrosion products. Magnetite (Fe_3O_4) and Fe sulphides (FeS, FeS_2) are the only products currently considered in conjunction with steel/iron corrosion in anoxic alkaline conditions and it is assumed that iron corrosion products, in particular Fe(II), cannot be taken up by cement phases. Thus, it is presently unclear whether or not the interaction between the corrosion products and cement paste can occur and if so, whether or not this interaction will affect the long-term barrier performance of cementitious materials in the L/ILW repository. A PhD project funded by the Swiss National Science Foundation (SNSF) (SNSF grant No 200021_162342) was started in 2016 with the aim of developing a mechanistic view of Fe(II,III) interaction with cement phases and thus improving the current understanding of iron/steel-cement interaction over the time scale of the L/ILW repository. In this project, the Fe speciation is being investigated a) upon the interaction of Fe(II,III) with single cement phases by using wet chemistry experiments and by synchrotron-based techniques, and b) in aged Fe(0)-containing slag cements sampled from concrete structures that had been exposed to environmental conditions for several years.

In 2018 batch sorption studies with Fe(III) on calcium silicate hydrates (C-S-H phases) were continued. C-S-H phases are the main hydration products of Portland cement and strongly control the mobility of many radionuclides in a cementitious near field because of their long-term stability and high immobilization potential for metal cations. Thus, Fe(III) released during iron/steel corrosion could compete with radionuclide uptake by C-S-H phases provided that Fe(III) is strongly bound by these phases. Results for Fe(III) uptake by a C-S-H phase with C/S ratio of 1.5 are exemplarily shown in Fig. 5.6.

The Fe(III) kinetic experiments reveal a very strong uptake of Fe(III) by the C-S-H phase and further that the chemical equilibrium is reached within ~35 days (Fig. 5.6a). The relatively long time required to reach equilibrium suggests that the Fe(III) uptake mechanism is not only the consequence of Fe(III) adsorption onto the surface of the C-S-H phase, which is a fast process reaching equilibrium within ~ 1 day, but rather that Fe(III) is taken up into the structure of the C-S-H phase. Measurements of the Fe(III) uptake at increasing initial Fe(III) concentration further show linear sorption of Fe(III) with increasing concentration up to 5000 ppm surface loading (Fig. 5.6b). Interestingly, the formation of $Fe(OH)_3(s)$ was not observed over the entire concentration range although, at the higher concentrations, the solution was oversaturated with respect to the solubility limit of crystalline $Fe(OH)_3(s)$ (ferrihydrate). Extended X-ray absorption fine structure (EXAFS) spectroscopy confirmed absence of $Fe(OH)_3(s)$ precipitation up to 12'000 ppm Fe(III) loading and further indicated the same coordination environment of Fe(III) in the range of linear sorption. Nevertheless, $Fe(OH)_3(s)$ precipitation was clearly observed on the C-S-H phase loaded with 50'000 ppm Fe(III) as the spectral features of this sample are comparable to those of $Fe(OH)_3(s)$ (Figs. 5.6c/d). This shows that precipitation of $Fe(OH)_3(s)$ occurs in the C-S-H system, however at significantly higher solubility. Interpretation of the EXAFS spectra is ongoing with the aim of developing a structural model for Fe(III) uptake by C-S-H phases. The latter information is essential with a view to future mechanistic sorption studies on the Fe(II) uptake by cement phases.

Complementary to the Fe(II,III) sorption studies on C-S-H phases, micro-spectroscopic investigations were carried out in 2018 with the aim of determining the oxidation state of Fe in slag cements that had been sampled from aged concrete structures and a laboratory sample. The aim is to assess the Fe speciation around Fe(0) particles embedded in the cement matrix that had been aged for many years both under oxic and anoxic conditions. Very little to nothing is currently known about the long-term reactivity of finely dispersed Fe(0) in slag-containing cements, in particular the interaction of Fe(II,III) with cement phases, although the content of metallic Fe(0) particles is substantial (~2 - 5 wt.% as Fe_2O_3). It is anticipated that the same chemical processes are operative at the interface between iron/steel waste materials and solidifying concrete in the L/ILW repository. Thus, the spectroscopic study on the long-term reactivity of Fe(0) in slag cements will enable us to assess the long-term effect of iron/steel on the performance of the cementitious barrier in the L/ILW repository.

In 2018 redox mapping was performed at the microXAS beamline of the Swiss Light Source (SLS) on different slag-containing cement thin sections in order to identify the Fe redox states 0, +II, and +III around aged slag particles.

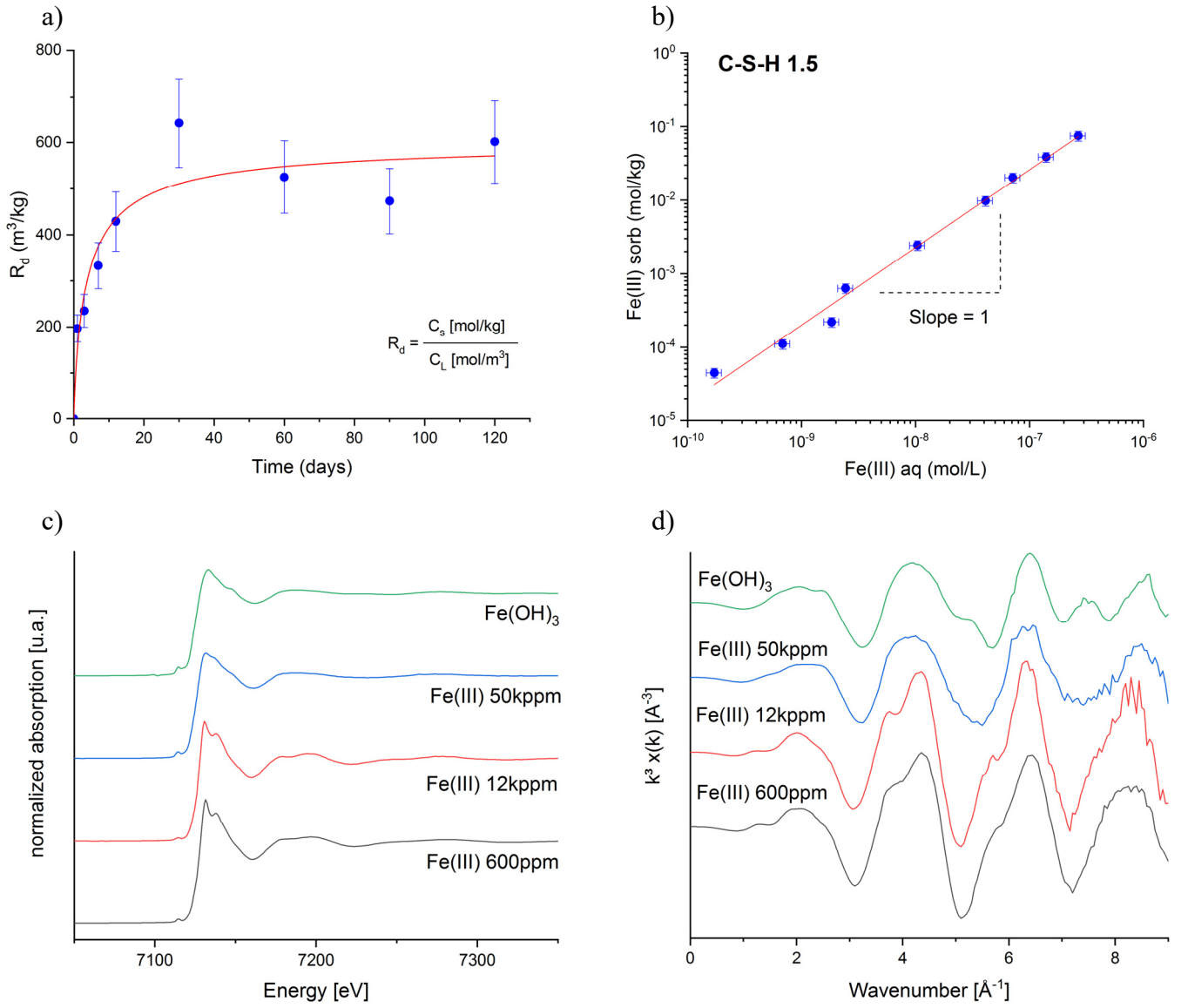

Fig. 5.6: Wet chemistry studies: a) Kinetics of Fe(III) uptake by a C-S-H phase with C/S = 1.5 (pH 12.3), b) Fe(III) sorption isotherm; Spectroscopic investigations: c) Fe K-edge XANES of a C-S-H phase with C/S = 1.5 at different Fe(III) loadings (600 ppm, 12'000 ppm and 50'000 ppm) and a Fe(III) hydroxide reference, d) k^3-weighted EXAFS spectra of the same samples.

The micro-spectroscopic study was conducted on three different slag-containing cement samples: a concrete sample from the Danish Vejle Fjord bridge aged for more than 30 years in marine environment, a concrete sample from the German Auw an der Kyll bridge aged for 7 years in continental environment, and a laboratory specimen aged for 7 years in closed containers with limited oxygen ingress. X-ray absorption near edge structure (XANES) spectra were collected on selected spots of thin sections prepared from the above materials. These data were fitted using the least-square linear combination (LC) approach in order to determine the contribution of the main Fe-containing phase around slag particles and in the bulk material. Fig. 5.7 exemplarily shows the redox map for the specimen aged for 7 years in laboratory conditions. The results from the LC fitting are listed in Table 5.1.

The Fe oxidation state maps and the LC fits reveal major compositional differences among the different samples. Almost no Fe(0) was observed in the sample from the Vejle Fjord bridge and the Auw an der Kyll bridge exposed to environmental conditions (data not shown). In these samples Fe(0) was almost completely corroded to form Fe(II,III) corrosion products. In contrast, Fe(0) was the dominant oxidation state in the sample aged in laboratory conditions (Fig. 5.7a) suggesting that in these conditions oxygen ingress and therefore Fe(0) oxidation are strongly inhibited.

LC fitting of the bulk XANES spectrum shows that, as expected, magnetite (Fe_3O_4) is the main corrosion product (Table 5.1). At present, the possibility of an interaction of the Fe(II,III) species with cement phases at the magnetite-cement interface cannot be assessed from micro-spectroscopy. A proposal for complementary micro-X-ray diffraction measurements on these samples at the microXAS of SLS has been submitted.

Table 5.1: Proportion of minerals determined from the least-square LC fitting of the Fe K-edge XANES spectra.

	Fe(0)	Fe_3O_4	C_4AF	Residual (R-factor)
Bulk-XANES	0.80(3)	0.08(3)	0.12(2)	0.0021
µ-XANES	1.00(5)	-	-	0.0010

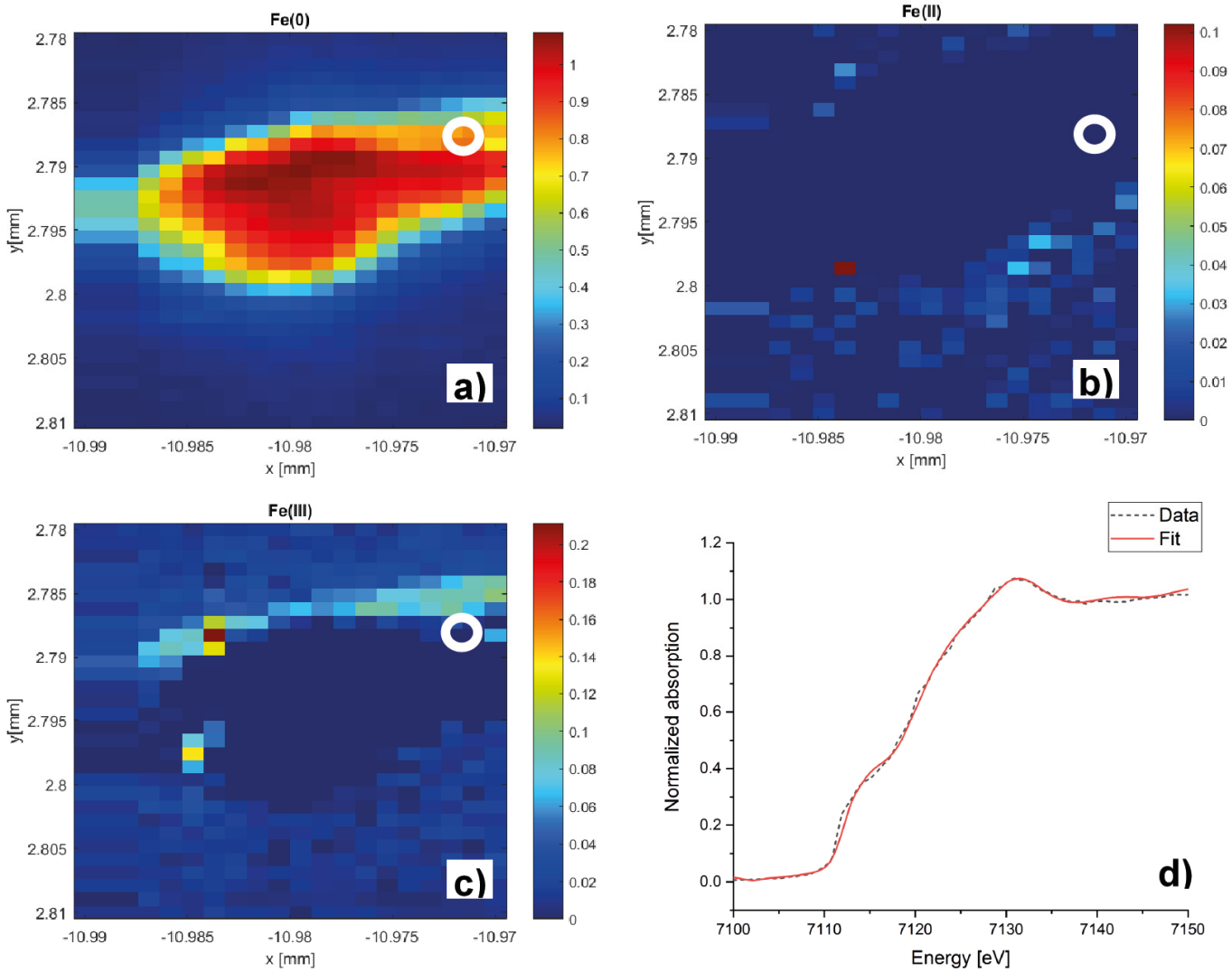

Fig. 5.7: Redox mapping and XANES performed on a slag-containing cement sample aged in laboratory conditions. Grey circles indicate the spot where the XANES spectrum was collected. a) Fe(0), b) Fe(II), c) Fe(III), d) XANES data and fitting. The results from LC fitting are presented in Table 5.1.

5.5 Alkali-silica reaction in concrete

The alkali-silica reaction (ASR) is a deterioration mechanism, which can severely shorten the durability of concrete structures. The ASR between concrete aggregate and the alkaline pore solution produces expansive solid in the concrete porosity and initiates significant cracking. Despite decades of study, the crystal structure of the ASR products remains largely unclear. This project aims to investigate the molecular configuration of the ASR product and its correlation with the physical properties related to the expansion phenomena. In step I, pure ASR samples with systematically varied chemical compositions are synthesized, which are then subjected to crystal-chemical characterization. In step II, microscale crystal-chemical information are collected and compared with the database of reference samples established in step I.

This project is carried out in the framework of a SNSF funded Sinergia project in which researchers from Empa, EPFL and PSI have teamed up with the aim to gain insights into the mechanisms of the reaction and to acquire knowledge about how ASR develops with time. Additional funding could be acquired from the European Union's Horizon 2020 research and innovation programme under the Marie Skłodowska-Curie grant agreement No 701647. Thus, funding for this project is fully provided by SNSF and the EU Horizon 2020 research programme.

In 2018, we have focused on, and roughly completed step I, i.e. the crystal-chemical characterization of synthesized ASR products. According to the reported composition of the ASR product, three sets of samples were synthesized in the laboratory, with chemical compositions of $(K_2O)_m(CaO)_n(SiO_2)$ (the K-gel), $(Na_2O)_m(CaO)_n(SiO_2)$ (the Na-gel) and $[(K_2O)_x–(NaO)_y]_m(CaO)_n(SiO_2)$ (the Na-K-gel), where m = 0 - 1.0, n = 0 - 0.5 and x/y = 0.5 -10. A total number of 30 samples were expected to cover the broad geochemical boundary conditions of ASR. For the characterization, a series of synchrotron-based methods have been used, including XANES, EXAFS spectroscopy, powder X-ray diffraction (XRD) and high-pressure X-ray diffraction (HP-XRD). The XANES and EXAFS experiments were conducted at the Phoenix beamline of the SLS. The powder samples were dust onto carbon tapes and placed in a vacuumed chamber. In particular, Ca, K and Na *K*-edges were measured within the energy range of 3900 - 4500, 3550 - 4000 and 1000 - 1600 eV, respectively. The step size was 0.1 eV at the absorption edge, whereas 2 - 5 eV at the pre- and post-edge. The powder XRD study was conducted at beamline 6-ID-D of the Advanced Photon Source (APS, USA). Powder samples were packed into capillary tubes made of Kapton film, which was then placed between a 100 keV X-ray beam and a 2D detector. The distance between the sample and the detector was adjusted such that the resolution of the diffractograms and the Q-range were balanced to allow both powder XRD Rietveld refinement and a pair distribution function (PDF) analysis. The HP-XRD experiments were conducted at beamline P02 of DESY (Germany) and beamline I15 of the Diamond Light Source (United Kingdom). Small amounts of the powders were loaded in a micro-sized cylindrical hole pre-drilled on a stainless-steel sheet, filled with ethanol-methanol solution and closed with diamond anvils on both sides. A gask membrane was used to apply increasing hydrostatic load (~ 1 eV each step) up until ~ 10 GPa. At each step, the diffraction (exposure to an X-ray beam of 20 - 25 keV) was recorded. Such data was later on analysed to yield the lattice constants as a function of the applied pressure. In the past year, our proposals were assigned over 350 beamtime hours to conduct the above-mentioned experiments.

Fig. 5.8 shows selected results from the synchrotron-based studies. The diffraction of some lab-synthesized samples (Fig. 5.8a) indicates that the lab-reaction leads to either a crystalline phase (namely skc) when the initial water-to-solid (w/s) ratio is ~ 5, or poorly crystalline phases, namely C-S-H phase (blue arrows) and/or a product 1 (P1) (red arrows) when the initial w/s is ~ 10. The real ASR products exhibit strong crystallinity when forming inside an aggregate yet they are amorphous when forming in the cement paste (Fig. 5.8b). The micro-XANES results of the selected points show that the K environments in both regions are similar and resemble the chemical environment in the reference mineral Mountainite (Fig. 5.8c). Meanwhile, the Ca environment in the crystalline region is in line with that of Shlykovite (natural crystalline form of skc), and the Ca environment in amorphous regions is consistent with Ca in C-S-H phases. The above structural information is essential to finally decipher the structure of the ASR products with various degree of crystallinity.

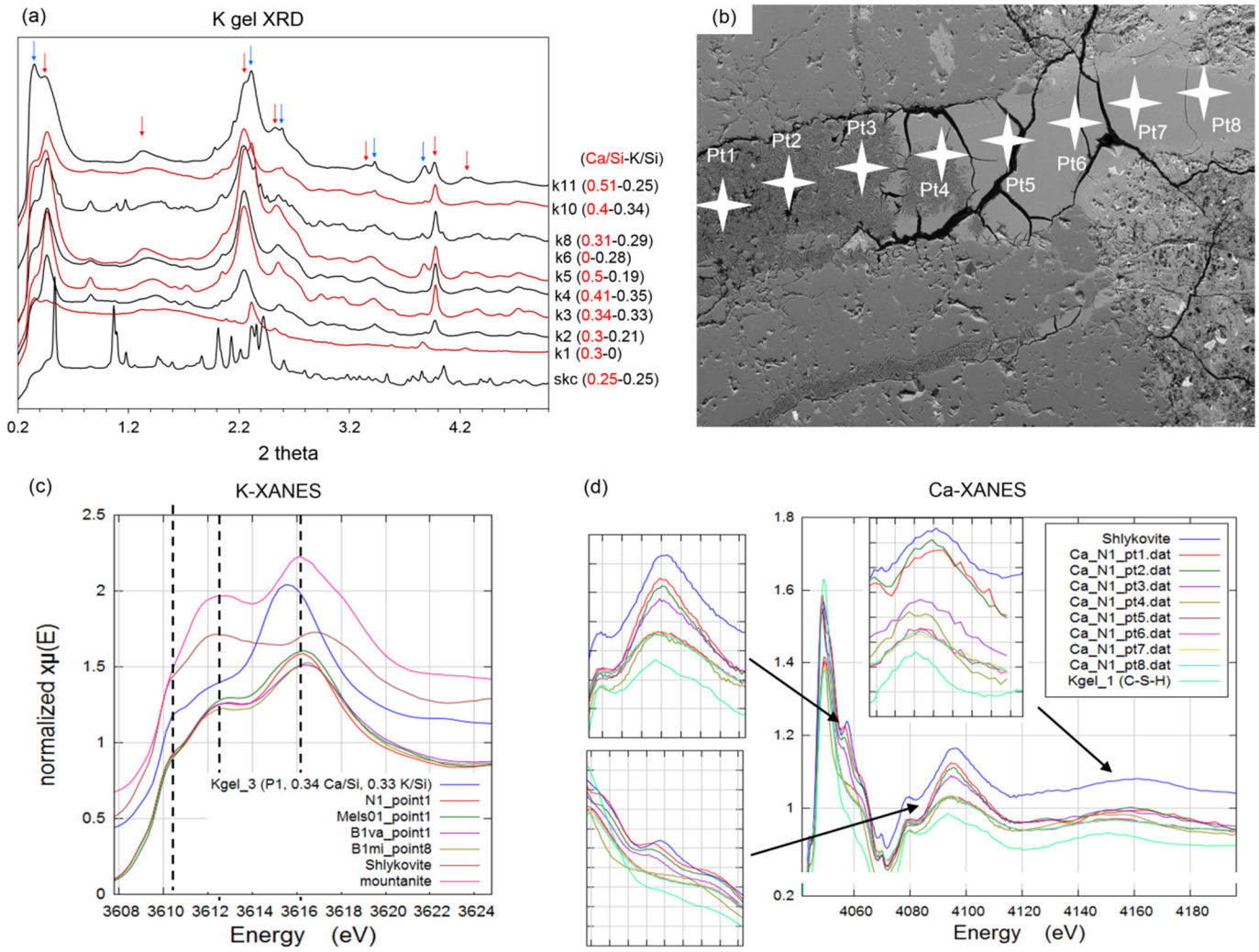

Fig. 5.8: Selected data of the XRD and spectroscopic studies of the ASR products: a) powder XRD of the lab-synthesized ASR products; b) the micro-morphology of the study region in an ASR affected concrete (N1); c) the K K-edge and d) Ca K-edge XANES of the studied regions and the reference samples.

5.6 Resolving carbonation mechanisms of cement-based materials through multi-scale microstructural simulations

The PSI-fellow 3i project *"Resolving carbonation mechanisms of cement-based materials through multiscale microstructural simulations"* (R. Patel) started in 2017. The project receives partial funding from the European Union's Horizon 2020 research and innovation programme under the Marie Sklodowska-Curie grant agreement No 701647.

During the first year of this project, the work focused on simulating cement paste microstructure evolution due to combined leaching and carbonation under fully saturated conditions. Such conditions are commonly encountered at cement-clay interfaces, as well as in CO_2 sequestration wells. In such systems, ingress of low pH solution that contains dissolved carbonate ions can lead to precipitation of calcite, and at the same time to the dissolution of calcium-bearing phases in cement paste. To simulate such systems, an extension to capture precipitation processes was made to Yantra, a lattice Boltzmann method based reactive transport tool (PATEL 2016). The extended code was first applied to simulate the influence of the composition of an ingressing solution on an idealized porous media consisting of portlandite ($Ca(OH)_2$) as cement phase. Fig. 5.9 shows the evolution of the microstructure in

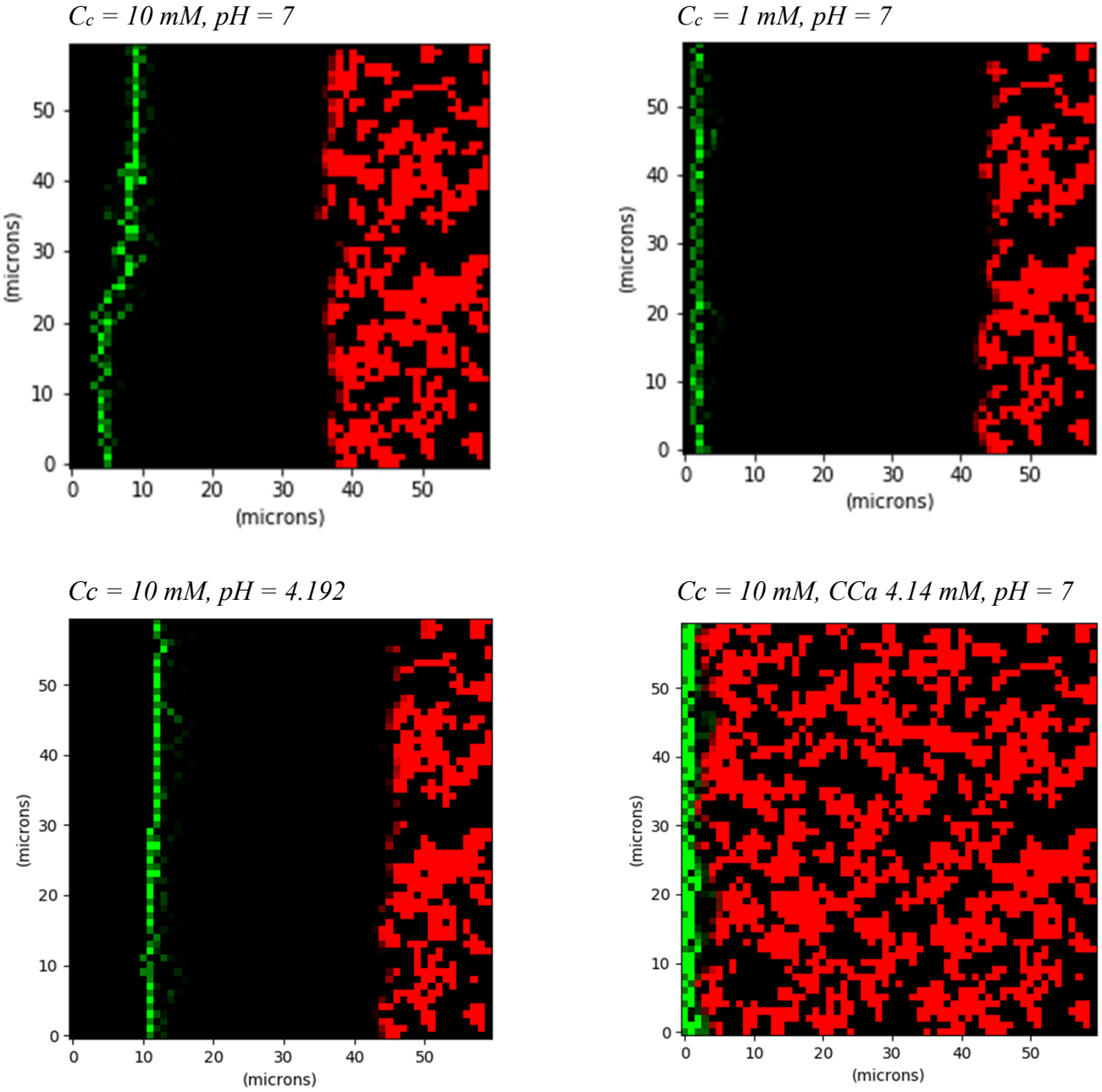

Fig. 5.9: Evolution of the pore structure at 400 s. Calcite, portlandite, and pores are represented in green, red and black respectively. Shading of color is proportional to the volume fraction of the phase.

terms of portlandite dissolution and calcite precipitation after 400 sec for four cases with different aqueous carbon concentration (C_C), aqueous calcium concentration (C_{Ca}) and pH of the solution. It was observed that changes in the aqueous carbon concentration and pH can affect the dissolution rate of portlandite and the location of the calcite precipitation front. Large amounts of calcium ions in the ingressing solution can lead to the formation of a calcite layer, which can clog the surface and prohibit the further dissolution of portlandite from the pore structure. The detailed results of this study have been published in a conference paper (PATEL & PRASIANAKIS 2018). This study was then extended on 3D virtual microstructures generated from HYMOSTRUC (VAN BREUGEL 1995) to obtain a comparison between the model and experimental results of DUGUID & SCHERER (2010). Fig. 5.10 shows volume rendering of calcite and portlandite solid phases at the end of 1 day for these simulations.

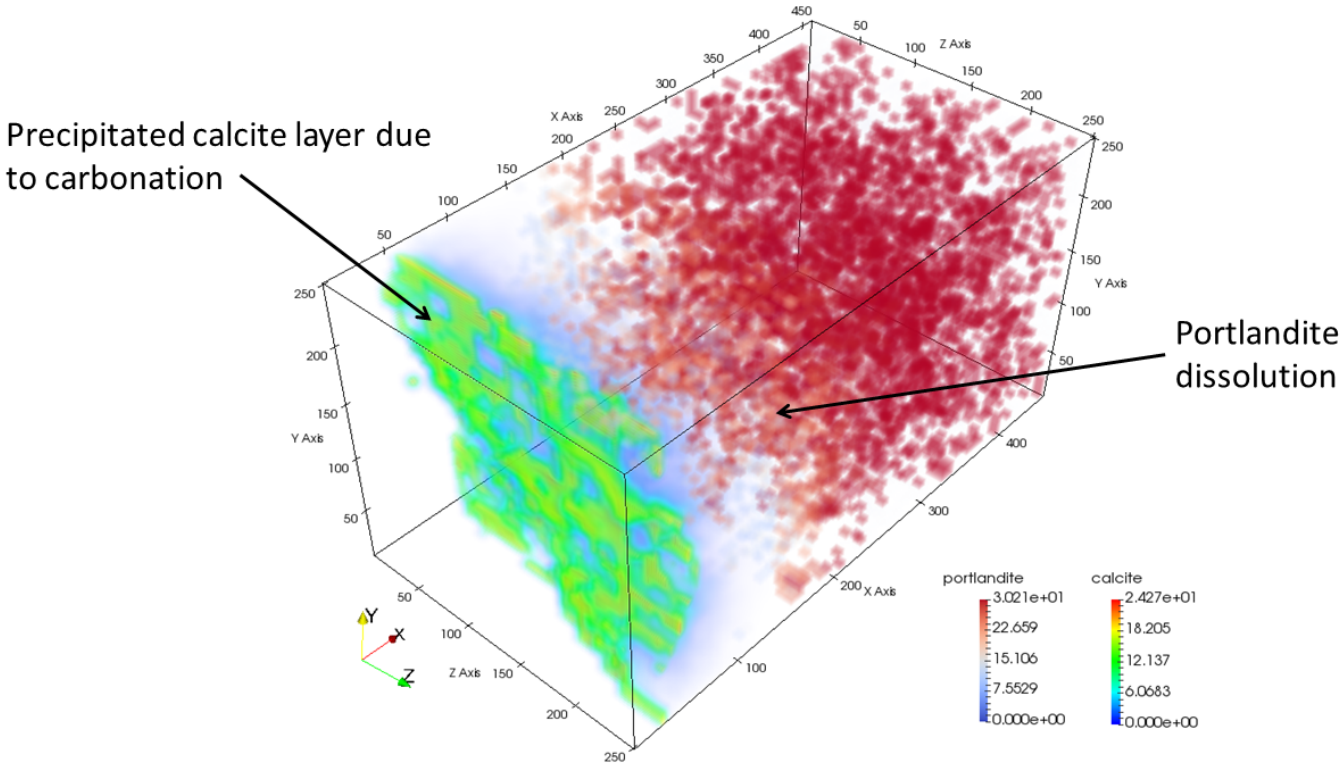

Fig. 5.10: Portlandite and calcite volume rendering at 1 day for 3D simulations of the virtual microstructure.

5.7 References

DIOMIDIS N. (2014)
Scientific basis for the production of gas due to corrosion in a deep geological repository. Nagra Work Rep. NAB 14-21.

DUGUID A., SCHERER G.W. (2010)
Degradation of oilwell cement due to exposure to carbonated brine. Int. J. Greenh. Gas Con. 4(3), 546-560.

HUANG Y., KOLDITZ O., SHAO H. (2015)
Extending the persistent primary variable algorithm to simulate non-isothermal two-phase two-component flow with phase change phenomena. Geotherm. Energy 3, 13.

HUANG Y., NAGEL T., SHAO H. (2017)
Comparing global and local implementations of nonlinear complementary problems for the modeling of multi-component two-phase flow with phase change phenomena. Environ. Earth Sci. 76, 643.

HUANG Y., SHAO H., WIELAND E., KOLDITZ O., KOSAKOWSKI G. (2018)
A new approach to coupled two-phase reactive transport simulation for long-term degradation of concrete. Constr. Build. Mater. 190, 805-829.

KOSAKOWSKI G., BERNER U., WIELAND E., GLAUS M.A., DEGUELDRE C. (2014)
Geochemical evolution of the L/ILW near field. Nagra Tech. Rep. NTB 14-11.

KULIK D.A., WAGNER T., DMYTRIEVA S.V., KOSAKOWSKI G., HINGERL F.F., CHUDNENKO K.V., BERNER U. (2013)
GEM-Selektor geochemical modeling package: revised algorithm and GEMS3K numerical kernel for coupled simulation codes. Computat. Geosci. 17, 1-24.

NAGRA (2002)
Project Opalinus Clay. Safety report. Demonstration of disposal feasibility for spent fuel, vitrified high-level waste and long-lived intermediate-level waste (Entsorgungsnachweis). Nagra Tech. Rep. NTB 02-05.

NAGRA (2014)
Modellhaftes Inventar für radioaktive Materialien MIRAM 14. Nagra Tech. Rep. NTB 14-04.

PATEL R.A. (2016)
Lattice Boltzmann method-based framework for simulating physico-chemical processes in heterogeneous porous media and its application to cement paste, PhD thesis, Ghent University, Belgium.

PATEL R.A., PRASIANAKIS N.I. (2018)
Development of pore-scale model for ingress of CO_2 brine through cement paste. SynerCrete'18 - International conference on interdisciplinary approaches for cement-based materials and structural concrete. Funchal, Maderia, Portugal.

TROTIGNON L., THOUVENOT P., MUNIER I., COCHEPIN B., PIAULT E., TREILLE E., BOURBON X., MIMID S. (2011)
Numerical simulation of atmospheric carbonation of concrete components in a deep geological radwaste disposal site during operating period. Nucl. Technol. 174, 424–437.

VAN BREUGEL K. (1995)
Numerical simulation of hydration and microstructural development in hardening cement paste (II): Applications. Cem. Concr. Res. 25(3), 522–530.

WIELAND E. (2018)
Geochemical modelling of the temporal evolution of waste packages of L/ILW waste sorts with siliceous and calcareous aggregates. PSI Technical Report TM-44-18-07, Paul Scherrer Institut, Villigen, Switzerland.

WIELAND E., KOSAKOWSKI G., LOTHENBACH B., KULIK D.A., CLOET V. (2018)
Preliminary assessment of the temporal evolution of waste packages in the near field of the L/ILW repository. Nagra Work Rep. NAB 18-05.

6 WASTE CHARACTERIZATION

E. Wieland, E. Curti, J. Tits, D. Kunz, A. Laube, B. Z. Cvetković (postdoc)

6.1 Introduction

This chapter summarizes the research activities at LES related to the characterization of radioactive waste materials, currently focusing on irradiated steel, spent fuel and vitrified high-level waste. The projects aim at providing important information on the source term of radionuclide release from the waste materials in the planned repositories for high-level (HLW) and low- and intermediate-level waste (L/ILW). The source term influences directly and indirectly several safety assessment parameters and calculations related to the other repository compartments (near field, geosphere, biosphere). In addition, the source term is a time-dependent parameter strongly affected by the temporal evolution of the waste materials, which are subjected to chemical degradation processes, such as corrosion of irradiated steel, (bio)chemical degradation of organic matter, or the dissolution of spent fuel and vitrified high-level waste. Besides changes caused by the evolution of physical-chemical conditions such as pH, temperature and redox potential, time dependence of radionuclide release from waste materials is thus a direct consequence of the degradation of waste materials themselves. For this reason, investigations of the waste properties have been identified as an area of research that is important for Nagra over the next 5 years and possibly also beyond the general licence application.

6.2 C-14 Project: Release and speciation of ^{14}C-bearing compounds

Carbon-14 has been identified as a key radionuclide in safety assessment and a major contributor to the activity release rate (mSv per year) from the cement-based L/ILW repository into the host rock. Activated steel is the main source of ^{14}C in the radioactive waste produced in Switzerland. The chemical form of the ^{14}C-bearing compounds produced during the anoxic corrosion of activated steel is only poorly known while the overall ^{14}C inventory in the radioactive waste is well known. The aim of this project is to investigate i) the release of ^{14}C-bearing organic compounds from waste materials (e.g. during the corrosion of activated steel) and their speciation, ii) the chemical stability of these organic compounds in repository relevant conditions, and iii) the retardation of the organics in the near field of a repository for radioactive waste.

Partial funding of the ^{14}C project by swissnuclear (Project title: *"Investigation of the chemical speciation of ^{14}C released from activated steel"*) and by the EU FP7 collaborative project *"CAST"* (CArbon Source Term) ended on March 31st, 2018. Since then the project receives partial funding solely by Nagra.

Compound-specific radiocarbon analysis (CSRA) is being developed in co-operation with Prof. Dr. S. Szidat and Dr. G. Salazar (Department of Chemistry & Biochemistry at the University of Bern, Switzerland).

6.2.1 Corrosion experiment with activated steel

The corrosion experiment with activated steel was started in May 2016 (LES PROGRESS REPORT 2016) and since then several samplings of the liquid phase have been carried out (LES PROGRESS REPORT 2017). CSRA was applied to identify and quantify the ^{14}C-bearing compounds present in the liquid phase. CSRA is based on the separation of individual compounds with liquid chromatography and ^{14}C quantification by ^{14}C accelerator mass spectrometry (AMS). In 2018, preparation and submission of publications was the main activity, reporting details of the experimental set-up, the development of CSRA for the analysis of the liquid phase and first CSRA results from the sampling of the corrosion experiment with activated steel (WIELAND et al. 2018; CVETKOVIĆ et al. 2018a; CVETKOVIĆ et al. 2018b).

6.2.2 Development of CSRA for gaseous compounds

At present, the concentration of the ^{14}C-bearing gaseous compounds in the corrosion experiment with activated steel cannot be determined using standard gas chromatography with mass spectrometry detection (GC-MS) as their concentration is below the detection limit of the current analytical setup. Thus, the CSRA-based analytical method is being further developed to improve the detection of gaseous ^{14}C-bearing compounds at very low concentrations. To this end, the LES owned GC system operated in the PSI HOTLAB has been modified in the past years and allows for the separation of individual ^{14}C-bearing gaseous organic compounds, their oxidation to $^{14}CO_2$ in a combustion (oxidation) reactor and collection of $^{14}CO_2$ in the fraction collector (Fig. 6.1). The fraction collector (Fig. 6.1) was developed specifically for this project by Brechbühler AG, the commercial partner in the project.

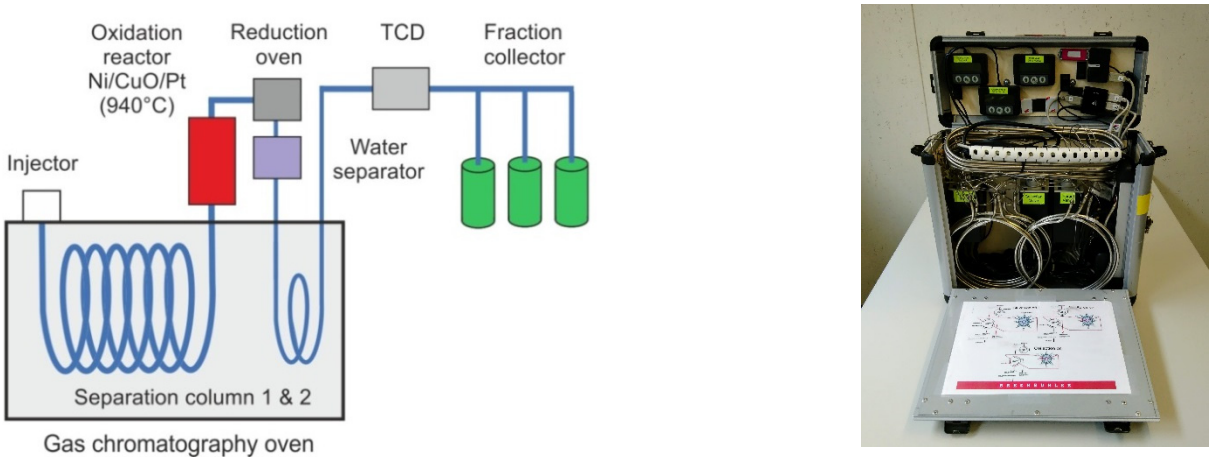

Fig. 6.1: Left: Schematic presentation of the modified GC system used for CSRA of gaseous species. Right: Picture of the fraction collector.

The analytical method is based on the separation of target analytes (separation column 1) and their online oxidation to CO_2 in the oxidation reactor (Fig. 6.1). The oxidation products (ideally only CO_2) pass through a water separator to remove residual water and a reduction oven to remove traces of oxygen and nitrous oxides. The oxidation products further pass through a short second separation column that was installed to separate CO_2 from the rest of the gaseous compounds, e.g. hydrocarbons that have not been oxidized. The analytes are detected by a non-destructive method with thermal conductivity detection (TCD) and, based on their retention times, they are eventually collected as separate fractions in the fraction collector.

Performance of the combustion reactor was evaluated and optimized in the last reporting year (LES PROGRESS REPORT 2017). In 2018, we mainly focused on testing and optimizing performance of the fraction collector. To this end, repeatability and recovery of the sampling process were elaborated. The tests were performed by injecting 20 µg stable carbon CH_4. It emerged from the tests that keeping a constant pressure and gas flow during separation, oxidation and sampling is essential to improve repeatability and recovery of the sampling process. In particular, it emerged that injection of the target analyte had to be optimized. Fig. 6.2 shows the TCD recordings for N_2 (carrier gas) and CO_2 (product of CH_4 oxidation) before and after optimizing the injection system during gas sampling by the selected sampling loops. Initially, injection was carried out by using an injection loop with an inner diameter of 0.25 mm which gave rise to pressure fluctuation during sample injection, and consequently to changes in the flow rate of the carrier gas. The pressure fluctuations led to shifts in the retention time of the analyte, which further reduced recovery due to the fixed time interval applied for gas sampling (Fig. 6.2a). Thus, both retention time and recovery were found to be specific for each of the selected sampling loops. In particular, recovery was less than 100% for some sampling loops. After installing an injection loop with a larger inner diameter of 0.5 mm, however, pressure fluctuation could be strongly minimized during injection, which resulted in identical retention times for all the selected sampling loops and further resulted in almost 100% recovery (Fig. 6.2b). Currently, we are testing the connection between the fraction collector and the AMS and optimizing injection of CO_2 collected in the sampling loops into the gas injection system (GIS) of the AMS.

6.2.3 Identification and quantification of organic compounds released during anoxic iron corrosion

Corrosion experiments with non-activated steel powders have been carried out in recent years aiming at identifying and quantifying both aqueous and gaseous carbon-containing compounds produced during anoxic corrosion (LES PROGRESS REPORTS 2015/2016). A recent publication summarizes the results from these studies (CVETKOVIĆ et al. 2018c). They show that only a limited number of small organic molecules are formed during anoxic iron corrosion. These compounds have less than five carbon atoms and a low molecular weight. The findings from the corrosion studies with non-activated materials are complementary to those resulting from the ongoing corrosion study with activated steel because, in the long term, it can be expected that the impact of gamma irradiation (which enables radiolysis) on the carbon speciation generated during the anoxic corrosion of activated steel will decrease with the decay of the relatively short-lived gamma emitters like ^{60}Co.

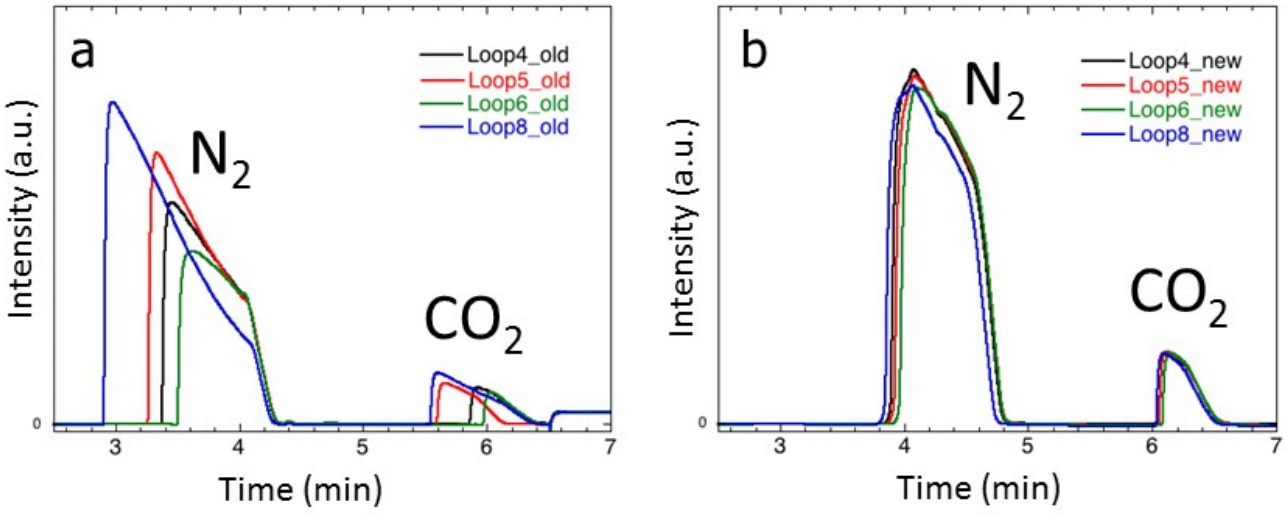

Fig. 6.2: Recordings of the TCD signals for N_2 and CO_2. Retention time and recovery a) before and b) after modification of the injection loop.

The influence of gamma irradiation on the carbon speciation is expected to be diminished at the latest after 1000 years. Hence, a long-term assessment of the type of carbon species present in the L/ILW repository should also be undertaken by considering the findings from corrosion studies with non-activated iron/steel materials.

In 2018 a series of corrosion experiments with iron powder were carried out. The objective was to also analyse and quantify H_2, which is formed during anoxic corrosion of iron, in addition to the aqueous and gaseous organic compounds that are produced in the course of the corrosion process (Fig. 6.3). The experiments were carried out in NaOH solution at pH 11. The results show that all the relevant corrosion products can be quantified reproducibly, however, only over a very short time spread of the experiments up to 8 days as gas tightness of the vials used for the corrosion experiments was not ensured in the long run. The production of H_2 and gaseous organic compounds resulted in a pressure build-up that leads to an escape of gas over longer time spans.

The results displayed in Fig. 6.3a will be used to develop a stoichiometric relationship between the production of gaseous organic compounds and H_2 in short-term experiments. By contrast, Fig. 6.3b clearly reveals that time dependence of the concentration of the carboxylates is not related to H_2 production and therefore to anoxic iron corrosion. Detailed analysis of the data is ongoing.

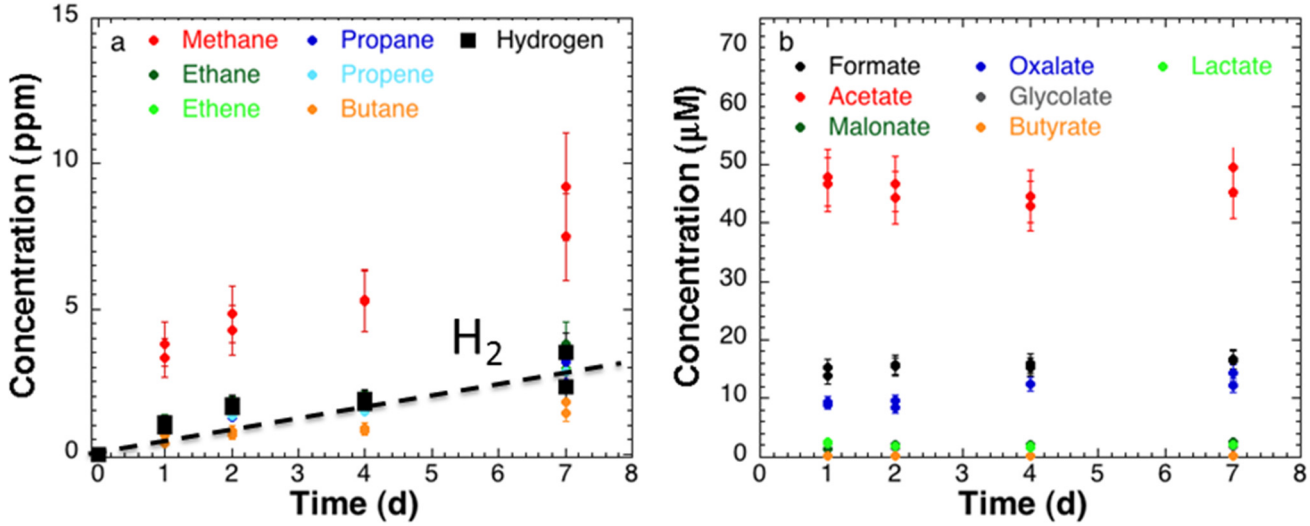

Fig. 6.3: Time-dependent increase of the concentrations of a) gaseous organic compounds and hydrogen, and b) carboxylates in aqueous phase during the anoxic corrosion of iron powder in 1mM NaOH.

6.2.4 Chemical stability of organic compounds in repository relevant conditions

^{14}C-containing low molecular weight (LMW) organics, such as formate and acetate, are expected to be released during the anoxic corrosion of activated steel in a cement-based L/ILW repository (Fig. 6.3b; WIELAND & HUMMEL 2015). At ambient temperature and pressure, these LMW organics are metastable. Assuming complete thermodynamic equilibrium a subsequent decomposition into CO_2 and/or CH_4 can be expected. However, without the interaction of micro-organisms or catalysts, decomposition processes are extremely slow. It is noteworthy that temperatures up to 80°C and H_2 partial pressures up to 100 atm can be expected in the near field of the L/ILW repository (XU et al. 2008), and in addition, the decomposition process may be accelerated due to the presence of magnetite as catalyst (WERSIN et al. 2003). It is further noted that the decomposition of ^{14}C-bearing aqueous LMW organics would enhance ^{14}C release via gas phase and therefore, this process is currently being investigated. The studies are carried out under conditions relevant to the L/ILW repository near field, i.e. in highly alkaline solution and with anoxic and reducing atmosphere. The results are expected to allow a more thorough appraisal of the relevance of abiotic decomposition of organic compounds in the L/ILW repository.

In the last year, the stability of formate was studied under anoxic conditions (N_2 atmosphere) and under reducing conditions (2 atm forming gas (FG, 95% N_2/ 5% H_2)) at temperatures between 150°C and 200°C to accelerate potential decomposition reactions. The total pressure in the gas-tight pressurized reactors used for these experiments was maintained at 5.5 bar (2 bar forming gas + 3.5 bar water vapour pressure at 150°C). The mixture of ^{13}C- and ^{14}C-labelled formate was used in these experiments to avoid misinterpretation of the data due to the presence of organic contaminants originating from the reactor equipment (LES PROGRESS REPORT 2016). In deionised (Milli-Q) water, ^{13}C- and ^{14}C-labelled formate was found to be stable over a period up to eight months (LES PROGRESS REPORT 2017) whereas in alkaline conditions a significant reduction of the aqueous concentration of ^{13}C- and ^{14}C-labelled formate was observed within two months. The reduction in the formate concentration was found to be more pronounced in the presence of Ca in the concentration range 0.001 – 0.02 M.

Several experiments were repeated in 2018 to ensure reproducibility of the results. In particular, the decomposition of formate was studied in order to further substantiate the effect of Ca in solution. Temperature and pressure were identical to the earlier experiments described above. The aim of these experiments was to identify the products formed during the decomposition of formate and to develop a mass balance for the process. To this end, the inner surfaces of the reactors were cleaned with 0.1 M HCl at the end of each experiment to dissolve corrosion products that had been accumulated on the reactor surface. After 1-day equilibration in the closed reactors, the acidic solutions were sampled and the gas phases were purged through alkaline gas traps to collect ^{13}C- and ^{14}C-labelled CO_2 dissolved during the washing procedure. The liquid samples were analysed by using high performance ion exchange chromatography either coupled with mass spectrometry (HPIEC-MS) for the determination of ^{13}C-labelled formate or coupled with a conductivity detector (HPIEC-CD) for the determination of total formate. The activity of ^{14}C-labelled formate was determined by liquid scintillation counting (LSC).

Fig. 6.4 shows the results from experiments carried out at different $Ca(OH)_2$ concentrations, i.e. 0.02 M, 0.005 M and 0.001 M, and in the absence of $Ca(OH)_2$. Note that the concentration of ^{13}C- and ^{14}C-labelled formate in the stability test carried out in 0.001 M $Ca(OH)_2$, was a factor 6 higher (300 μM) than in the other stability experiments (50 μM). At the same initial ^{13}C-labelled/^{14}C-labelled formate concentration (50 μM), the decrease in formate was more pronounced in the presence of Ca and only ~10% of the added H^{13}COONa was recovered after 60 days reaction. In the NaOH system, i.e. in the absence of $Ca(OH)_2$, and in the system with 0.001 M $Ca(OH)_2$, however, the decrease in the concentration of ^{13}C-labelled formate was much weaker. Thermodynamic calculations showed that, at a temperature of 150°C and a total pressure of 5.5 atm, the systems containing 0.02 M $Ca(OH)_2$ and 0.005 M $Ca(OH)_2$ are likely oversaturated w.r.t. portlandite ($Ca(OH)_2$(s)). Thus, co-precipitation may explain the stronger reduction of the concentration of both ^{13}C- and ^{14}C-labelled formate in these systems compared to the experiments carried out in NaOH and 0.001 M $Ca(OH)_2$.

Table 6.1 shows the mass balance for ^{13}C- and ^{14}C-labelled formate at the end of some experiments. Neither ^{13}C-labelled LMW organic compounds other than ^{13}C-labelled formate were detected in the aqueous phase by HPIEC-MS nor ^{13}C-labelled LMW compounds were identified by GC-MS in the gas phase. The washing procedure with 0.1 M HCl at the end of the experiments allowed a small but significant portion of the aqueous ^{14}C to be recovered (measured with LSC) thus suggesting that co-precipitation with $Ca(OH)_2$(s) occurred (Table 6.1). A small but still significant portion of ^{14}C was detected in the NaOH solutions of the two gas-sampling units connected to

the reactors after exposing the inner surface of the reactors to HCl solution and flushing the gas phase with N_2 (Table 6.1). It is likely that this ^{14}C fraction was present as solid carbonate in the reactor and released as CO_2 during the washing procedure with HCl. Nevertheless, complete recovery of ^{13}C- and ^{14}C-labelled formate that was removed from solution was not achieved and therefore, an important sink of ^{13}C- and ^{14}C-labelled formate has not yet been identified. Future tasks will focus on identifying the unknown sink.

In 2018, additional experiments were carried out at lower temperature. These stability tests were carried out in autoclaves containing a $3 \cdot 10^{-4}$ M ^{13}C-labelled/^{14}C-labelled formate solution and 25 $g \cdot L^{-1}$ Fe(0) powder. The autoclaves were stored in an oven at 80°C for 60 days. It should be noted that the maximum H_2 partial pressure was much higher in these batch autoclave experiments than in the decomposition experiments described above using the gas-tight pressurized reactors. At the end of the experiments, the solutions were analysed by HPIEC-MS and LSC. After 2 months reaction, approximately 3 % of the formate was found to be decomposed (measured with both LSC and HPIEC-MS). Note that the small decrease in the formate concentration is analytically significant. These preliminary results show that the decomposition of formate also takes place at lower temperature relevant to the near-field conditions of the L/ILW repository.

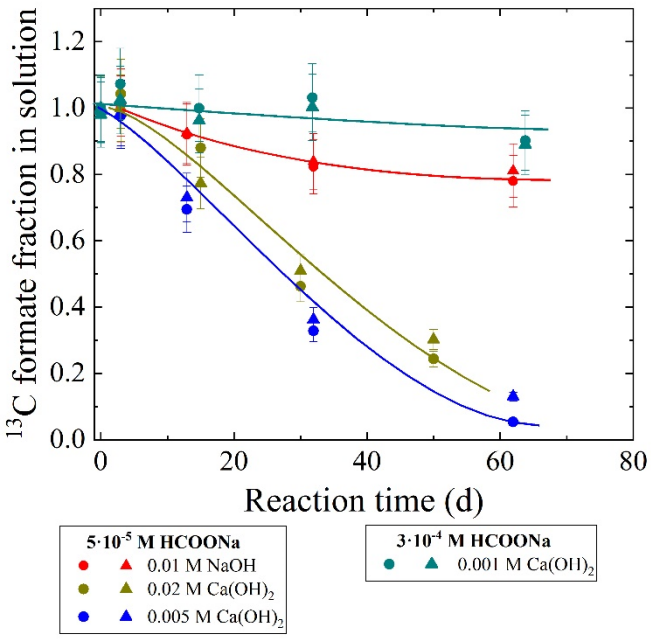

Fig. 6.4: Reaction of ^{13}C-labelled Na-formate in various alkaline solutions under a forming gas atmosphere at 150°C. The fraction of ^{13}C-labelled formate in solution is shown as function of the reaction time. Dots: ^{13}C HPIEC-MS measurements, triangles: ^{14}C LSC measurements.

Table 6.1: Mass balance for ^{13}C- and ^{14}C-labelled formate.

	$5 \cdot 10^{-5}$ M ^{13}C+^{14}C formate 0.01 M NaOH	$5 \cdot 10^{-5}$ M ^{13}C+^{14}C formate $5 \cdot 10^{-3}$ M $Ca(OH)_2$	$3 \cdot 10^{-4}$ M ^{13}C+^{14}C formate 10^{-3} M $Ca(OH)_2$
$(^{13}C+^{14}C)_{initial}$	$2 \cdot 10^{-5}$ mol	$2 \cdot 10^{-5}$ mol	$1.20 \cdot 10^{-4}$ mol
$(^{13}C+^{14}C)_{end, sol}$	$1.32 \cdot 10^{-5}$ mol (66%)	$2.03 \cdot 10^{-6}$ mol (10.15%)	$1.08 \cdot 10^{-4}$ mol (90.00%)
$(^{13}C+^{14}C)_{end, gas}$	0	0	0
$(^{13}C+^{14}C)_{HClsol}$	$1.31 \cdot 10^{-7}$ mol (0.66%)	$1.98 \cdot 10^{-6}$ mol (9.90%)	$8.00 \cdot 10^{-7}$ mol (0.67%)
$(^{13}C+^{14}C)_{HClgas}$	$5.90 \cdot 10^{-8}$ mol (0.30%)	$3.39 \cdot 10^{-6}$ mol (16.95%)	$6.00 \cdot 10^{-7}$ mol (0.50%)
$(^{13}C+^{14}C)_{missing}$	$6.60 \cdot 10^{-6}$ mol (33.04%)	$1.26 \cdot 10^{-5}$ mol (63.00%)	$1.06 \cdot 10^{-5}$ mol (8.83%)

$(^{13}C+^{14}C)_{initial}$ = total amount ^{13}C+^{14}C formate in solution at the start of the experiment (mol)

$(^{13}C+^{14}C)_{end, sol}$ = total amount ^{13}C+^{14}C formate in solution at the end of the experiment (mol)

$(^{13}C+^{14}C)_{end, gas}$ = total amount ^{13}C+^{14}C formate in the gas phase at the end of the experiment (mol)

$(^{13}C+^{14}C)_{HClsol}$ = amount of ^{13}C+^{14}C formate in the acidic washing solution (mol)

$(^{13}C+^{14}C)_{HClgas}$ = amount of ^{13}C+^{14}C CO_2 in the gas phase from the washing procedure with 0.1 M HCl (mol)

$(^{13}C+^{14}C)_{missing}$ = unidentified ^{13}C+^{14}C sink in the experiment based on mass balance calculations

6.3 DisCo project: Thermodynamics of Cr-doped UO_2 fuel

LES is participating in the EU project **DisCo** (Modern spent fuel **Dis**solution and chemistry in failed **Co**ntainer conditions) which started on June 1st 2017 on a 4 years basis. LES is involved with the development and application of solid solution models for Cr-doped UO_2 fuel. The aim is to determine the impact of this dopant on the oxygen potential of the fuel, a central parameter affecting system behaviour both under in-reactor and repository conditions. For instance, a high oxygen potential favours the inner-side corrosion of Zircaloy cladding. The main objective of our study in the framework of DisCo is, however, to find out whether the use of Cr-doped fuel could modify the oxidation state of redox-sensitive fission products, as this could affect their source term release and solubility limits.

For this task, a set of thermodynamic data for Cr had to be selected and integrated into the GEMS-PSI code used for the calculations. Standard state thermodynamic data for eskolaite (Cr_2O_3), metallic Cr and other species of interest were adopted from the Tables of BARIN (1989) and their consistency with the experimental data of JEANNIN et al. (1963) and TOKER et al. (1991) was verified. Heat capacities were interpolated from Barin's tabulated data to obtain the coefficients for the 10-term equation built-in in the GEMS-PSI code.

Preliminary calculations were carried out based on an ideal solid solution model with $Cr(III)O_{3/2}$, $U(IV)O_2$ and $U(V)O_{2.5}$ as end-members. The selection of end-members is consistent with the two dominant Cr(III) substitutions in stoichiometric and hyper-stoichiometric urania (MIDDLEBURGH et al. 2012, GUO et al. 2017). Both involve replacement of two regular U(IV) ions by two Cr(III) ions. In stoichiometric UO_2, the charge balance is provided by a vacancy in the oxygen sub-lattice, according to the reaction (6.1). The reactions are set up using a slightly modified form of the standardized Kröger-Vink notation, in which absolute charges are used in place of relative charges for the lattice sites:

$$Cr_2O_3 + 2\ U_u^{4+} + O_o^{2-} <=> 2\ Cr_u^{3+} + V_o^0 + 2\ UO_2 \qquad (6.1)$$

In hyper-stoichiometric UO_{2+x} it is achieved by addition of an interstitial oxygen atom:

$$Cr_2O_3 + 2\ U_u^{4+} + O_i^{2-} + 1/2\ O_2(g) <=> 2\ Cr_u^{3+} + V_i^0 + 2\ UO_{2.5} \qquad (6.2)$$

Note that the latter mechanism involves the oxidation of U^{4+} to U^{5+} and is coupled to pO_2, which is not the case for the former substitution.

Fig. 6.5 shows the results of GEMS calculations in the form of an Ellingham diagram, in which the oxygen potential ($\Delta G_{O2} = -RT\ ln\ pO_2$) is displayed as a function of temperature. The plot also shows the equilibrium oxygen potentials of the pure metal/oxide pairs for selected fission products (from KLEYKAMP 1985) and for pure Cr/Cr_2O_3 (from our selected data).

Two series of calculations, in which Cr(III) is assumed to be incorporated in the aforementioned ternary ideal solid solution, were carried out. The first series (orange line) shows oxygen potentials in equilibrium with a simple system composed only of UO_2 with 0.5 mol% Cr_2O_3 (thus excluding fission products and actinides). Compared to the pure $Cr(s)$-$Cr_2O_3(s)$ equilibrium, slightly lower oxygen potentials were obtained, with the difference increasing with temperature. The second series (violet line) shows the analogous results for a full model spent fuel composition, i.e. including the entire fission products and actinide inventory. The resulting ΔGO_2–values are much higher and cross the field defined by oxygen potential measurements on conventional light water reactor (LWR) fuels taken from the literature (MATZKE 1994 & 1995).

The following conclusions can be drawn from the calculations presented in Fig. 6.5:

(I) The fact that the oxygen potential of the irradiated fuel is calculated to be well above the Cr/Cr_2O_3 curve implies that the stable final oxidation state in the fuel will be Cr(III), independently of the initial oxidation state of Cr.

(II) The calculated difference in oxygen potential between a simple $UO_2 + Cr_2O_3$ system and spent fuel is considerable. Fission reactions during fuel burning produce free oxygen, which is only partially bound to fission products, thus increasing ΔG_{O2} compared to a pure Cr-UO_2 system.

(III) Ideal solid solution calculations for the Cr-doped spent fuel predict oxygen potentials, which fall within the range measured for non-doped LWR fuels. Therefore, they suggest that Cr-doping should not affect the fuel oxygen potential significantly. Changes in the oxidation state of redox-sensitive nuclides are thus not expected.

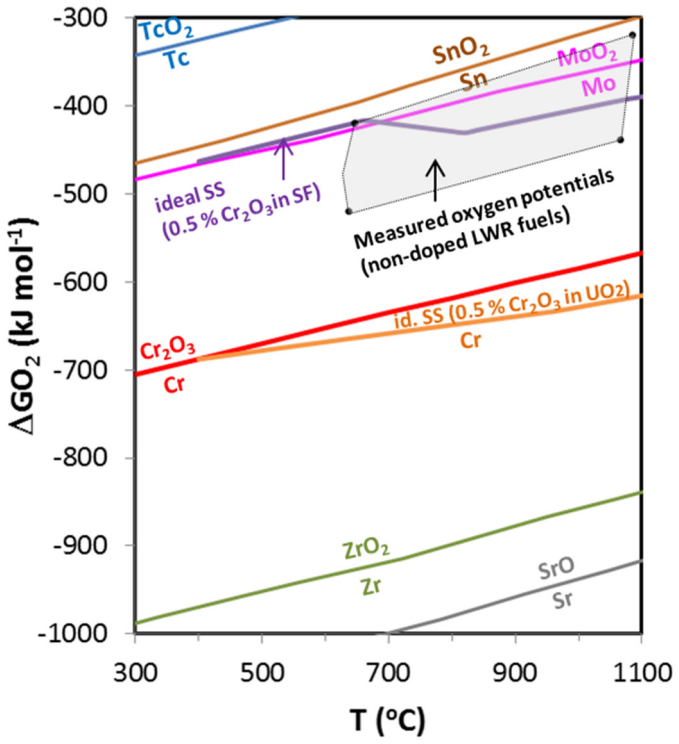

Fig. 6.5: Ellingham diagram showing calculated oxygen potential curves for various systems and redox pairs compared with measured oxygen potentials of non-doped UO_2 fuels.

The calculations shown in Fig. 6.5 are, however, based on the assumption of ideality, which is unrealistic considering the charge and cation size mismatch between Cr(III) and U(IV). In fact, high non-ideality is expected for this system. Moreover, mixing with Pu and minor actinides in the UO_2 phase is not yet taken into account. A major task in the coming project year will be the refinement of the solid solution model to include actinide dissolution and non-ideality for Cr. This will be done by deriving interaction parameters with the help of available experimental data on the solubility of Cr in UO_2 (RIGLET-MARTIAL et al. 2014) and *ab initio* calculations (MIDDLEBURGH et al. 2012, GUO et al. 2017).

Acknowledgment: This project has received funding from the European Union's Horizon 2020 research and innovation programme under grant agreement No. 755443 - DISCO - NFRP-2016-2017/NFRP-2016-2017-1.

6.4 References

BARIN I.B. (1989)
Thermodynamic data of pure substances, VCH Verlagsgesellschaft mbt-l, 0-6940 Weinheim (Vol. 1, p. 418).

CVETKOVIĆ B.Z, SALAZAR G., KUNZ D., SZIDAT S., WIELAND E. (2018a)
Analysis of ^{14}C-containing compounds released by corrosion of irradiated steel using accelerator mass spectrometry. Analyst 143, 3059-3063.

CVETKOVIĆ B.Z, SALAZAR G., KUNZ D., TITS J., SZIDAT S., WIELAND E. (2018b)
Quantification of dissolved organic carbon-14-containing compounds by accelerator mass spectrometry in a corrosion experiment with irradiated steel. Radiocarbon (in press).

CVETKOVIĆ B.Z, ROTHARDT J., BÜTTLER A., KUNZ D., SCHLOTTERBECK G., WIELAND E. (2018c)
Formation of low-molecular-weight organic compounds during anoxic corrosion of zero-valent iron. Environ. Eng. Sci. 35, 447-461.

GUO Z., NGAYAM-HAPPY R., KRACK M., PAUTZ A. (2017)
Atomic-scale effects of chromium-doping on defect behaviour in uranium dioxide fuel. J. Nucl. Mat. 488, 160-172.

JEANNIN Y., MANNERSKANTZ C., RICHARDSON F.D. (1963)
Activities in iron-chromium alloys. Trans. Metallurgical Soc. AIME 227, 300-305.

KLEYKAMP H. (1985)
The chemical state of the fission products in oxide fuels. J. Nucl. Mat. 131, 221-246.

MATZKE H.J. (1994)
Oxygen potential in the rim region of high burnup UO_2 fuel. J. Nucl. Mat. 208, 18-26.

MATZKE H.J. (1995)
Oxygen potential measurements in high burnup UO_2 fuel. J. Nucl. Mat. 223, 1-5.

MIDDLEBURGH S.C., PARFITT D.C., GRIMES R.W., DORADO B., BERTOLUS M., BLAIR P.R., HALLSTADIUS L., BACKMAN K. (2012)
Solution of trivalent cations into uranium dioxide. J. Nucl. Mat. 420, 258-261.

RIGLET-MARTIAL CH., MARTIN PH. ET AL. (2014)
Thermodynamics of chromium in UO_2 fuel: A solubility model. J. Nucl. Mat. 447, 63-72.

TOKER N.Y., DARKEN L.S., MUAN A. (1991)
Equilibrium phase relations and thermodynamics of the Cr-O system in the temperature range of 1500 °C to 1825 °C. Metallurgical Trans. B, 22B, 225-232.

WERSIN P., JOHNSON L.H., SCHWYN B., BERNER U., CURTI E. (2003)
Redox conditions in the near field of a repository for SF/HLW and ILW in Opalinus Clay. Nagra Tech. Rep. NTB 02-13.

WIELAND E., CVETKOVIĆ B.Z., KUNZ D., SALAZAR G., SZIDAT S. (2018)
Carbon-14 speciation during anoxic corrosion of activated steel in a repository environment. *ATW* 63, 34-37.

WIELAND E., HUMMEL W. (2015)
Formation and stability of carbon-14 containing organic compounds in alkaline iron-water-systems: Preliminary assessment based on a literature survey and thermodynamic modelling. Mineral. Mag. 79, 1275-1286.

XU T., SENGER R., FINSTERLE S. (2008)
Corrosion-induced gas generation in a nuclear waste repository: Reactive geochemistry and multiphase flow effects. Appl. Geochem. 23, 3423-3433.

7 THERMODYNAMIC MODELS AND DATABASES

W. Hummel, D.A. Kulik, G.D. Miron (postdoc), T. Thoenen

7.1 Introduction

The aim of this project is to develop thermodynamic models and databases to be applied in the preparation of various reports for the general license applications (RBG). Solubility and sorption databases and synthesis reports are an important part of the documentation for RBG.

The timely finalisation of the thermodynamic database is an important task because the carefully selected thermodynamic data provide the basis for the solubility databases, the development of the sorption databases and simulation of the repository *in situ* conditions. The consistent and consequent use of the approved thermodynamic dataset throughout all types of thermodynamic calculations is of crucial importance.

To support the thermodynamic calculations and maintenance of thermodynamic databases, the GEM Software (GEMS) code collection has been developed at PSI/LES since 2000 by a community team lead by D.A. Kulik. The most resent application of GEMS focuses on the development of new solid solution models for calcium silicate hydrate (C-S-H) phases of variable composition. These phases determine the most relevant properties and durability of hydrated cement pastes and concretes.

7.2 Update of the Thermodynamic Data Base (TDB)

A high-quality Thermodynamic Data Base (TDB) is currently in place. This database needs to be kept state-of-the-art and remaining gaps need to be filled where this is safety relevant. As the availability of an approved TDB is an essential prerequisite for preparing solubility limits and sorption database reports for the next safety assessments related to Nagra's general license applications (RBG), updates and filling gaps of the TDB need to be finished before work on solubility and sorption databases commences, planned for 2021. The current update of TDB has been planned for the period 2017-2019 with a final document to be published in 2020.

The TDB update has been started in 2017 with reviews of Hg (HUMMEL 2017a), Cu (THOENEN 2017a), Pb (HUMMEL 2017b), Fe (THOENEN 2017b) and Po (HUMMEL 2017c). With the exception of Fe all the other elements are new in the TDB.

The review work was continued in 2018 with the update of Nb and Sn data, and the review of data for Ti, Ag, Ac, Pa and Cf which are new elements in the TDB.

In 2019, the review work will be finished with the reviews of selected organic ligands, silicates, Pd, and the rare earth elements Sm, Eu and Ho.

7.2.1 Tin

The evaluation of thermodynamic data for Sn was based on the NEA review by GAMSJÄGER et al. (2012). The NEA reviews are widely recognized as very carefully executed and valuable critical reviews and the selected data are of high quality. The volume on Sn makes no exception. Striving for high quality, however, may sometimes lead to pitfalls, as shown in the case of the temperature dependence of the stability constants of Sn(II) chloride. These constants were studied by MÜLLER & SEWARD (2001) using UV spectrophotometry at saturated vapor pressure and temperatures between 25 and 300˚C. GAMSJÄGER et al. (2012) accepted these data and included the stability constants at 25˚C in their SIT analyses, together with stability constants determined in several other studies. Nonetheless, GAMSJÄGER et al. (2012) did not take advantage of the data obained at higher temperatures for extracting temperature functions and values for $\Delta_r H_m°$(298.15 K) and $\Delta_r C_{p,m}°$(298.15 K) and considered calorimetric determinations of $\Delta_r H_m°$(298.15 K) for the formation reactions of $SnCl^+$ and $SnCl_2$(aq) as more reliable. However, even if they appear to be of very good quality and were even measured at various ionic strengths, they are either not sufficient to extrapolate $\log_{10}\beta°$ to higher temperatures, as in the case of $SnCl_2$(aq), which requires a three-term temperature extrapolation equation

$$\log_{10}\beta^{\circ}(T) = \log_{10}\beta^{\circ}(T_0) - \left(\frac{1}{T} - \frac{1}{T_0}\right)\frac{\Delta_r H^{\circ}_m(T_0)}{R\ln(10)} - \left(1 - \frac{T_0}{T} + \ln\frac{T_0}{T}\right)\frac{\Delta_r C^{\circ}_{p,m}(T_0)}{R\ln(10)}$$

involving $\log_{10}\beta°$(298.25 K), $\Delta_r H_m°$(298.15 K), and $\Delta_r C_{p,m}°$(298.15 K) — instead of the linear two term van 't Hoff equation — involving $\log_{10}\beta°$(298.25 K) and $\Delta_r H_m°$(298.15 K) — (see Fig. 7.1 b), or are clearly discordant to the measured data, as is the case for $SnCl^+$ (see Fig. 7.1 a). Therefore, we decided to include in TDB 2020 the values for $\Delta_r H_m°$(298.15 K) and $\Delta_r C_{p,m}°$(298.15 K) derived from the temperature variation of the stability constants and not the calorimetrically determined value for $\Delta_r H_m°$(298.15 K).

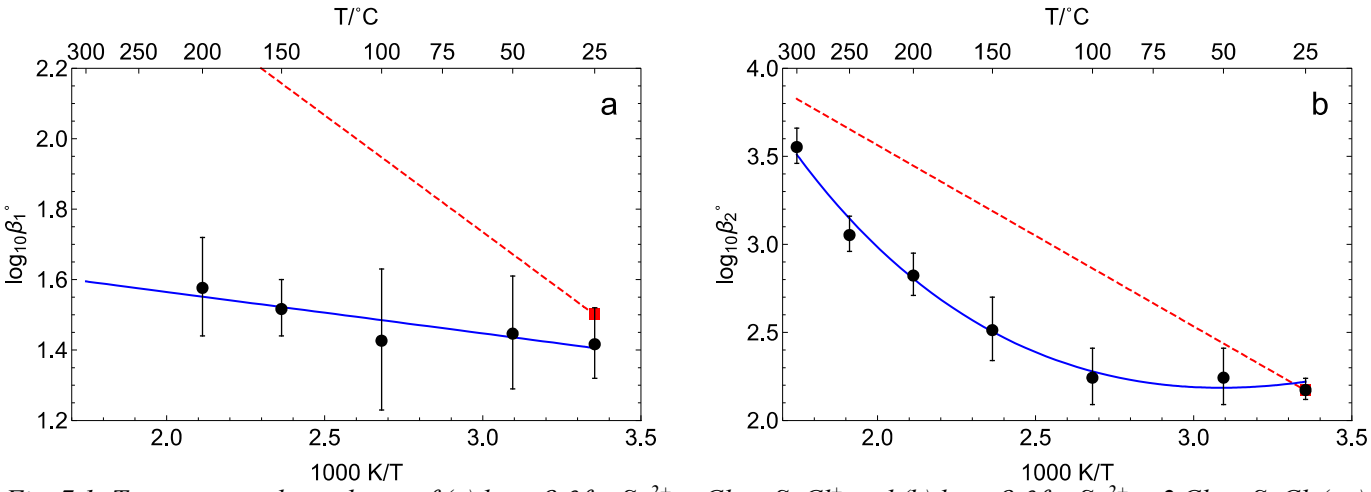

Fig. 7.1: Temperature dependence of (a) $\log_{10}\beta_1°$ for $Sn^{2+} + Cl^- \rightleftharpoons SnCl^+$ and (b) $\log_{10}\beta_2°$ for $Sn^{2+} + 2\ Cl^- \rightleftharpoons SnCl_2(aq)$. Experimental data (filled circles) by MÜLLER & SEWARD (2001). The data can be represented by the functions (a) $\log_{10}\beta_1°(T) = 1.800 - 117.6/T$ and (b) $\log_{10}\beta_2°(T) = -63.92 + 3158/T + 9.759\ \ln T$ (blue lines). For comparison, (a) $\log_{10}\beta_1°(298.15)$ and (b) $\log_{10}\beta_1°(298.15)$ selected by GAMSJÄGER et al. (2012) (filled squares) are shown together with the extrapolation to higher temperatures (dashed lines) based on the calorimetric values for $\Delta_r H_m°$ selected by GAMSJÄGER et al. (2012).

7.2.2 Silver

If the speciation and solubility of silver is calculated under reducing conditions with data usually found in thermodynamic databases, unusual results are obtained. With decreasing redox potential metallic silver, Ag(cr), becomes the thermodynamically stable solid phase and the calculated solubility of silver in water drops to improbably low values. The reason for these strange results is the ignorance of dissolved silver in redox state zero, Ag(aq), in all thermodynamic data bases (HUMMEL 2017d).

In the chemically similar system of the heavy metal mercury, metallic mercury, Hg(l), becomes the stable phase under reducing conditions. Here, we find that the existence of the species Hg(aq) and the solubility of mercury, Hg(l) ⇌ Hg(aq), is well established (CLEVER et al. 1985) and is now included in TDB 2020 (HUMMEL 2017a).

By contrast, the experimental determination of the solubility of metallic silver, Ag(cr) ⇌ Ag(aq), by KOZLOV & KHODAKOVSKIY (1983) and DOBROWOLSKI & OGLAZA (1963) went unnoticed. The very similar values for the solubility of Hg(aq) and Ag(aq) at 25°C and the also similar temperature dependence (Fig. 7.2) might be just coincidences. Nevertheless, thermodynamic data for Ag(aq) are now included in TDB 2020 which will prevent the above-mentioned improbable modelling results in future TDB applications.

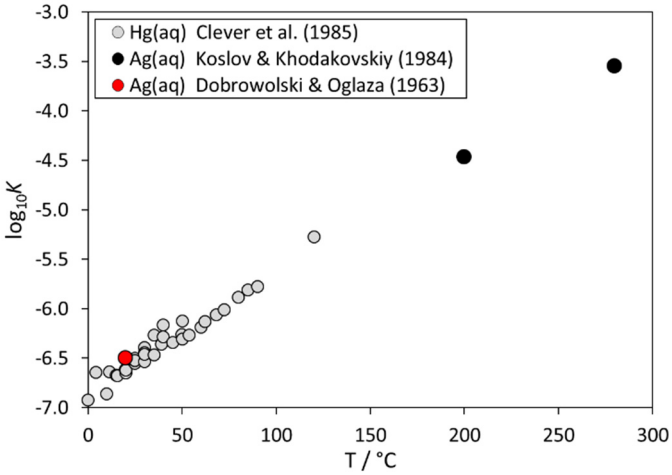

Fig. 7.2: Temperature dependence of $\log_{10}K$ for Hg(l) ⇌ Hg(aq) and Ag(cr) ⇌ Ag(aq).

7.3 New solid-solution model of C-S-H with alkali and aluminium uptake

Calcium silicate hydrate (C-S-H) phases of variable composition determine the most relevant properties and durability of hydrated cement pastes and concretes. Hence, accurate thermodynamic modelling predictions of stability, density, composition and solubility of C-S-H (including water content and minor cations Na, K, Al, Sr, U, Zn, ...), in response to changes in cement recipe, water addition, humidity, temperature, carbonation, leaching, and other factors, comprise a major challenge in cement chemistry and in the use of cement materials as a waste matrix or repository backfill.

The actual atomistic understanding (KUNHI MOHAMED et al. 2018) suggests that most varieties and compositions of C-S-H can be derived from 14Å- or 11Å- tobermorite structures by introducing various defects, i.e. substitutions of silica by other moieties or vacancies at bridging tetrahedral BT sites, as well as by related (via the charge balance) cation- or vacancy substitutions at interlayer cationic IC sites; the non-gel water content of C-S-H is determined by a substitution of H_2O by vacancy at interlayer water IW sites in response to relative humidity (Fig. 7.3).

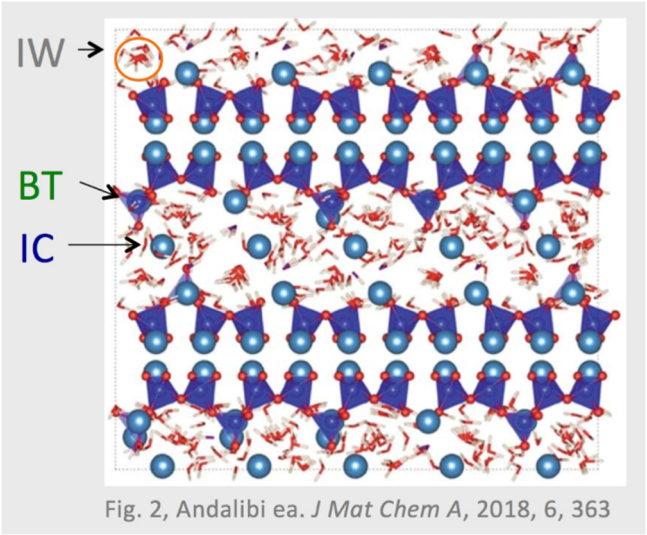

Fig. 7.3: C-S-H structure based on tobermorite model with defects in the tetrahedral chain. The model includes sublattice sites: IW: Interlayer Water (species: H_2O, Va); BT: Bridging Tetrahedral (Si, Al, Ca, Va); IC: Interlayer Cation (Ca, K, Na, Va). Va stands for a vacancy.

In chemical thermodynamic terms, this can be expressed by modelling C-S-H as a sublattice solid solution, where the mixing occurs by simultaneous substitutions of moieties and vacancies in two or three sublattices, i.e. sets of all structural sites of the same type (KULIK 2011). To certain extent, such models are consistent with the atomistic structure of the solid, and thus are expected to be more flexible, predictive, and incremental than older semi-empirical models with simple mixing of end members.

Our newly developed "level 3" CNKASH sublattice solid solution model (KULIK et al. 2018; MIRON et al. 2018) is capable of describing composition, solubility, density, non-gel water content, and mean silicate chain length (MCL) in a wide range of Ca/Si ratios. The main assumption, supported by results of CHURAKOV et al. (2014) and CHURAKOV & LABBEZ (2017), is that the charges acting on IC sites originate at BT sites due to a partial deprotonation of OH groups sitting either on a bridging silicon (aluminum) or on a dimeric silicon. End members can be constructed by permutation of moieties using a template formula IC:BT:IW:[DU], where [DU] is a constant dimeric unit of the tobermorite structure; IW site is occupied by H_2O or vacancy; Ca and Al enter both BT and IC sites, whereas Na and K probably enter IC sites only. Moieties and vacancies in BT and IC sites (Fig. 7.4) are chosen to provide charge-compensated end members and to yield realistic non-gel water contents at various Ca/Si mole ratios between 0.67 and 2.0 and full hydration at 100% relative humidity. We were not sure if Na and K moieties in BT sublattice sites are really needed, but included them into the initial sublattice model. The vacancy in IW sites was added for future extensions of the model to cover partially dried C-S-H phases, but was not used here.

Due to the complexity of sublattice solid solution models, with many parameters to be adjusted at the same time, we used GEM-Selektor and GEMS3K codes (KULIK et al. 2013) with the TSolMod library of solution models (WAGNER et al. 2012) and the GEMSFITS code (MIRON et al. 2015) for multiple parameter optimization following a stepwise fitting strategy. Thermodynamic data for other phases except C-S-H were taken from PSI/Nagra (THOENEN et al. 2014) and Cemdata18 (LOTHENBACH et al. 2018) chemical thermodynamic databases.

Sites	IC (interlayer cation)		BT (bridging tetrahedral)		IW (interlayer water)		DU (dimeric unit)	
Stoich. factor	1		1		2		1	
Moieties (species)	H^+	v	SiO_2OH^-	S	H_2O	h	$[(CaSiO_3)_2H_2O]^0$	T
	$CaOH^+$	C	OH^-	v	Va	v		
	Na^+	N	$CaOOH^-$	C				
	K^+	K	NaO^-	N	← Needed or not?			
	AlO^+	A	KO^-	K				
			AlO_2^-	A				

Fig. 7.4: Moieties chosen to substitute in different sublattices in C-S-H structure (those excluded from the final model are indicated in grey font).

At step 1, several selected experimental solubility datasets were used for parameter optimization restricted to the C-S-H sub-system at 25 °C (298.15 K), 1 bar. To improve the fit to MCL data derived from ^{29}Si NMR spectroscopy, the MCL data were also involved. Standard Gibbs energies G^o_{298} of six end members, with four regular site interaction parameters, and optionally G^o_{298} of $CaSiO_3$(aq) complex as a fitting parameter, were optimized (Fig. 7.5).

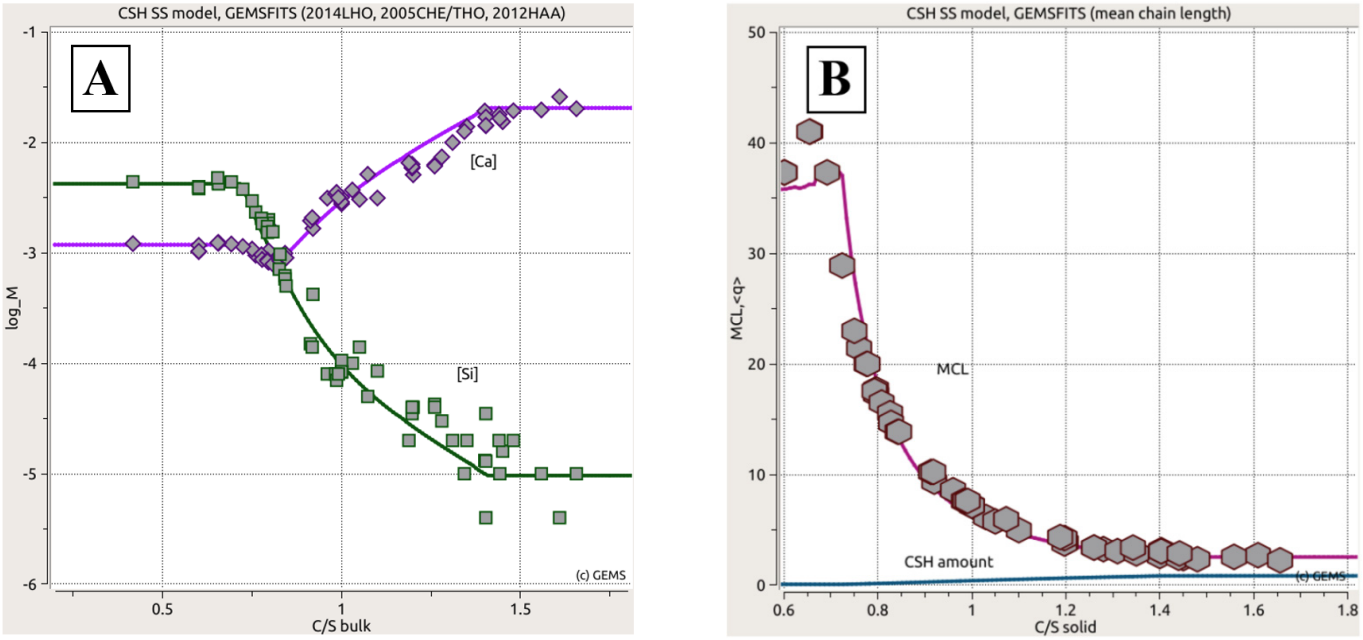

Fig. 7.5: C-S-H sub-model comparison between measured and calculated values for A) Solubility of C-S-H; B) MCL as a function of bulk Ca/Si mole ratio (C/S). Experimental data points from L'HÔPITAL (2014), CHEN et al. (2004), and HAAS & NONAT (2015).

At step 2, selected experimental datasets on the Na and K uptake in C-S-H were used to refine G^{o}_{298} values and interaction parameters for the added moieties and end members, while keeping constant those previously optimized for the C-S-H sub-system. Initially we assumed that K and Na can enter both sublattices (see Fig. 7.4), but the fitting results showed that alkalis most probably enter IC sites only. This reduces the number of added end members from six to three, and the number of site interaction parameters from five to two per cation. Good fits (not shown here) demonstrated that the model is indeed incremental and can be extended stepwise for more cations of interest for cement chemistry and waste management. Even though the scarce MCL dataset for the C-Na-S-H sub-system was not used in fitting, the model independently predicts the decrease in MCL upon the alkali uptake (Fig. 7.6). This remarkable feature shows that, even if Na or K ions most probably do not enter BT sites, they still compete with Ca in the interlayer, thus forcing more Ca into BT sites, which causes a decrease in the MCL.

The resulting internally consistent set of parameters (manuscript in preparation) can now be used to model the uptake of Na and K in fully hydrated C-S-H phases at various Ca/Si ratios and from low to high Na/Si or K/Si ratios. Further model extensions for Al entering BT and IC sites comprises the on-going work. It is already clear that the CNKASH "level 3" model performs more accurately than any previous thermo-

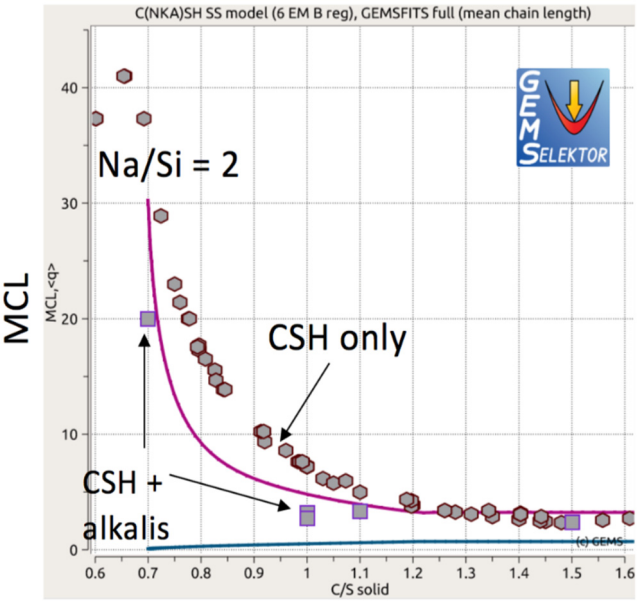

Fig. 7.6: C-Na-S-H solid solution model prediction (curve) of the MCL shift upon addition of Na to the C-S-H sub-system. No fitting to MCL data (squares) in the C-Na-S-H system has been performed.

dynamic model of C-S-H, and can be efficiently used in studies of ordinary, CSA, and blended hydrated cements.

This study is part of the SNF CASH-II project 200021_169014/1 (lead B. Lothenbach, Empa).

7.4 Cemdata18 chemical thermodynamic database

Thermodynamic modelling can reliably predict hydrated cement phase assemblages and chemical compositions, including their interactions with prevailing service environments, provided that an accurate and complete thermodynamic database is used. D.A. Kulik and G.D. Miron (LES) contributed to the compilation and critical assessment of the Cemdata18 database (LOTHENBACH et al. 2018) covering hydrated Portland, calcium aluminate, calcium sulfoaluminate and blended cements, as well as alkali-activated materials for the temperature range from 0 to 100 ºC and ambient pressure. The new database includes thermodynamic properties determined from various experimental data published in recent years, and is available in GEMS and PHREEQC computer code formats (from http://www.empa.ch/cemdata). Solid solution models for AFm, AFt, C-S-H, and M-S-H are also included.

Some popular geochemical codes such as PHREEQC (PARKHURST & APPELO 1999) use the LMA (Law of Mass Action) reactions-based thermodynamic data. In the past, there were third party attempts to recast the GEMS Cemdata TDB into PHREEQC format, e.g. by JACQUES et al. (2013). Hence, we decided to export the original Cemdata18 TDB from GEM (Gibbs Energy Minimization) format (KULIK et al. 2013) into the PHREEQC "dat" format. This has been done using a ThermoMatch code (MIRON et al. in preparation), our new tool for managing thermodynamic data both for substances (GEM format) and reactions (LMA format) in a modern graph database.

The Cemdata18 for the GEM dataset was imported from the GEM-Selektor code into ThermoMatch, which automatically generated a set of reactions from a list of substances and a selection of master species, and exported this set into a PHREEQC*.dat file. The supplementary data for aqueous, gaseous and solid species required for Cemdata18 TDB were selected from the PSI/Nagra 12/07 database (THOENEN et al. 2014). Based on generic predominance in cement porewater, the following *master* species were chosen: Ca^{2+}, Mg^{2+}, Sr^{2+}, Na^{+}, K^{+}, H^{+}, CO_3^{2-}, SO_4^{2-}, Cl^{-}, NO_3^{-}, AlO_2^{-}, FeO_2^{-}, SiO_2^{0}, H_2O^{0}. For the remaining *product* species, the reactions of formation from master species were automatically generated together with their thermodynamic properties (effects) at 25 °C and 1 bar. To allow calculations of $\log_{10}K°$ as a function of temperature up to 100°C, the parameters for $\log_{10}K° = f(T)$ analytical expressions were derived using the 3-term extrapolation method that assumes the $\Delta_r Cp°$ to be not zero and independent of temperature.

7.5 References

CHEN J.J., THOMAS J.J., TAYLOR H.F.W., JENNINGS H.M. (2004)
Solubility and structure of calcium silicate hydrate. Cem. Concr. Res. 34, 1499-1519.

CHURAKOV S.V., LABBEZ CH., PEGADO L., SULPIZI M. (2014)
Intrinsic acidity of surface sites in calcium cilicate hydrates and its implication to their electrokinetic properties J. Phys. Chem. C, 118, 11752-11762.

CHURAKOV S.V., LABBEZ C. (2017)
Thermodynamics and molecular mechanism of Al incorporation in calcium silicate hydrates. J. Phys. Chem. C, 121, 4412-4419.

CLEVER H.L., JOHNSON S.A., DERRICK M.E. (1985)
The solubility of mercury and some sparingly soluble mercury salts in water and aqueous electrolyte solutions. J. Phys. Chem. Ref. Data 14, 631-679.

DOBROWOLSKI J., OGLAZA J. (1963)
Zastoswanie izotopu ^{110}Ag do badania rozpuszczalnosci srebra metalicznego i chlorku srebra w roztworach wodnych siarczanu cynku [use of the isotope ^{110}Ag in studying the solubility of silver metal and silver chloride in aqueous solutions of zinc sulphide]. Nucleonika 8, 79-81 (in Polish).

GAMSJÄGER H., GAJDA T., SANGSTER J., SAXENA S.K., VOIGT W. (2012)
Chemical Thermodynamics of Tin. Chemical Thermodynamics Series, Vol. 12, OECD NEA, Paris, France, 609 pp.

HAAS J., NONAT A. (2015)
From C–S–H to C–A–S–H: Experimental study and thermodynamic modelling. Cem. Concr. Res. 68, 124–138.

HUMMEL W. (2017a)
The PSI Chemical Thermodynamic Database 2020: Data Selection for Mercury. PSI Technical Report TM-44-17-04, Paul Scherrer Institut, Villigen, Switzerland.

HUMMEL W. (2017b)
The PSI Chemical Thermodynamic Database 2020: Data Selection for Lead. PSI Technical Report TM-44-17-06, Paul Scherrer Institut, Villigen, Switzerland.

HUMMEL W. (2017c)
The PSI Chemical Thermodynamic Database 2020: Data Selection for Polonium. PSI Technical Report TM-44-17-08, Paul Scherrer Institut, Villigen, Switzerland.

HUMMEL W. (2017d)
Chemistry of selected dose-relevant radionuclides. Nagra Tech. Rep. NTB 17-05.

JACQUES D., WANG L., MARTENS E., MALLANTS D. (2013)
Thermodynamic database (CEMDATA07) for concrete in PHREEQC format. Belgian Nuclear Research Centre SCK·CEN, Mol, Belgium.

KOZLOV V.K., KHODAKOVSKIY I.L. (1983)
The thermodynamic parameters of atomic silver in aqueous solution at 25-280 °C. Geochemistry International 20, 118-131 (translated from Geokhimiya 6 (1983) 836-848).

KULIK D.A. (2011)
Improving the structural consistency of C-S-H solid solution thermodynamic models. Cem. Concr. Res. 41, 477-495.

KULIK D.A., WAGNER T., DMYTRIEVA S.V., KOSAKOWSKI G., HINGERL F.F., CHUDNENKO K.V., BERNER U. (2013)
GEM-Selektor geochemical modeling package: revised algorithm and GEMS3K numerical kernel for coupled simulation codes. Comp. Geosci. 17, 1-24.

KULIK D.A., MIRON G.D., LOTHENBACH B. (2018)
A realistic three-site solid solution model of C-S-H. Goldschmidt 2018 Conference, Boston MA, USA, 12-17 August 2018.

KUNHI MOHAMED A., PARKER S.C., BOWEN P., GALMARINI S. (2018)
An atomistic building block description of C-S-H - Towards a realistic C-S-H model. Cem. Concr. Res. 107, 221-235.

L'HÔPITAL E. (2014)
Aluminium and alkali uptake in calcium silicate hydrates (C-S-H). PhD Thesis.
(https://doi.org/10.5075/epfl-thesis-6389)

LOTHENBACH B., KULIK D.A., MATSCHEI T., BALONIS M., BAQUERIZO L., DILNESA B.Z., MIRON G.D., MYERS R. (2018)
Cemdata18: A chemical thermodynamic database for hydrated Portland cements and alkali-activated materials. Cem. Concr. Res. in press (https://doi.org/10.1016/j.cemconres.2018.04.018).

MIRON G.D., KULIK D.A., DMYTRIEVA S.V., WAGNER T. (2015)
GEMSFITS: Code package for optimization of geochemical model parameters and inverse modeling. Appl. Geochem. 55, 28-45.

MIRON G.D., KULIK D.A., LOTHENBACH B. (2018)
Parameterization of a new C-S-H solid solution model for alkali uptake. Goldschmidt 2018 Conference, Boston MA, USA, 12-17 August 2018.

MÜLLER B., SEWARD T.M. (2001)
Spectrophotometric determination of the stability of tin(II) chloride complexes in aqueous solution up to 300˚C. Geochim. Cosmochim. Acta, 65, 4187-4199.

PARKHURST D.J., APPELO C.A.J. (1999)
User's Guide to PHREEQC (version 2) - A computer program for speciation, batch reaction, one dimensional transport, and inverse geochemical calculations. Water-Resources Investigations Report 99-4259, USGS, Denver, Colorado.

THOENEN T., HUMMEL V., BERNER U., CURTI E. (2014)
The PSI/Nagra Chemical Thermodynamic Data Base 12/07, PSI Bericht 14-04, Paul Scherrer Institut, Villigen, Switzerland.

THOENEN T. (2017a)
The PSI Chemical Thermodynamic Database 2020: Data Selection for Copper. PSI Technical Report TM-44-17-05, Paul Scherrer Institut, Villigen, Switzerland.

THOENEN T. (2017b)
The PSI Chemical Thermodynamic Database 2020: Data Selection for Iron. PSI Technical Report TM-44-17-07, Paul Scherrer Institut, Villigen, Switzerland.

WAGNER T., KULIK D.A., HINGERL F.F., DMYTRIEVA S.V. (2012)
GEM-Selektor geochemical modeling package: TSolMod library and data interface for multicomponent phase models. Can. Mineral. 50, 1173-1195.

8 FUNDAMENTAL ASPECTS OF MINERAL REACTIVITY AND STRUCTURAL TRANSFORMATIONS

S.V. Churakov, Th. Armbruster, U. Eggenberger, G. Cametti, F. Di Lorenzo, M. Fisch, I. Kurganskaya, G. Weibel, R. Schliemann (PhD student)

8.1 Introduction

Since 2015, PSI/LES and the Institute for Geological Science at the University of Bern (UBERN/IfG) have established research collaboration in the field of mineralogy and crystallography. The research field of the Mineralogy group at the University of Bern covers fundamental aspects of mineral dissolution and precipitation, chemical aspects of crystal structure stability and temperature driven phase transitions in minerals. The dedicated laboratories operated by the group are equipped with powder and single-crystal diffractometers for structural studies of minerals and an atomic force microscopy laboratory for *in situ* characterization of mineral surfaces. The experimental studies are widely supported by modelling activities. Main research activities are focused on structural transformation in natural and synthetic zeolite material and on the mechanistic understanding of dissolution/precipitation reaction pathways on minerals surfaces. These processes are investigated by molecular simulations, crystal structure refinement and surface analysis.

8.2 Crystal chemistry and thermal stability of zeolites

Natural zeolites are mainly framework silicates with large open cavities occupied by cations and H_2O molecules. These minerals are abundant all over the world and applied as ion exchangers for large-scale remediation (e.g. radionuclides extraction from contaminated soils in Chernobyl and Fukushima). The arrangement of extra-framework cation of natural zeolites is studied under different environmental conditions (temperature and humidity) by single crystal X-ray diffraction methods to understand the bonding between framework and cavity occupants and its influence on framework distortions. This basic research approach has strong bearing on application of zeolites in chemical technology and environmental remediation.

Zeolites are characterized by reversible hydration/dehydration and the ability to exchange, to different extent, their extra-framework cations in contact with aqueous solutions. Structural rearrangements in zeolite-type materials arise as a consequence of the loss of water previously bonded to extra framework cations. Such changes can involve severe structural modifications (decrease of unit-cell volume, channels contraction and in some cases structural collapse) and lead to the formation of new phases. For this reason, the study of the thermal stability of this group of minerals, from a structural point of view, is particularly interesting considering that many applications involved a pre-heat treatment of the zeolites.

8.2.1 Thermal behavior of stilbite and stellerite: Memory effect of the STI framework type

This project addresses the role of extra-framework cations in **STI** framework-type zeolites, namely barrerite $Na_{16}Al_{16}Si_{56}O_{144}\cdot 52H_2O$, stellerite $Ca_8Al_{16}Si_{56}O_{144}\cdot 58H_2O$ and stilbite $Na_2Ca_8Al_{18}Si_{54}O_{144}\cdot 60H_2O$. The thermal behavior of Na-exchanged stellerite and stilbite was investigated by *in situ* single crystal X-ray diffraction. For comparison with the exchanged forms, new data were collected on natural stellerite and stilbite under the same experimental conditions. With the increase in temperature, strong disorder at T and O sites of the tetrahedra of the four-membered ring developed in natural forms. Such disorder was associated with the rupture of T-O-T connections and transition from the A to the B phase (Fig. 8.1). Differently from previous studies, stellerite B at T >300°C was found to be monoclinic (space group *A*2/*m*). In addition, at 400°C, a new T-O-T connection occurred, analogous to that in the B phase of barrerite (CAMETTI et al. 2016).

At room temperature Na-stellerite and Na-stilbite were stable as monoclinic phases with space group *F*2/*m*. Upon heating, they showed the same structural modifications as observed in natural barrerite and Na-barrerite and adopted space group *A*2/*m*. However, compared to natural stellerite and stilbite different T-O-T connections were ruptured in Na-exchanged forms leading to a different topology of the B phase. The total volume contraction measured for the Na-exchanged forms was -16% at 350°C as compared to -8% in the pristine materials. The highly condensed D phase, which does not form in natural stellerite and stilbite, was obtained by heating a Na-stellerite crystal *ex-situ* at 525°C. The structure corresponded to the D phase of natural barrerite and Na-barrerite (CAMETTI et al. 2017).

All investigated **STI** members, after being exchanged with Na, have identical symmetry and demonstrate corresponding behavior upon heating and associated dehydration. Thus, a previously assumed memory

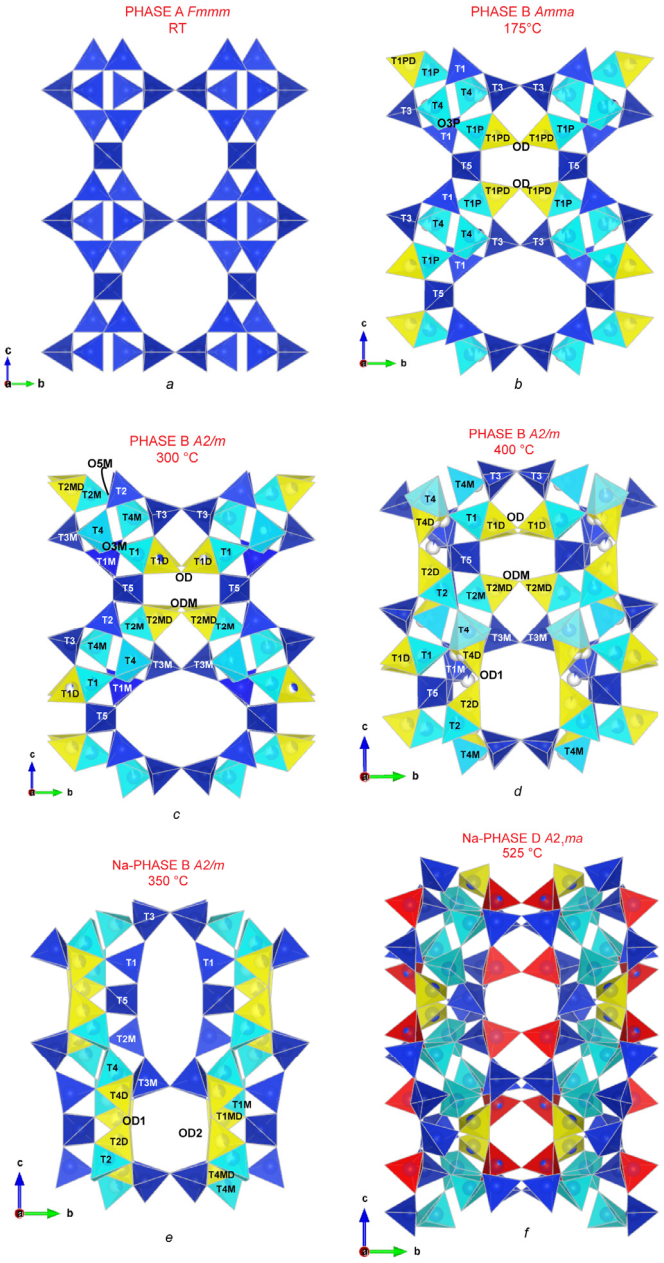

Fig. 8.1: Framework of the A phase of stellerite at RT (a) and of the B phase of stellerite at 175°C (b) and 300°C (c). (Si,Al)O_4 tetrahedra are depicted in blue. The original tetrahedra involved in the T-O-T rupture are shown in cyan whereas the new T sites originating as a consequence of the T migration are yellow. Sites are labelled to show the correspondence between the nomenclature of tetrahedra in orthorhombic and monoclinic symmetry. (d) Framework of the stellerite B phase at 400°C. The irregular shape of (Si,Al)O_4 tetrahedra is due to split oxygen sites. Partially coloured spheres show low occupancy T sites. (e) B phase of Na-exchanged forms of stellerite and stilbite at 350°C. (f) D phase of Na-stellerite obtained ex-situ in air. Red tetrahedra correspond to those flipped inside the cage (CAMETTI et al. 2017).

effect of the symmetry of the natural parent structure is not confirmed. These results demonstrate that even minor changes in extra framework composition influence the dehydration path of the minerals, changing their stability field and leading to the formation of different structural modifications.

8.2.2 New topology of B-levyne under quasi-equilibrium conditions

Ca-Levyne is a common mineral in vugs of massive volcanic rocks. Its chemical composition shows a rather constant Si/(Si + Al) ratio (0.62–0.70) with Ca and Na as the dominant extra framework cations. The mineral group levyne, belongs to a natural porous material with **LEV** topology. Microporous materials of **LEV** framework-type are characterized by a sequence of single six-membered rings (6mR) and double six-membered rings (D6R) stacked along the c-axis following the ...AABCCABBCAA… sequence. The dehydration behavior of natural Ca-levyne was investigated from 25 to 400°C by *in situ* single-crystal X-ray diffraction under dry conditions. The dehydration started at 50°C. From 125 to 250°C the structure changed to B-levyne topology, characterized by statistical breaking of T1-O-T1 bonds in the original D6R units. At 275°C, additional rupture of T2-O-T2 bonds in 6mR units started. This second rupture, associated with the release of remaining water, was not reported before. At 300°C, the structure is assumed to be anhydrous. The new B-levyne topology, referred to B'-levyne, is characterized by 37% T1B and 15% T2B. These are new tetrahedral sites arising as a consequence of the T-O-T breaking process. In contrast to the T1B site, T2B is at general position, originating from a system of mutually exclusive T2B face sharing tetrahedra. Complete migration of T sites to the new positions would lead to different **LEV** topologies with different kinds of cages and, as a consequence, of stacking sequences depending on the position occupied by the T2B tetrahedra (Fig. 8.2). The different results obtained in this study compared to previous ones, confirm that the applied experimental set-up is fundamental in tracking the transformations upon dehydration in zeolitic materials. Understanding these differences is crucial for subsequent applications of these microporous compounds (CAMETTI 2018).

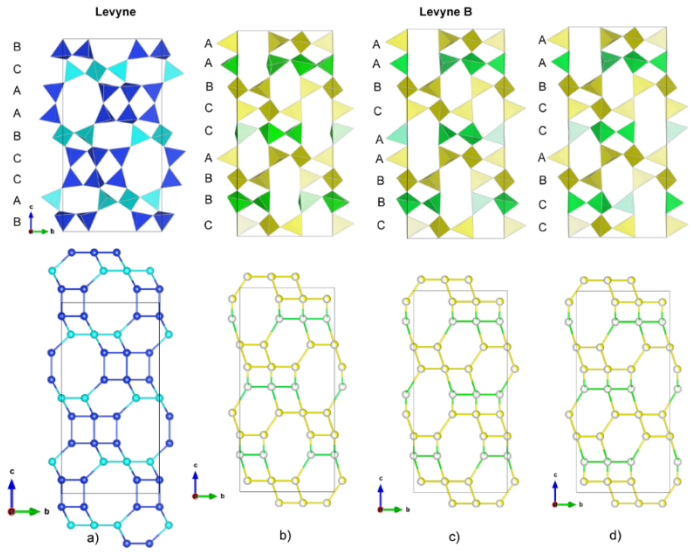

Fig. 8.2: Stacking sequence (polyhedral and nodal representation) of the LEV framework type for Ca-levyne at RT (a) and of the new topology of levyne B considering 100% migration of T1 and T2 sites toward the new positions, T1B and T2B. Three possible topologies of levyne B (b,c,d), obtained by the random removal of one of the two T2B tetrahedra, mutually exclusive, are shown.

8.3 Clay mineral dissolution mechanism from atomic scale simulations

Due to the high sorption capacity, clay minerals and clay-rich rocks are widely used as backfill material in disposal sites to protect the environment from toxic waste, heavy metal contaminants, and radionuclides. The interplay between adsorption and desorption, crystal growth and dissolution and changes in porewater chemistry is of key importance for the prediction of the pollutants transport and their retention in the geochemical environment over time. Atomistic simulations can help to obtain a deeper understanding of the underlying mechanisms and their respective time scales. In particular, the dissolution and growth of clay platelets at the edge sites are most likely to modify the surface topography and the availability of sorption sites. These processes are responsible for a durable entrapment of contaminants since they involve direct structural incorporation or release of hazardous ions.

In the SNF funded PhD project (SNF-200021 165548) *"Dissolution, growth and ion uptake at phyllosilicate surfaces: Coupling atomistic interactions at the mineral-water interface with Kinetic Monte Carlo (KMC) model"* a coarse grain simulation strategy is used to formulate a mechanistic model for clay minerals reactivity. KMC simulations have been widely applied for the modelling mineral dissolution (KURGANSKAYA & LUTTGE 2013a & b). The most important input parameters for KMC simulations are the free energy path for attachment and detachment of the Si tetrahedra and Al octahedra to the edge surface of clay particles. To obtain these parameters the molecular mechanism of dissolution of clay minerals at edge surfaces was studied by DFT-based metadynamics simulations.

The breaking of chemical bonds at mineral surfaces is associated with a high activation energy. In particular at low temperatures, the kinetic energy of atoms is not sufficient to overcome the activation barriers. Therefore, the dissolution process cannot be observed in a short equilibrium molecular dynamics simulation. To overcome the time scale problem the so-called metadynamics approach is applied (LAIO & PARRINELLO 2002). In the metadynamics method the dissolution process is described by a set of reaction coordinates (e.g. coordination number and/or bond distances). During the simulation, the system is biased via time-dependent external potential to facilitate the transition from reactants to products. At the end of the simulations, the corresponding biasing time dependent potential represents the activation free energy of the reaction.

Fig. 8.3 shows a sequence of snapshots representing stepwise detachment of Si tetrahedra from the (110) edge surface. The simulation results show that the dissolution process starts with the hydrolysis of the Si-O-Al bond, which is the weakest in the system. A bi-dentate dangling Si tetrahedron connected to the tetrahedral sheet is formed. In the next series of steps Si-O-Si bonds are hydrolyzed and the newly formed $Si(OH)_4$ group leaves the surface. The simulations for the idealized pyrophyllite surface are now finalized. Ongoing simulations aim at investigating the role of Al-Mg and Al-Si substitutions on the activation barrier for the dissolution process.

8.4 Kinetics of Pb^{2+} uptake via carbonation of Pb^{2+}-bearing solutions.

The formation of carbonate minerals is raising renewed interest due to the development of carbon storage techniques which aim at the mitigation of anthropogenic release of carbon dioxide release to the atmosphere. In this context, the possibility of combining geological carbon storage (GCS) with the disposal of contaminated water could help to mitigate the high cost of conventional GCS processes.

Lead and other divalent transition metals (i.e. Cd, Co, Ni, Zn, etc.) are released from mining processes and recycling. The disposal of waste waters containing heavy metals undergoes specific laws for the protection of the environment. The combination of GCS with heavy-metals decontamination could help reducing the overall economic impact of the environmental remediation.

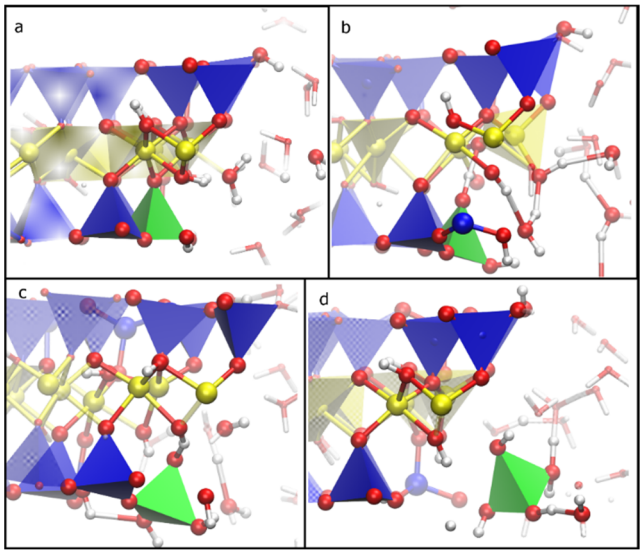

Fig. 8.3: Step-by-step detachment mechanism of a silicon tetrahedron from the (110) edge surface of ideal pyrophyllite; a) First, the oxygen bridge linking the tetrahedron to the octahedral sheet detaches, b) then the bond with one neighbouring tetrahedron breaks, c) before the third bond to the silicon sheet is dissociated and, d) the silicon is in solution.

The development of industrial applications relying on geological resources requires accurate kinetic data for mineral dissolution/precipitation. These data are only partially available for Pb-Ca-CO_2-H_2O system. To fill the knowledge gap, we conducted three different types of experiments that investigate the reactivity of Pb-bearing solutions towards carbonation processes: i) kinetics of the Pb^{2+} uptake by $CaCO_3$ crystals powder, ii) titration experiments to determine the effect of the presence of Pb^{2+} on the precipitation of $CaCO_3$, iii) *in situ* AFM observation of the replacement of calcite by cerussite (DI LORENZO et al. 2019).

The uptake of Pb^{2+} to form cerussite was investigated using calcite and aragonite powders ($66 < \emptyset < 250$ µm) as the carbonate source. The acidity of the $Pb(NO_3)_2$ 10 mM solution (pH = 4.3) favours $CaCO_3$ dissolution and as a consequence inorganic carbon is released to the solution, supersaturation with respect to cerussite is achieved and the replacement process takes place. The structural difference between the two $CaCO_3$ polymorphs controls the replacement process (Fig. 8.4). The evolution of the system as a function of time was derived from independent experiments (each experiment was repeated at least twice) with incremental reaction times ranging from 4 hours to 10 days. The solid products were filtrated and analysed by XRD and SEM. The aqueous solutions were analysed by ICP-OES to determine the amount of Pb and Ca. The pH and the electrical conductivity were also measured. The analytical measurements, combined with geochemical modelling, allowed describing the path followed by the system to approach equilibrium.

The titration experiments aimed at observing the influence of Pb^{2+} ions on the nucleation of $CaCO_3$ from a supersaturated solution. The experiments were carried on with the pH controlled by the addition of NaOH, the formation of the solid phase was tracked by detection of turbidity through variation of visible light transmittance from the solution (Optrode, Metrohm). Also Ca^{2+}-ISE and conductivity probes were used to monitor the system and to observe the influence of lead on the pre-nucleation stage of $CaCO_3$ precipitation. After filtration the solid products were analysed by FT-IR, XRD and SEM.

The replacement of calcite by cerussite was observed *in situ* using the AFM Cypher Asylum, a solution of $Pb(NO_3)_2$ 10 mM was flowed onto a freshly cleaved {104} calcite surface. The evolution of the surface topography was recorded in tapping mode. This allowed to observe at nanoscale the intrinsic properties of the reaction $CaCO_3 + Pb^{2+} = PbCO_3 + Ca^{2+}$ (Fig. 8.5). The distortion of the normal etch pit geometry of calcite was demonstrated to be univocally related to the presence of Pb^{2+} by comparative studies performed with $NaNO_3$. The flow through experiments also provided insight into the growth mechanism of Pb-carbonate, the replacing phase was observed growing via hillock formation in our experimental conditions.

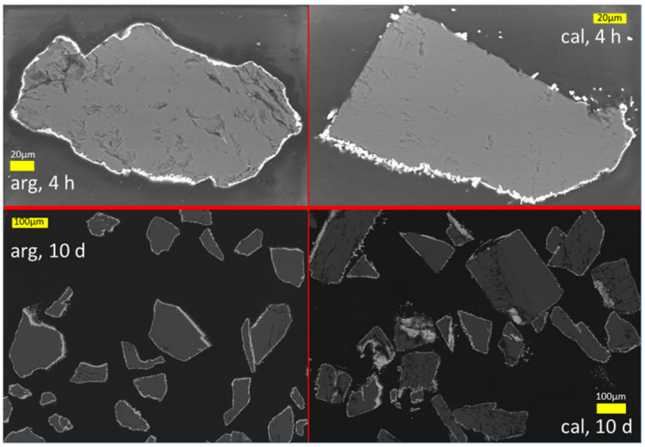

Fig. 8.4: Left: Passivation layer forming by epitaxial growth of Pb-carbonate on the surface of aragonite crystals after few hours of interaction time. The formation of the passivation layer prevents further supply of carbonate ions necessary for Pb-carbonate precipitation and slows down the Pb^{2+} uptake. Right: Growth of Pb-carbonate crystals on calcite surface. The passivation layer is not formed. The calcite dissolution continuously supplies carbonate ions necessary for precipitation of Pb-carbonate.

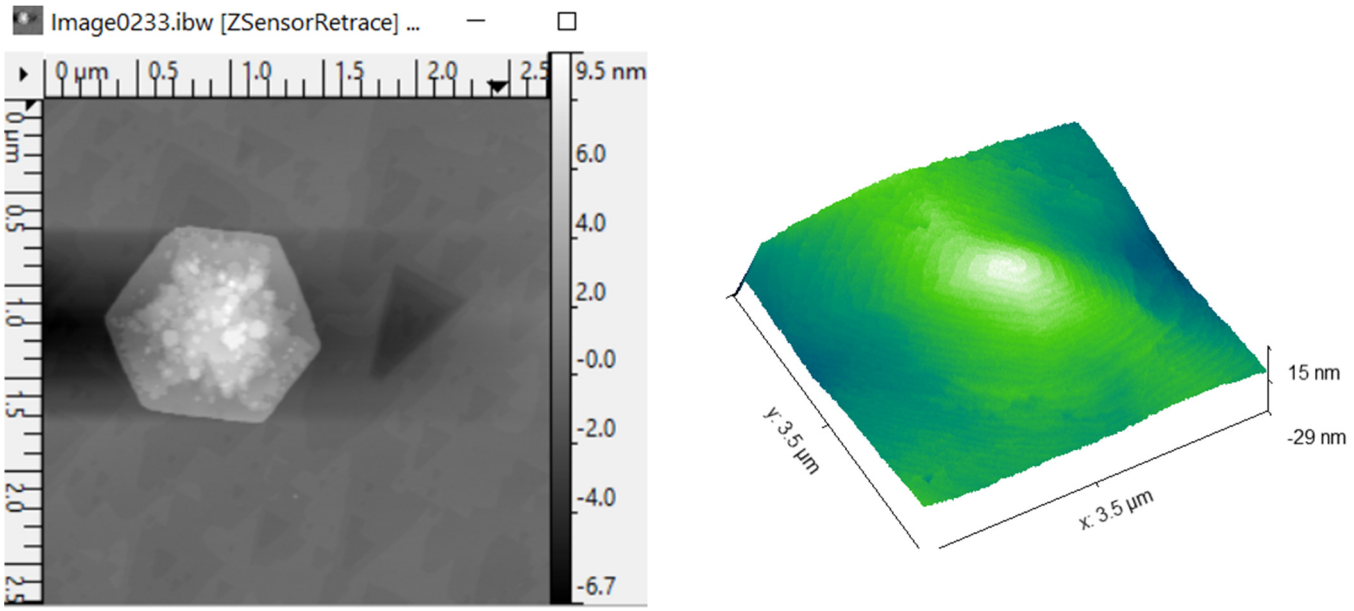

Fig. 8.5 Left: Pseudo hexagonal crystal of orthorhombic Pb-carbonate growing on calcite surface. The surface of calcite shows characteristic triangular shaped etch pitting typically observed in presence of $Pb(NO_3)_2$ solution. Right: In situ observation of Pb-carbonates forming by spiral growth mechanism.

8.5 Molecular scale carbonates dissolution in a wide range of chemical environments revealed by Grand Canonical and Kinetic Monte Carlo modelling

Experimental observations of carbonate dissolution show systematic discrepancies between results obtained by different measurement techniques or sample preparation protocols (ARVIDSON et al. 2003). Dissolution/precipitation reactions of minerals take place in contact with fluids of variable chemical composition in complex heterogeneous environments including a variety of rock textures, pore geometries, and fluid flow regimes. The surface of a carbonate mineral has a complex topography built by different morphological features such as steps, kinks and etch pits. The differences in reactivity of step and kink sites reflect their crystallographic orientation and coordination, and the distribution of these sites is an important source of rate variance at the atomic scale (KURGANSKAYA & LUTTGE 2016). The influence of the fluid chemical composition on rate variance is a complex problem not fully understood yet, primarily due to the following reasons: (1) adsorption of ions and protons at the carbonate-water interface is difficult to quantify experimentally, and (2) the influence of surface charge on dissolution kinetics is not well-characterized.

Currently, available dissolution models for carbonates do not consider dependence of the surface speciation on the local surface topography. We have developed a new approach, combining Grand Canonical (GCMC) and Kinetic Monte Carlo (KMC) methods to investigate the influence of pH and electrolyte concentration in water onto processes of surface charging and dissolution of carbonates. GCMC simulations of the calcite-electrolyte system are used to calculate populations of protonated sites. The modelling approach was used to systematically evaluate the behaviour of different speciation models distinguished by spatial charge distributions at the surface. The best results in comparison with the experimental AFM model were obtained considering explicit oxygen sites on the surface. The model could reproduce both calcite dissolution rate and surface morphology (Fig. 8.6) as function of pH (KURGANSKAYA & CHURAKOV 2018).

The speciation model developed in this study does not rely on fitting experimental data. The outcome of the speciation modelling is determined by the charge distribution of sites on the surface, the effective ion size and the intrinsic acidity constant of the bicarbonate molecule (an experimental quantity). The current model is developed for dissolution at far from equilibrium conditions and does not take into account the potential contribution of re-precipitation processes. This limitation will be resolved in subsequent work.

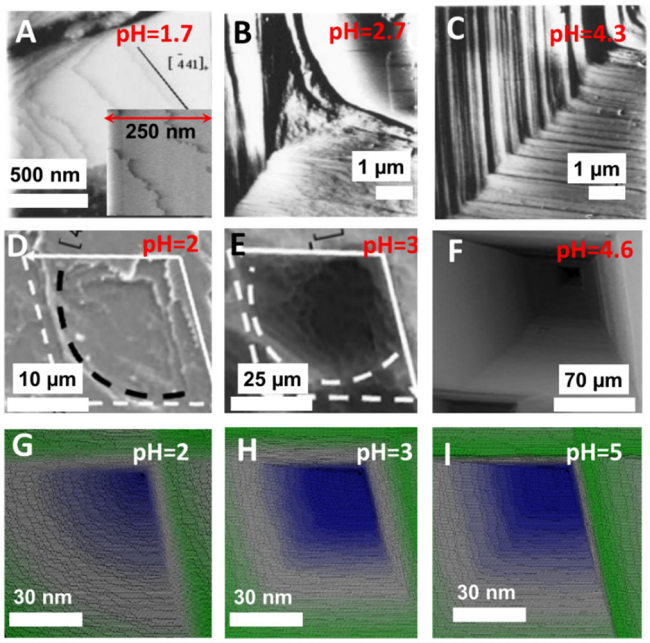

Fig. 8.6. Surface morphologies and etch pit structure reported in experimental studies of calcite dissolution. Panels A-C: 0.1M NaCl, pH adjusted by HCl/NaOH (GIUDICI et al. 2002); panels D-F: pure water, pH adjusted by HCl/NaOH (ATANASSOVA et al. 2013). Panels G-I KMC simulations. Comparison of these data with our modelling results demonstrates that the model reproduces the typical, experimentally observed step morphologies as a function of pH (KURGANSKAYA & CHURAKOV 2018).

8.6 Mineralogy of solid municipal waste incineration residues

Switzerland has a long tradition of waste incineration and today combustible municipal waste that cannot be recycled has to be thermally treated in one of the 31 municipal solid waste incineration (MSWI) plants that are coupled to the distribution of district heat. The advantages of incineration are reduction of mass (75%) and volume (90%) as well as the immobilization of metals and destruction of organic compounds. However, around 6×10^5 tons of bottom ash (BA) and 6×10^4 tons of fly ash (FA) annually remain as residues after waste incineration and have to be disposed of due to their elevated concentrations of toxic substances. For both residues the regulations for metal-depletion have recently been tightened by Swiss Waste Ordinance of Waste (VVEA, 2016). In the context of the elaboration of detailed guidelines to the ordinance, a series of studies on the mineralogical characterisation and the leaching behaviour of the solid residues have been initiated.

The chemical bulk composition and the mineralogical characteristics of fly ash (FA) and acid washed filter cakes (FC) from six Swiss MSWI plants with variable waste input and incineration conditions were investigated for metal content, type of chemical bonding and matrix composition for further optimization of the acidic FA leaching (FLUWA process). The same information is necessary for the remaining FC to evaluate its quality for deposition. Three particle morphologies with heavy metal contents of 4-10 wt.% which are mainly condensed as coatings on larger particles were identified. Approximately 40 wt.% of the phases are present in a crystalline form such as gehlenite, calcite, K_2ZnCl_4, halite and anhydrite. The concentrations of Zn, Pb, Cu, Cd and Sb in the acidic leached FC are strongly reduced and a mass loss of ca. 30 wt.% occurred due to leaching of soluble matrix components such as salts. The FLUWA process allows separation and recovery of heavy metals and significant lesser amounts of residues have to be disposed of (WEIBEL et al. 2017).

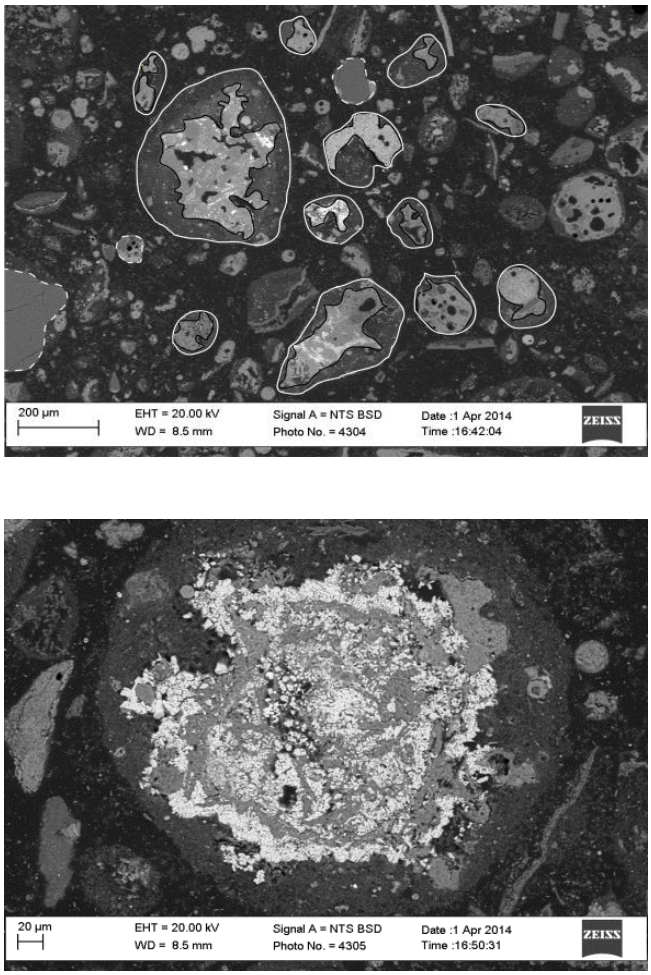

Fig. 8.7: BSE image of FA. Fine grained condensate (top, white framed) which encapsulates metal-bearing particles (top, black framed). Dashed are refractory minerals such as SiO_2.

Focusing on the determination of parameters influencing metal mobilization by leaching, three different leaching processes of FA from MSWI plants in Switzerland comprise neutral, acidic and optimized acidic (+ oxidizing agent) FA leaching. Metals are carried along with the flue gas (Fe-oxides, brass) and are enriched in mineral aggregates (quartz, feldspar, wollastonite, glass) or vaporized and condensed as chlorides or sulphates. Parameters controlling the mobilization of neutral and acidic fly ash leaching are pH and redox conditions, liquid to solid ratio, extraction time and temperature. Almost no depletion for Zn, Pb, Cu and Cd is achieved by performing neutral leaching. Acidic fly ash leaching results in depletion factors of 40% for Zn, 53% for Cd, 8% for Pb and 6% for Cu. The extraction of Pb and Cu are mainly limited due to a cementation process and the formation of a $PbCu^0$-alloy-phase and to a minor degree due to secondary precipitation ($PbCl_2$). The addition of hydrogen peroxide during acidic fly ash leaching (optimized acidic leaching) prevents this reduction through oxidation of metallic components and thus significantly higher depletion factors for Pb (57%), Cu (30%) and Cd (92%) are achieved. The elevated metal extraction using acidic leaching in combination with hydrogen peroxide justifies the extra effort not only by reduced metal loads to the environment but also by reduced deposition costs (WEIBEL et al. 2018).

To enhance the extraction rate of heavy metals from MSWI fly ash, hydrochloric acid and sodium chloride solution were tested. The investigation and optimization of the FLUWA process is of increasing interest and an industrial solution for direct metal recovery within Switzerland is under development. A detailed laboratory study on different filter cakes from fly ash leaching using HCl 5% (represents the FLUWA process) and concentrated sodium chloride solution (300 g/L) were performed. This two-step leaching of fly ash is an efficient combination for the mobilization of a high percentage of heavy metals from fly ash (Pb, Cd > 90% and Cu, Zn 70 - 80%). The depletion of these metals is mainly due to a combination of redox reaction and metal-chloride-complex formation. The results indicate a way forward for an improved metal depletion and recovery from fly ash that has potential for application at industrial scale. Similar investigations are currently performed on wood ashes, since the annual amount of these residues is in the same range as the fly ash from MSWI.

8.7 References

ARVIDSON R.S., ERTAN I.E., AMONETTE J.E., LUTTGE A. (2003)
Variation in calcite dissolution rates: A fundamental problem? Geochim. Cosmochim. Acta 67, 1623-1634.

ATANASSOVA R., CAMA J., SOLER J.M., OFFEDDU F.G., QUERALT I., CASANOVA I. (2013)
Calcite interaction with acidic sulphate solutions: A vertical scanning interferometry and energy-dispersive XRF study. Eur. J. Mineral. 25 (3), 331-351.

CAMETTI G., ARMBRUSTER T., NAGASHIMA M. (2016)
Thermal stability of barrerite and Na-exchanged barrerite: An *in situ* single crystal X-ray diffraction study under dry conditions. Micropor. Mesopor. Mat. 236, 71-78.

CAMETTI G., FISCH M., ARMBRUSTER T.M. (2017)
Thermal behavior of stilbite and stellerite revisited and dehydration of their Na-exchanged forms: Considerations on the memory effect of the **STI** framework type. Micropor. Mesopor. Mat. 253, 239-250.

CAMETTI G. (2018)
New topology of levyne B under quasi-equilibrium conditions: A temperature-dependent *in situ* single crystal X-ray diffraction study. Micropor. Mesopor. Mat. 265, 162-171.

DI LORENZO F., RUIZ-AGUDO C., CHURAKOV S.V. (2019)
Experimental determination of the kinetics of PbII uptake and storage via carbonation of Pb^{2+} bearing solutions. Environ. Sci. Technol. (submitted).

GIUDICI G.D. (2002)
Surface control vs. diffusion control during calcite dissolution: Dependence of step-edge velocity upon solution PH. Am. Mineral. 87 (10), 1279-1285.

KURGANSKAYA I., LUTTGE A. (2013a)
A comprehensive stochastic model of phyllosilicate dissolution: Structure and kinematics of etch pits formed on muscovite basal face. Geochim. Cosmochim. Acta 120, 545-560.

KURGANSKAYA I., LUTTGE A. (2013b)
Kinetic Monte Carlo simulations of silicate dissolution: Model complexity and parametrization. J. Phys. Chem. C 117, 24894-24906.

KURGANSKAYA I., LUTTGE A. (2016)
Kinetic Monte Carlo approach to study carbonate dissolution. J. Phys. Chem. C 120, 6482-6492.

KURGANSKAYA I., CHURAKOV S.V. (2018)
Carbonates dissolution mechanisms in the presence of electrolytes revealed by Grand Canonical and Kinetic Monte Carlo modelling. J. Phys. Chem. C 122, 29285-29297.

LAIO A., PARRINELLO M. (2002)
Escaping free-energy minima. Proceedings of the National Academy of Sciences of the United States of America 99, 12562-12566.

VVEA (2016)
Swiss Confederation, Verordnung über die Vermeidung und die Entsorgung von Abfällen. 1-46.

WEIBEL G., EGGENBERGER U., SCHLUMBERGER S., MÄDER U.K. (2017)
Chemical associations and mobilization of heavy metals in fly ash from municipal solid waste incineration. Waste Manage. 62, 147-159.

WEIBEL G., EGGENBERGER U., KULIK D.A., HUMMEL W., SCHLUMBERGER S., KLINK W., FISCH M., MÄDER U.K. (2018)
Extraction of heavy metals from MSWI fly ash using hydrochloric acid and sodium chloride solution. Waste Manage. 76, 457-471.

9 PUBLICATIONS

9.1 Peer reviewed journals

Alt-Epping P.[1], Gimmi T., Wersin P.[1], Jenni A.[1]
Incorporating electrical double layers into reactive-transport simulations of processes in clays by using the Nernst-Planck equation: A benchmark revisited. Appl. Geochem. 89, 1-10 (2018).
[1] University of Bern, Bern, Switzerland

Bestel M., Glaus M.A., Frick S., Gimmi T., Juranyi F.[1], Van Loon L.R., Diamond L.W.[2]
Combined tracer through-diffusion of HTO and Na-22 through Na-montmorillonite with different bulk dry densities. Appl. Geochem. 93, 158-166 (2018).
[1] LNS, Paul Scherrer Institut, Villigen, Switzerland
[2] University of Bern, Bern, Switzerland

Chen Y., Glaus M.A., Van Loon L.R., Mäder U.[1]
Transport of low molecular weight organic molecules in compacted illite and kaolinite. Chemosphere 198, 226-237 (2018).
[1] University of Bern, Bern, Switzerland

Chen Y., Glaus M.A., Van Loon L.R., Mäder U.[1]
Transport behaviour of low molecular weight organic compounds in multi-mineral clay systems: a comparison between measured and predicted values. Appl. Clay Sci. 165, 247-256 (2018).
[1] University of Bern, Bern, Switzerland

Churakov S.V., Prasianakis N.I.
Review of the current status and challenges for a holistic process-based description of mass transport and mineral reactivity in porous media. Am. J. Sci. 318, 921-948 (2018).

Cvetković B.Z., Rothardt J., Büttler A.[1], Kunz D., Schlotterbeck G.[1], Wieland E.
Formation of low-molecular-weight organic compounds during anoxic corrosion of zero-valent iron. Environ. Eng. Sci. 35, 447-461 (2018).
[1] University of Applied Sciences Northwestern Switzerland, Muttenz, Switzerland

Cvetković B.Z., Salazar G.[1], Kunz D., Szidat S.[1], Wieland E.
Analysis of ^{14}C-bearing compounds released by the corrosion of irradiated steel using accelerator mass spectrometry. Analyst 143, 3059-3067 (2018).
[1] University of Bern, Bern, Switzerland

Endrizzi F.[1], Gaona X.[1], Marques Fernandes M., Baeyens B., Altmaier M.[1]
Solubility and hydrolysis of U(VI) in 0.5 mol/kg NaCl solutions at T=22 and 80 °C. J. Chem. Thermodyn. 120, 45-53 (2018).
[1] KIT-INE, Karlsruhe, Germany

Fazeli H.[1], Patel R.A., Hellevang H.[1]
Effect of pore-scale mineral spatial heterogeneity on chemically induced alterations of fractured rock: A lattice Boltzmann study. Geofluids Article ID 6046182 (2018).
[1] University of Oslo, Norway

Gaona X.[1], Kulik D.A., Macé N., Wieland E.
Corrigendum to "Aqueous-solid solution thermodynamic model of U(VI) uptake in C-S-H phases" [Appl. Geochem. 27 (2012), 81-95]. Appl. Geochem. 90, 150 (2018).
[1] KIT-INE, Karlsruhe, Germany

Gimmi T., Alt-Epping P.[1]
Simulating Donnan equilibria based on the Nernst-Planck equation. Geochim. Cosmochim. Acta 232, 1-13 (2018).
[1] University of Bern, Bern, Switzerland

Gysi A.P.[1], Harlov D.[2], Miron G.D.
The solubility of monazite ($CePO_4$), $SmPO_4$, and $GdPO_4$ in aqueous solutions from 100 to 250° C. Geochim. Cosmochim. Acta 242, 143-164 (2018).
[1] Colorado School of Mines, Golden, CO, USA
[2] GeoForschungsZentrum, Potsdam, Germany

Heberling F.[1], Metz V.[1], Böttle M.[1], Curti E., Geckeis H.[1]
Barite recrystallization in the presence of ^{226}Ra and ^{133}Ba. Geochim. Cosmochim. Acta 232, 124-139 (2018).
[1] KIT-INE, Karlsruhe, Germany

Huang Y.[1], Shao H.[1], Wieland E., Kolditz O.[1], Kosakowski G.
A new approach to coupled two-phase reactive transport simulation for long-term degradation of concrete. Constr. Build. Mater. 190, 805-829 (2018).
[1] Helmhotz Centre for Environmental Research - UFZ, Leipzig, Germany

Kurganskaya I., Churakov S.V.
Carbonates dissolution mechanisms in the presence of electrolytes revealed by Grand Canonical and Kinetic Monte Carlo modelling. J. Phys. Chem. C 122, 29285-29297 (2018).
[1] University of Bern, Bern, Switzerland

Lothenbach B.[1], Kulik D.A., Matschei T.[2], Balonis M.[3], Baquerizo L.[4], Dilnesa B.Z.[5], Miron G.D., Myers R.[6]
Cemdata18: A chemical thermodynamic database for hydrated Portland cements and alkali-activated materials. Cem. Concr. Res. 115, 472-506 (2018).

[1] Empa, Dübendorf, Switzerland
[2] HTW Dresden University of Applied Sciences, Dresden, Germany
[3] University of California, Los Angeles, USA
[4] Lafarge-Holcim Centre de Recherche, Saint-Quentin Fallavier, France
[5] BASF Schweiz AG, Kaisten, Switzerland
[6] University of Sheffield, Sheffield, UK

Montoya V.[1], Baeyens B., Glaus M.A., Kupcik T.[1], Marques Fernandes M., Van Laer L.[2], Bruggeman C.[2], Maes N.[2], Schäfer T.[1]
Sorption of Sr, Co and Zn on illite: Batch experiments and modelling including Co in-diffusion measurements on compacted samples. Geochim. Cosmochim. Acta 223, 1-20 (2018).
[1] KIT-INE, Karlsruhe, Germany
[2] SCK-CEN, Mol, Belgium

Patel R.A., Perko J.[1], Jacques D.[1], De Schutter G.[2], Ye G.[2,3], Van Bruegel K.[3]
Effective diffusivity of cement pastes from virtual microstructures: Role of gel porosity and capillary pore percolation. Constr. Build. Mater. 165, 833-845 (2018).
[1] SCK-CEN, Mol, Belgium
[2] Ghent University, Belgium
[3] T U Delft, Netherlands

Patel R.A., Perko J.[1], Jacques D.[1], De Schutter G.[2], Ye G.[2,3], Van Breugel K.[3]
A three-dimensional lattice Boltzmann method based reactive transport model to simulate changes in cement paste microstructure due to calcium leaching. Constr. Build. Mater. 166, 158-170 (2018).
[1] SCK-CEN, Mol, Belgium
[2] Ghent University, Belgium
[3] T U Delft, Netherlands

Prasianakis N.I., Gatschet M., Abbasi A., Churakov S.V.
Upscaling strategies of porosity-permeability correlations in reacting environments from pore-scale simulations. Geofluids Article ID 9260603 (2018).

Rojo H., Scheinost A.C.[1], Lothenbach B.[2], Laube A., Wieland E., Tits J.
Retention of selenium by calcium aluminate hydrate (AFm) phases under strongly reducing radioactive waste repository conditions. Dalton Trans. 47, 4209-4218 (2018).
[1] HZDR, Dresden, Germany; ROBL, Grenoble, France
[2] Empa, Dübendorf, Switzerland

Rufer D.[1], Waber H.N.[1], Gimmi, T.
Identifying temporally and spatially changing boundary conditions at an aquifer - aquitard interface using helium in porewater. Appl. Geochem. 96, 62-77 (2018).
[1] University of Bern, Bern, Switzerland

Seetharam S.C.[1], Patel R.A., Perko J. [1], Jacques D. [1]
Quantification of leaching kinetics in OPC mortars via a mesoscale model. Constr. Build. Mater. 180, 614-628 (2018).
[1] SCK-CEN, Mol, Belgium
[2] Ghent University, Belgium
[3] T U Delft, Netherlands

Sui R., Essebbar E.T., Mantzaras J., Prasianakis N.I.
Experimental and numerical investigation of fuel-lean H_2/CO/air and H_2/CH_4/air catalytic microreactors. Comb. Sci. Technol. 190, 336-362 (2018).

Van Loon L.R., Leupin O.X.[1], Cloet V.[1]
The diffusion of SO_4^{2-} in Opalinus Clay: Measurements of effective diffusion coefficients and evaluation of their importance in view of microbial mediated reactions in the near field of radioactive waste repositories. Appl. Geochem. 95, 19-24 (2018).
[1] Nagra, Wettingen, Switzerland

Vespa M.[1], Lothenbach B.[2], Dähn R., Huthwelker T.[3], Wieland E.
Characterisation of magnesium silicate hydrates (M-S-H): A combined approach using synchrotron-based absorption spectroscopy and ab initio calculations. Cem. Concr. Res. 109, 175-183 (2018).
[1] GeochEnv Consulting, Herrischried, Germany
[2] Empa, Dübendorf, Switzerland
[3] SLS, Villigen PSI, Switzerland

Vinograd V.L.[1], Kulik D.A., Brandt F.[1], Klinkenberg M.[1], Weber J.[1], Winkler B.[2], Bosbach D.[1]
Thermodynamics of the solid solution - aqueous solution system (Ba,Sr,Ra)SO_4 + H_2O: I. The effect of strontium content on radium uptake by barite. Appl. Geochem. 89, 59-74 (2018).
[1] IEK-6, Forschungszentrum Jülich, Germany
[2] J.W. Goethe University, Frankfurt am Main, Germany

Vinograd V.L.[1], Kulik D.A., Brandt F.[1], Klinkenberg M.[1], Weber J.[1], Winkler B.[2], Bosbach D.[1]
Thermodynamics of the solid solution - aqueous solution system (Ba,Sr,Ra)SO_4 + H_2O: II. Radium retention in barite-type minerals at elevated temperatures. Appl. Geochem. 93, 190-208 (2018).
[1] IEK-6, Forschungszentrum Jülich, Germany
[2] J.W. Goethe University, Frankfurt am Main, Germany

Weibel G.[1], Eggenberger U.[1], Kulik D.A., Hummel W., Schlumberger S.[1], Klink W.[1], Fisch M.[1], Mäder U.K.[1]
Extraction of heavy metals from MSWI fly ash using hydrochloric acid and sodium chloride solution. Waste Manage. 76, 457-471 (2018).
[1] University of Bern, Bern, Switzerland

Wersin P.[1], Gimmi T., Mazurek M.[1], Alt-Epping P.[1], Pękala M.[1], Traber, D.[2]
Multicomponent diffusion in a 280 m thick argillaceous rock sequence. Appl. Geochem. 95, 110-123 (2018).
[1] University of Bern, Bern, Switzerland
[2] Nagra, Wettingen, Switzerland

Wick S.[1], Baeyens B., Marques Fernandes M., Voegelin A.[1]
Thalium adsorption onto illite. Environ. Sci. Technol. 52, 571-580 (2018).
[1] Eawag, Dübendorf, Switzerland

Wieland E., Cvetković B.Z., Kunz D., Salazar G.[1], Szidat S.[1]
Carbon-14 speciation during anoxic corrosion of activated steel in a repository environment. Atw-International Journal for Nuclear Power 63, 34-38 (2018).
[1] University of Bern, Bern, Switzerland

Wigger C., Gimmi T., Müller A.C.A.[1], Van Loon L.R.
The influence of small pores on the anion transport properties of natural argillaceous rocks – A pore size distribution investigation of Opalinus Clay and Helvetic Marl. Appl. Clay Sci. 156, 134-143 (2018).
[1] Ecole Polytechnique Fédérale de Lausanne, Lausanne, Switzerland

Wigger C., Kennell-Morrison L.[1], Jensen M.[1], Glaus M., Van Loon L.R.
A comparative anion diffusion study on different argillaceous low permeability sedimentary rocks with various pore waters. Appl. Geochem. 92, 157-165 (2018).
[1] Nuclear Waste Management Organisation, Toronto, Canada

Wigger C., Plötze M.[1], Van Loon L.R.
Pore geometry as a limiting factor for anion diffusion in argillaceous rocks. Clay. Clay Miner. 66, 329-338 (2018).
[1] Swiss Federal Institute of Technology, Zurich, Switzerland

Wigger C., Van Loon L.R.
Effect of the pore water composition on the diffusive anion transport in argillaceous, low permeability sedimentary rocks. J. Contam. Hydrol. 213, 40-48 (2018).

Wu T.[1], Wang Z.[2], Tong Y.[1], Wang Y.[1], Van Loon L.R.
Investigation of Re(VII) diffusion in bentonite by trough-diffusion and modeling techniques. Appl. Clay Sci. 166, 223-229 (2018)
[1] Huzhou University, PR China
[2] East China Institute of Technology, Nanchang, PR China

9.2 Books and book chapters

Baeyens B, Marques Fernandes M.
Adsorption of heavy metals including radionuclides. In: R. Schoonheydt, C.T. Johnston and F. Bergaya, editors, *Developments in Clay Science, Vol. 9*, Oxford: Elsevier, 2018, pp. 125-172.

Churakov S., Liu X.[1]
Quantum-chemical modelling of clay mineral surfaces and clay mineral–surface–adsorbate interactions. In: R. Schoonheydt, C.T. Johnston and F. Bergaya, editors, *Developments in Clay Science, Vol. 9*, Oxford: Elsevier, 2018, pp. 49-87.
[1] Nanjing University, Nanjing, PR China

9.3 PSI and Nagra reports

Glaus M.A., Frick S., Van Loon L.R.
Diffusion of selected cations and anions in compacted montmorillonite and bentonite. PSI Bericht Nr.17-08 and Nagra Tech. Rep. NTB 17-12 (2018).

Kulik D.A., Marques Fernandes M., Baeyens B.
The 2SPNE SC/CE sorption model in GEM-Selektor v.3.4 code package (ClaySor): Implementation, tests, and user guide. Nagra Work Rep. NAB 18-27, 130 pp. (2018).

Tits J., Wieland E.
Actinide sorption by cementitious materials. PSI Bericht Nr. 18-02 and Nagra Work Rep. NAB 18-04 (2018).

Wieland E., Kosakowski G., Lothenbach B.[1], Kulik D.A., Cloet V.[2]
Preliminary assessment of the temporal evolution of waste packages in the near field of the L/ILW repository. Nagra Work Rep. NAB 18-05, 135 pp. (2018).
[1] Empa, Dübendorf, Switzerland
[2] Nagra, Wettingen, Switzerland

9.4 Conference proceedings

Patel R.A., Prasianakis N.I., Kulik D.A.
Pore-scale modeling: A tool for exploring mechanisms of reactive transport processes in cementitious materials. Workshop on Concrete Modelling and Materials Behaviour in Honor of Professor Klaas Van Breugel, pp. 84-91 (2018) Delft, 26-29 August 2018.

Patel R.A., Prasianakis N.I.
Development of pore-scale model for ingress of CO_2 brine through cement paste. SynerCrete'18 International Conference on Interdisciplinary Approaches for Cement-Based Materials and Structural Concrete, Funchal, Portugal, 24-26 October 2018.

9.5 Invited talks

Churakov S.V.
Coarse-grain simulations of ions uptake in cement. Topical Day - High performance multiscale modelling V, Empa, Dübendorf, AKADEMIE, 31 May 2018, (Key Note).

9.6 Conferences/workshops/presentations

Bentz J., Patel R.A., Kroener E.
Lattice-Boltzmann simulations describing how a heterogeneous distribution of hydrophobicity created by dry mucilage affects water retention, European Geosciences Union General Assembly, Vienna, Austria, 8-13 April 2018.

Cametti G., Churakov S.V.
Framework modification and dehydration path of the Ag-exchanged form of stellerite (STI) Zeolite 2018 The 10th International Conference on the Occurrence, Properties and Utilization of Natural Zeolites, Kraków, Poland, 24-29 June 2018.

Churakov S.V., Kosakowski G., Hax Damiani L., Patel R., Yang G., Curti E., Prasianakis N.I.
Efficient cross-scale modelling of geochemical interactions for nuclear waste geological disposal, International Symposium on Energy Geotechnics (SEG-2018), Lausanne, Switzerland, 26-28 September 2018.

Churakov S.V.
A holistic process-based description of mass transport and mineral reactivity in porous media. 6th Granada-Münster Discussion Meeting, Münster, Germany, 29-30 November 2018.

Curti E., Kulik D.A.
Effect of Cr-doping on UO_2 spent fuel thermodynamics: preliminary data and results. 1st annual workshop of the DisCo project, Sheffield, UK, May 15-16 2018.

Curti E., Churakov S.V., Leupin O. (2018)
Incorporation of Se fission products in the UO_2 lattice and consequences for the safety of radioactive waste disposal. International Conference on Uranium Biogeochemistry, CSF Monte Verità, Ascona, Switzerland, 21-26 October 2018.

Cvetković B.Z., Wieland E., Kunz D., Tits J., Salazar G., Szidat S.
Corrosion study with irradiated steel: Analytical developments and first results. Final Symposium EC CAST (Carbon-14 Source Term), Lyon, France, 16-18 January 2018.

Dähn R.
The fate of radionuclides in deep geological repository systems determined by synchrotron-based X-ray techniques. MARC XI, Methods & Applications of Radioanalytical Chemistry, Kailua-Kona, Hawaii, USA, 8-13 March 2018.

Hax Damiani L., Vinsot A., Kosakowski G., Churakov S.V.
HT – Hydrogen Transfer modeling with the Nernst-Planck Solver (NPS), Goldschmidt 2018, Boston, USA, 12-17 August 2018.

Detillieux V., Swahn J., Pellegrini D., Pfingsten W., Zeleznik N.
SITEX_NETWORK for the development of sustainable and independent technical expertise on radioactive waste management - General overview of the Network and its interactions with Civil Society. International Conference on Challenges Faced by Technical and Scientific Support Organizations (TSOs) in Enhancing Nuclear Safety and Security: Ensuring Effective and Sustainable Expertise, Brussels, Belgium, 15-18 October 2018.

Di Lorenzo F., Ruiz-Agudo C., Churakov S.V.
Experimental determination of the kinetics of PbII uptake and storage via carbonation of Pb^{2+}-bearing solutions. 6th Granada-Münster Discussion Meeting, Münster, Germany, 29-30 November 2018.

Gimmi T., Alt-Epping P.
Simulating Donnan equilibria based on the Nernst-Planck equation. Computational Methods in Water Resources XXII – Bridging gaps between data, models, and predictions, CMWR2018, Saint-Malo, France, 3-7 June 2018.

Kéri A., Dähn R., Krack M., Churakov S.V.
Combined *ab initio* and XAFS spectroscopy study on the characteristics of metal uptake by clay minerals. Goldschmidt 2018, Boston, USA, 12-17 August 2018 and 9th Mid-European Clay Conferences, Zagreb, Croatia, 17-21 September 2018.

Kosakowski G., Huang Y., Shao H., Wieland E.
Water and gas transport in a generic cemented waste package during intermediate storage. International Symposium on Cement-based Materials for Nuclear Waste (NUWCEM 2018), Avignon, France, 24-26 October 2018.

Krejci P., Gimmi T.
Modelling transport of sorbed species in clays. Computational Methods in Water Resources XXII – Bridging gaps between data, models, and predictions, CMWR2018, Saint-Malo, France, 3-7 June 2018.

Kulik D.A., Miron G.D., Lothenbach B.
A realistic three-site solid solution model of C-S-H. Goldschmidt 2018, Boston, USA, 12-17 August 2018.

Kulik D.A., Lothenbach B., Miron G.D.
Modern thermodynamic models of C-S-H in aid of predicting cement hydration and durability. Conference in honor of Centennial of Laboratory of Construction Materials and 60th Birthday Prof. K. Scrivener, Lausanne, Switzerland, 26-29 August 2018.

Kurganskaya I., Luttge A., Fischer C., Arvidson R.S., Churakov S.V.
A multi-scale approach to study mineral dissolution: Kinetic Monte Carlo models and experimental observations. CMWR2018, Saint-Malo, France, 3-7 June 2018.

Kurganskaya I., Luttge A., Churakov S.V.
Monte Carlo modelling of surface speciation and dissolution kinetics of carbonate minerals in the presence of electrolytes, Goldschmidt 2018, Boston, USA, 12-17 August 2018.

Kurganskaya I., Arvidson R.S., Churakov S.V., Luttge A.
Formulating Kinetic Monte Carlo models of crystal dissolution and growth, GeoBonn 2018 conference, Bonn, Germany, 2-6 September, 2018.

Kurganskaya I., Arvidson R.S., Fischer C., Churakov S.V., Luttge A.
Fundamental problems in mineral-fluid reaction kinetics modelling: system size, parameterization, complexity and scalability GeoBonn 2018 conference, Bonn, Germany, 2-6 September, 2018.

Mancini A., Wieland E., Lothenbach B., Barzgar S., Wehrli, B.
Uptake of aluminium and iron by C-S-H. 2nd Workshop on C-S-H Containing Aluminium: C-A-S-H II, Dübendorf, Switzerland, 23-24 April 2018.

Mancini A., Wieland E., Lothenbach B., Dähn R., Wehrli B.
Interaction of Fe(II, III) with cement phases in anoxic conditions. International Symposium on Cement-based Materials for Nuclear Waste (NUWCEM 2018), Avignon, France, 24-26 October 2018.

Marafatto F.F., Ferreira-Sanchez D., Dähn R., Grolimund D., Voegelin A.
Overcoming radiation artifacts in X-ray cryomicrospectroscopy: Case study of thallium speciation in soil manganese concretions. Soleil User Meeting 2018, Paris, France, 18-19 January 2018.

Marafatto F.F., Ferreira-Sanchez D., Dähn R., Grolimund D., Voegelin A.
Synchrotron X-ray cryomicrospectroscopy on radiation sensitive samples: Thallium speciation in contaminated soils. European Geoscience Union General Assembly, Vienna, Austria, 7-12 April 2018.

Marafatto F.F., Ferreira-Sanchez D., Dähn R., Grolimund D., Voegelin A.
Beam damage in X-ray cryomicrospectroscopy: Thallium speciation and crystallography in contaminated soils from the Swiss Jura mountains. International conference on X-ray Absorption Fine Structure 2018, Krakow, Poland, 22-27 July 2018.

Marafatto F.F., Ferreira-Sanchez D., Dähn R., Grolimund D., Voegelin A.
Some like it cold: X-ray cryomicrospectroscopy for environmental science. Eawag symposium 2018, Dübendorf, Switzerland, 14 September 2018.

Mibus J., Diomidis N., Swanton S., Suzuki-Muresan T., Rodríguez Alcalá M., Leganés Nieto J.L., Bottomley D., Herm M., de Visser-Týnová E., Cvetković B.Z., Sakuragi T., Druyts F., Heikola T.
Speciation of carbon-14 released from activated steels under conditions of a geological repository. Final Symposium EC CAST (Carbon-14 Source Term), Lyon, France, 16-18 January 2018.

Miron G.D., Kulik D.A., Lothenbach B.
Parameterization of a new C-S-H solid solution model for alkali uptake. Goldschmidt 2018, Boston, USA, 12-17 August 2018.

Nedyalkova L., Lothenbach B., Tits J., Wieland E., Mäder U.
Effect of redox conditions on sulfur, selenium and iodine binding in AFm phases. 3rd Annual Project Workshop of the Horizon 2020 Project Cebama, Nantes, France, 17-18 April 2018.

Nedyalkova L., Lothenbach B., Tits J., Wieland E., Mäder U.
Effect of redox conditions on sulfur, selenium and iodine binding in AFm phases. Goldschmidt 2018, Boston, USA, 12-17 August 2018.

Nedyalkova L., Lothenbach B., Tits J., Wieland E., Mäder U.
Fate of sulfur and selenium under reducing conditions. CEMNET meeting, Bern, Switzerland, 24 September 2018.

Nedyalkova L., Lothenbach B., Tits J., Wieland E., Renaudin G., Mäder U.
Effect of redox conditions on sulfur and selenium binding in AFm phases. International Symposium on Cement-based Materials for Nuclear Waste (NUWCEM 2018), Avignon, France, 24-26 October 2018.

Patel R.A.
Modeling of leaching and carbonation of cementitious materials across different spatial scale. CEMNET meeting, Bern, Switzerland, 19 March 2018.

Patel R.A., Prasianakis N.I.
Towards multi-scale microstructure modelling of carbonation process in cement paste. Rilem technical committee TC 281-CCC meeting, Ghent, Belgium, 11 April 2018.

Patel R.A., Prasianakis N.I.
Pore-scale modelling of cement paste subjected to CO_2 rich brine. EMPA Postdocs-II & PSI-FELLOW II-3i retreat, Dübendorf, Switzerland, 21 September 2018.

Poonoosamy J., Prasianakis N.I., Westerwalbesloh C., Deissmann G., Brandt F., Klinkenberg M., Kohlheyer D., Bosbach D.
Dynamics of celestine precipitation and dissolution in confined spaces: a lab-on-a-chip experiment and complementary pore scale modelling. CMWR 2018, Saint-Malo, France, 3-7 June, 2018.

Prasianakis N.I., Safi A., Mantzaras J., Lamibrac A., Büchi F.N.
High performance full resolution modelling of mass transport and phase change phenomena in anode and cathode sides of PEFCs, 15th Symposium on Modelling and Experimental Validation of Electrochemical Energy Devices MODVAL 2018, Aarau, Switzerland, 12-13 April 2018.

Prasianakis N.I., Patel R., Mahrous M.M., Curti E., Churakov S.V.
Cross-scale reactive transport modelling of precipitation processes in porous media, CRYSPOM 2018 conference, Hamburg, Germany, 19-21 September 2018.

Scheinost A.C., Kvashnina K.O., Hennig C., Schmidt M., Marques Fernandes M.
Sorption, redox reactions and (nano-)particle formation of uranium and other early actinides at mineral-water interfaces: Lessons (to be) learned from synchrotron methods. International Conference on Uranium Biochemistry, CSF Monte Verità, Ascona, Switzerland, 21-26 October 2018.

Schliemann R., Kurganskaya I., Churakov S.V.
Molecular mechanism of dissolution, growth and ion incorporation of clay minerals at the mineral/water interface. Mid-European Clay Conference, Zagreb, Croatia, 17-21 September 2018.

Tits J.
Actinide uptake by cementitious materials. Review meeting of the Belgian program related to the behaviour of spent fuel in a cementitious environment. ONDRAF/NIRAS, Brussels, Belgium, 26-27 April 2018.

Tits J., Kunz D., Cvetković B.Z., Wieland E.
Chemical stability of formate in alkaline cement pore waters. International Symposium on Cement-based Materials for Nuclear Waste (NUWCEM 2018), Avignon, France, 24-26 October 2018.

Vespa M., Dähn R., Wieland E.
State-of-the-art synchrotron-based techniques and analytical approaches for the understanding of radionuclide uptake mechanisms by cement. MARC XI, Methods & Applications of Radioanalytical Chemistry, Kailua-Kona, Hawaii, USA, 8-13 March 2018.

Vespa M., Dähn R., Mancini A., Wieland E.
Chemical speciation and structural studies in heterogeneous cementitious materials using synchrotron-based spectroscopic and diffraction techniques. Conference in honor of Centennial of Laboratory of Construction Materials and 60th Birthday Prof. K. Scrivener, Lausanne, Switzerland, 26-29 August 2018.

Wick S., Baeyens B., Pfenninger N., Voegelin A.
Importance of illite for Tl uptake in soils**,** Interfaces against Pollution, La Grande Motte, France, 11-13 June 2018.

Wieland E., Tits J., Cvetković B.Z., Kunz D., Thoenen T.
Chemical stability of low molecular weight organic compounds in the cementitious near field of a repository for radioactive waste. Final Symposium EC CAST (Carbon-14 Source Term), Lyon, France, 16-18 January 2018.

Wieland E., Kosakowski G., Lothenbach B., Kulik D.A.
Geochemical modelling of the long-term evolution of chemical conditions in cement-stabilized waste sorts (L/ILW). International Symposium on Cement-based Materials for Nuclear Waste (NUWCEM 2018), Avignon, France, 24-26 October 2018.

Yang Y., Patel R.A., Kosakowski G., Churakov S.V., Prasianakis N., Wang M.
Multiscale modelling of ion transport in cementitious system: Surface charge effects. 2nd Workshop on C-S-H Containing Aluminium: C-A-S-H II, Dübendorf, Switzerland, 23-24 April 2018.

Yang Y., Patel R.A., Kosakowski G., Churakov S.V., Prasianakis N., Wang M.
Multiscale modelling of ion diffusion in cement paste: Electrical double layer effects. CONMOD conference, Delft, Netherlands, 26-29 August 2018.

Yang G.M., Churakov S.V., Prasianakis N.I.
The applications of fluid density functional theory (DFT) to ion exchange and ion transport in nano-channels of clay minerals: Comparison of different models. Empa Postdocs-II & PSI-FELLOW II-3i retreat. Empa Dübendorf, Switzerland. 21 September 2018.

9.7 Teaching

Churakov S.V.
Bachelor Course: Crystallography I + II, Institute for Geological Sciences, University of Bern.

Churakov S.V.
Bachelor Course: Crystall-optics, Institute for Geological Sciences, University of Bern.

Gimmi T.
Lecture and examinations "Fluids in the Crust", Master Course in Environmental and Resource Geochemistry, University of Bern, Fall semester 2018.

Hummel W., Plötze L.M.
Master Course: Landfilling, Contaminated Sites and Radioactive Waste Repositories, ETH Zurich.

Prasser H.-M., Günther-Leopold I., Hummel W., Zuidema P.K., Hirschberg S.
Master Course: Nuclear Energy Systems, ETH Zurich.

Kulik D.A., Miron G.D.
Training Workshop: Metasomatism and ore deposits in the Earth's crust: experimental and modeling methods. 11-12 August 2018, Boston University (Pre-Goldschmidt 2018-conference workshop).

9.8 PhD thesis defences

Baeyens B.
Examination of Doctoral thesis of Flavia Maia, IMT Atlantique, Université de Nantes, Nantes, France, 30 May 2018.

Kosakowski G.
Examination of PhD thesis of Yonghui Shao, University of Dresden, Dresden, Germany, 31 May 2018.

Kosakowski G.
Examination of PhD thesis of Emma Hipkins, The University of Edinburgh, Edinburgh, United Kingdom, 17 September 2018.

Kulik D.A.
Examination PhD thesis of Aslam Kunhi Mohamed, EPFL Lausanne, 27 June 2018.

Pfingsten W.
Examination of Doctoral thesis of Jesús Fernández Águila, Universidad de La Coruña, La Coruña, Spain, 9 February 2018.

9.9 Other

Churakov S.V., Cametti G.
Guest Editor: Minerals. Special Issue "Natural Zeolites"

Gimmi T.
Associate Editor of Applied Geochemistry

Gimmi T.
Co-Guest Editor of Special Issue for Clay Conference Davos 2017, Applied Geochemistry

Kulik D.A.
Associate Editor of Applied Geochemistry.

Patel R.
Secretary and member of RILEM technical committee TC 244-NUM

Pfingsten W.
Secretary General of SITEX_Network Association

Paul Scherrer Institut :: Forschungsstrasse 111 :: 5232 Villigen PSI :: Switzerland :: Tel. +41 56 310 21 11 :: www.psi.ch